Correlation between Grain Boundary Segregation of Alloying Elements and Grain Refinement Strengthening in Ferritic Steels

周, 裕雄

Correlation between Grain Boundary Segregation of Alloying Elements and Grain Refinement Strengthening in Ferritic Steels

ZHOU YUXIONG

周　裕雄

Context

Chapter 1 Introduction

1. 1 Background

Structural materials play an essential role in our daily life. They are widely used in large structures, such as towers or bridges, and in small structures, such as automobiles or motorcycles. As the structure materials are designed to keep people safe for their specific mechanical properties, they face more and more challenges in this developing society. Plastic deformation influences the failure of materials and is relevant to the critical stress or the yield stress of the materials, which is a crucial factor in material design.

As an essential part of structure materials, steels are in the leading role because of their specific mechanical properties and economic cost. So far, much research on yield stress and deformation characteristics under yielding have been carried out. The design of steels has gone through the Conventional High Strength Steels (CHSS), the first generation of Advanced High Strength Steels (AHSS), the 2nd AHSS, and reached the 3rd AHSS, which is focused on increasing the strength and ductility under minimum alloying elements addition.

Grain refinement is one of the polycrystalline materials' most attractive strengthening methods, known as the only general strengthening mechanism to improve strength and toughness. E. O. Hall first discovered the linear relationship between yield strength and average grain size in the 1950s, which is the famous Hall-Petch (HP) relationship [1,2]. The relationship expresses that the yield stress increases along with grain size reduction. Based on this regularity, efforts to gain smaller grain size were tried a lot to obtain steels with higher strength.

Wallace [3] focused on nucleation by controlling the crystallization conditions during solidification. He found that adding carbon or other alloy elements will promote grain refinement. Grange [4] introduced a heat treatment method called thermal cycling, a process of austenitizing steel by rapidly heating through A_{c1} to $A_{c3,}$ then quenching immediately, then repeating several times until an ultrafine grain size is obtained. Ueji et al. [5] and Najaf et al. [6] reported the formation of ultrafine-grained microstructure while tempering cold-rolled martensite in low-carbon steels. The recrystallization processes, including dynamic, metadynamics and static recrystallization, also gained a fine grain size [7-14]. Dong et al. [15] developed a kind of solid

state transformation induced by deformation-induced ferrite transformation to produce fine or ultrafine ferrite grains. The thermo-mechanical-controlled processing technique was designed to achieve a fine and uniform acicular ferrite microstructure by controlling the hot-deformation process [16].

However, although these processes can obtain a fine or ultrafine grain size, there is too much cost both in time and energy resources. It is either inconformity to the industry's mass production nor the themes of economized society. In addition, grain refinement has been reported to break down at a critical ultrafine area [17,18]. They reported that material softening happens as the grain size decreases beyond some point in the nanometer-scale, resulting from the dominant mechanism of deformation changing from a dislocation-mediated process to grain boundary sliding.

The strength of structure materials comes from the resistance to plastic deformation. The reason why the refinement of grain helps to increase the yield stress generally attribute to the grain boundary (GB). From a microcosmic point of view, plastic deformation is due to the movement of dislocations in their crystal lattice. Because the lattice structure of adjacent grains varies in orientation, it needs more energy for a dislocation to change directions and move into the adjacent grain. The GB is much more disordered than inside the grain, preventing dislocations from moving in a continuous slip plane. Impeding these dislocations` movement will hinder the onset of plasticity and hence increase the yield strength of the material.

A theoretical explanation for this interaction between dislocations and the GB is the Pile-up model [19, 20]. This model quantifies the relation between the number of dislocations stopped at the GB and the critical force on the GB that suffered from these dislocations, called the critical grain boundary shear stress. In addition, the slope of the HP relationship, called the Hall-Petch coefficient (k_y), had been expressed as a function of the critical grain boundary shear stress, which represents the efficiency of grain size refinement.

To focus on more effective and economical ways to apply grain size refinement, researchers have investigated the HP relationship from other angles. The friction stress was studied in steels with C and N addition [21, 22]. It has been found that friction stress has a linear relationship with the concentration of solute C and N. Although this can be used in strengthening steels, it needs too

much addition of alloy, which will deviate from the economic objective.

Comparing the HP relation profile of interstitial free steels [23] with low carbon [24] steels, there was a significant enhancement of k_y. Since the addition of C can enlarge the effect of grain size refinement, much relevant research on ferritic steels was carried out subsequently. Takeda et al. [25] investigated steels with various grain sizes and different contents of C and N. It has been found that the k_y is enlarged by only a small amount of solute C, but solute N didn`t show this effect. They concluded this phenomenon as the k_y is influenced by the grain boundary segregation of C and N. Nakada et al. [26] studied the effect of phosphorus in interstitial free (IF) steel and ultralow carbon steel. The Auger electron spectroscopy (AES) results revealed that phosphorus decreased the k_y by reducing the concentration of C segregated at GB. Hironaka et al. [27] discussed the influence of chromium in ferritic steels. They summarized that chromium hardly affects the k_y of ferritic steel. Akama et al. [28] investigated the effect of nickel addition in IF steels. They found an increase in k_y due to grain boundary segregation of nickel.

All this research indicates that the k_y change is due to the GB segregation level. When interstitial or substitute elements segregate at GB, they will help to block or impede dislocations that result in an enlargement in the efficiency of the refinement of grain size. Furthermore, why different atoms have various influences on the k_y and the exact mechanism of this reinforcement of GB segregation is still unclear. However, the GB's information is minimal because it is a relatively specific but fuzzy concept. It is tough to figure out the change in the GB segregation level without GB`s characteristics.

To make an approximate description of the GB, thermodynamic simulations on the GB have been used for many years, which is based on the partial information obtained in previous experiments. Many thermodynamic models tried to describe the situation of the GB to approach the actual circumstance. Such as the McLean model [29], the Hillert model [30], the Guttmann model [31], and so on. A new analysis technology called three-dimensional atomic probe tomography (3DAP) has been developed recently. The 3DAP offers extensive capabilities for 3D imaging and chemical composition measurements at the atomic scale. Nevertheless, the 3DAP requires a complex process for specimen making and observation, which makes this method not rapid and timely.

Therefore, finding a quick and effective way to evaluate GB segregation and the relationship between GB segregation and the change of the k_y is necessary.

1. 2 Previous studies on the refinement of grain size

1. 2. 1 Hall-Petch coefficient in commercial low-carbon steels

Generally, the yield strength of polycrystalline metals linearly increases as a function of the inverse of the square root of grain size, referred to as Hall-Petch (HP) relationship, written as Eq. (1).

$$\sigma = \sigma_0 + k_y \cdot d^{-\frac{1}{2}} \quad (1)$$

σ, σ_0, k_y and d are the yield strength, the friction stress, the HP coefficient and the grain size, respectively. Based on the previous data of commercial low-carbon steels, the relationship between grain size and yield strength is summarized by Takaki, shown in Fig. 1. 1.

Fig. 1. 1 shows a typical HP relation between grain size and yield strength of various kinds of steels. The different shapes of spots in the graphic represent the previous experimental data from other researchers [32-34]. Although these specimens have various components, their HP profile roughly obeys the same linear relation displayed by the black line. The HP relation of interstitial free (IF) steels was also shown to clarify the difference with low-carbon steels. Based on Takaki`s conclusion [35], this result suggests some influence of solute C on the grain size refinement mechanism.

1. 2. 2 The Pile-up model

The theoretical model incorporated to support the HP effect is the dislocation pile-up model reported by Cottrell and Bilby [19] and Eshelby [20]. The dislocation pile-up model explains that the dislocations move inside the grain until they reach the grain boundary (GB), which prevents their movement. Fig. 1. 2 illustrates the dislocation pile-up model. The dislocations can hardly pass the GB because of the mismatch between grains, and the grain boundary will act as an obstacle.

Dislocations piled up at the GB will give GB a concentrated stress, τ. The pile-up process will

continue until the stress concentration τ reaches a critical value of τ_{cr}. At this moment, the dislocations will pass through the GB into the adjacent grain, and steel yield occurs.

To formulate this model, it is assumed that the dislocation slip occurs as soon as the shear stress becomes more significant than τ_0. Then the formula has already been summarized [19, 20] by Eq. (2).

$$k_y = M\sqrt{\frac{2Gb\tau_{cr}}{\pi e}} \tag{2}$$

Where *M*, *G*, *b*, *e* are the Taylor factor, shear modulus, burgers vector and a constant of the order of unity, respectively. The k_y is only relative to the critical grain boundary shear stress (τ_{cr}) as the other factors are constant. Obviously, to obtain higher strength steels by increasing the k_y, the control of the τ_{cr} is essential. From the previous discussion, τ_{cr} represents the strength of the GB, which seem to be reinforced by the solute C.

1. 2. 3 Hall-Petch coefficients in Fe-C and Fe-N binary alloys

To make this relation more specific and verify the connection between k_y and solute elements, very little addition of C and N was added in IF steels, separately. Then their HP relation was investigated [25]. Fig. 1. 3 shows the results of two kinds of alloys. In the HP profile of Fe-C binary alloys, the addition of C is 0, 5, 28, and 56 mass ppm, respectively. The C content is far lower than the commercial low-carbon steels, and they exhibit a different tendency of k_y. The k_y goes up with the increment of the solute C. It is indicated that k_y will enlarge along with the increasing solute C. The same investigation was also carried out in Fe-N binary alloys containing 0, 9, 24, and 54 mass ppm of N, respectively. However, the k_y only increased slightly at first and kept almost no change with the solute N increasing. Based on the theory that solute elements will reinforce the k_y, the HP profile of Fe-N seems unusual. It must be some deep reasons for the influence of solute elements on the k_y.

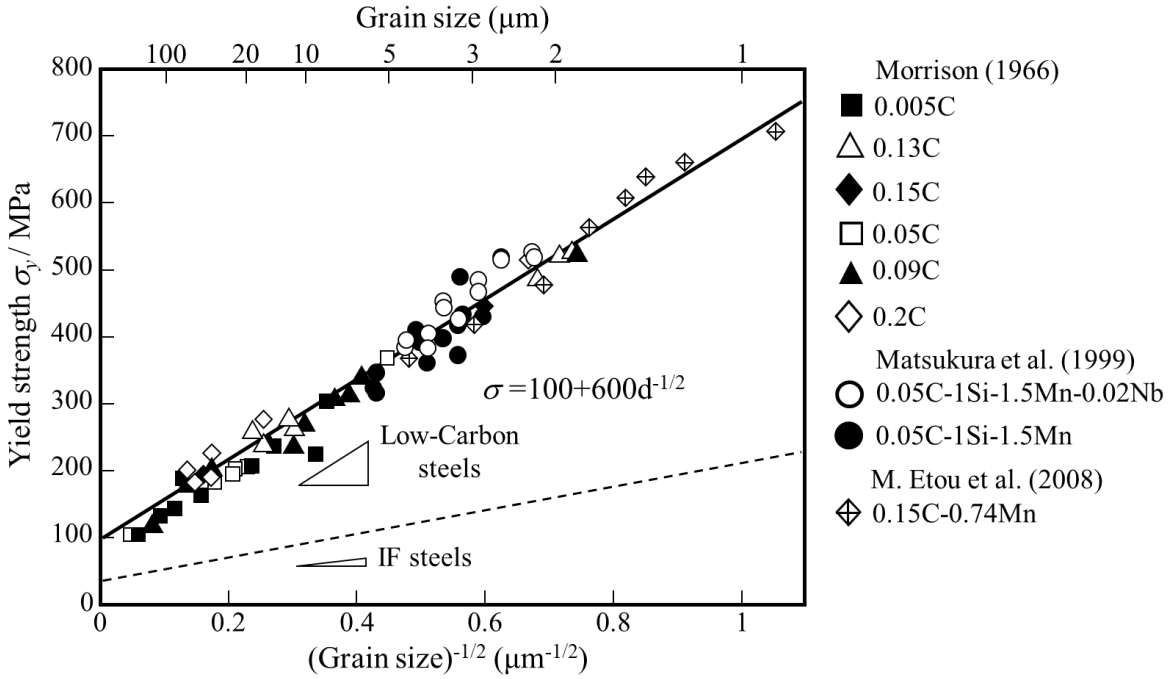

Fig. 1. 1 The Hall-Petch profiles in different Low-Carbon steels.

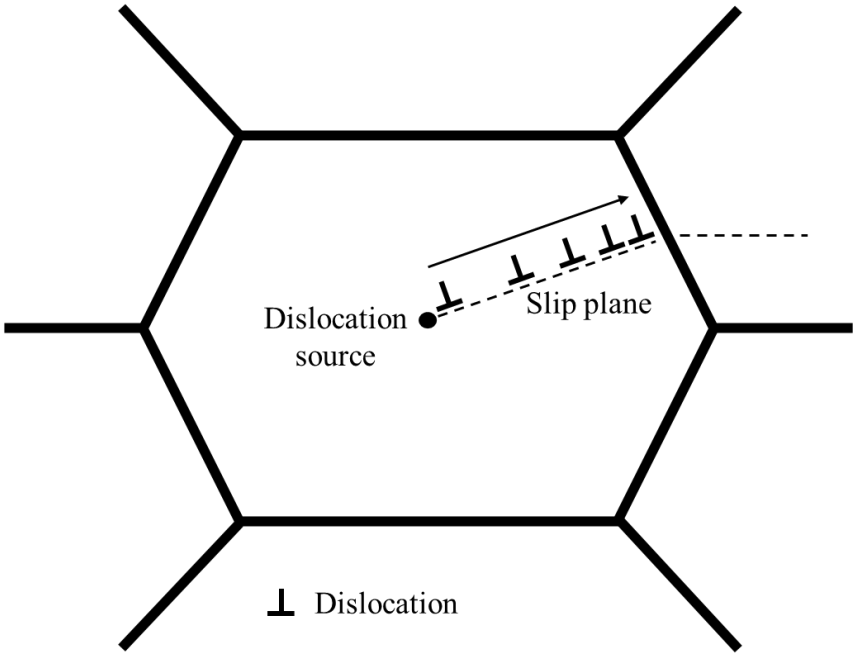

Fig. 1. 2 The pattern diagram of the pile-up model.

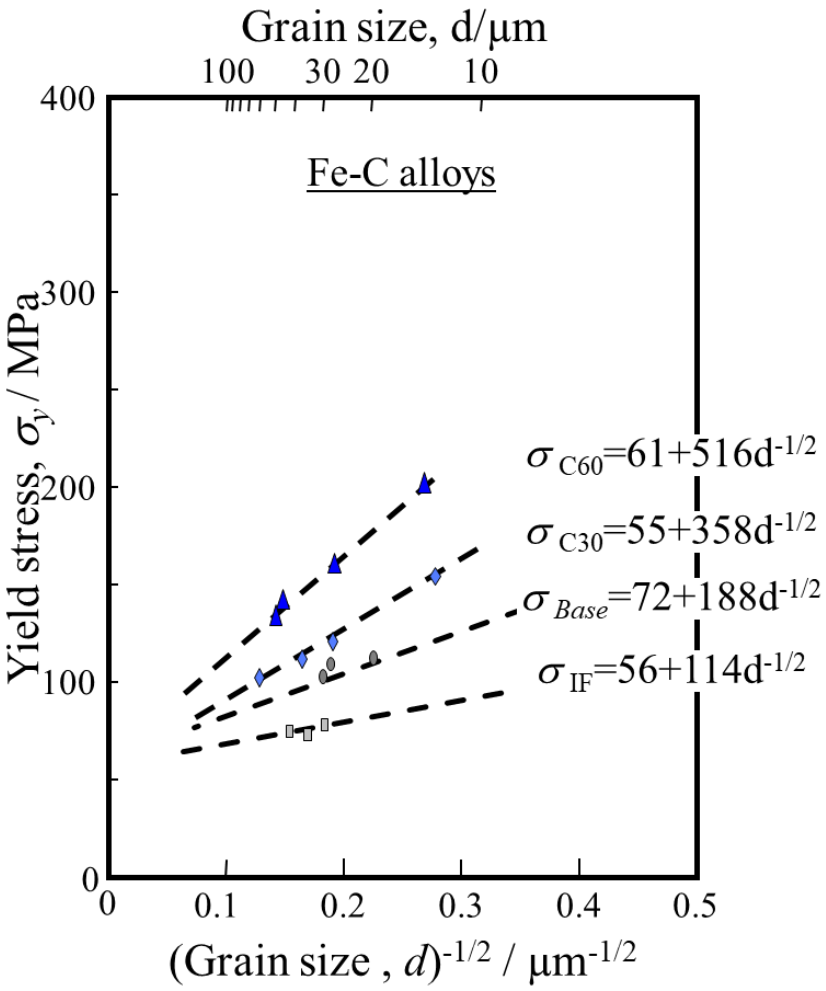

(a) Steels with different amount of C addition

Fig. 1. 3 The Hall-Petch profiles of (a) steels with different amount of C addition and (b) steels with different amount of N addition.

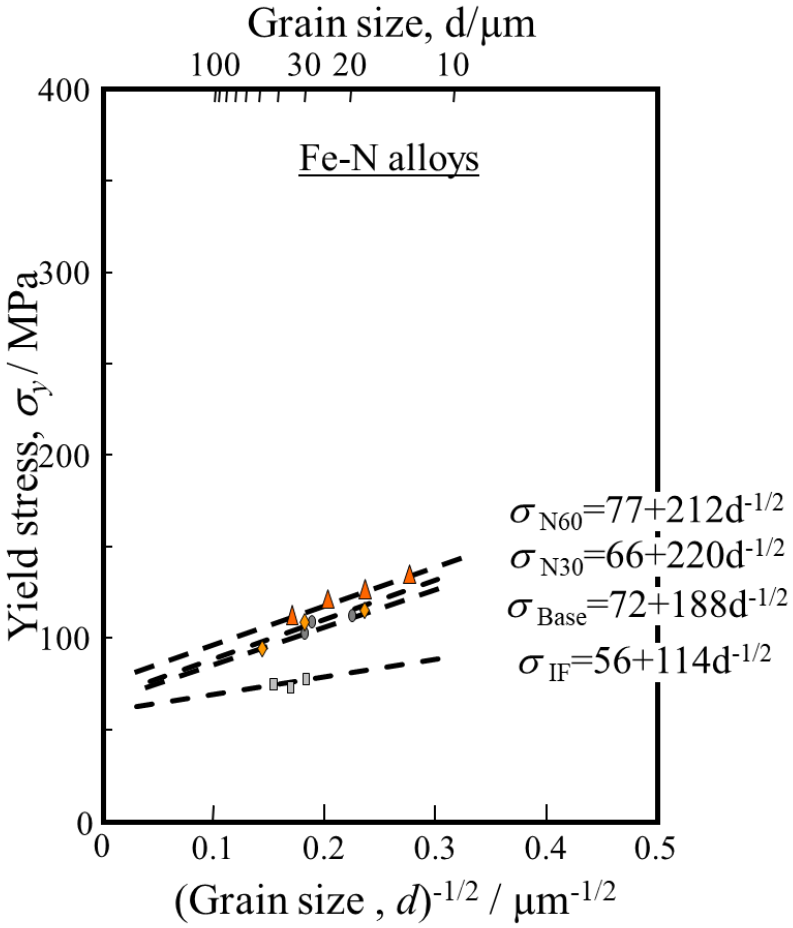

(b) Steels with different amount of N addition

Fig. 1. 3 The Hall-Petch profiles of (a) steels with different amount of C addition and (b) steels with different amount of N addition.

1. 3 Previous studies on grain boundary segregation

1. 3. 1 Structure and properties of the grain boundary

The grain boundary (GB) plays a vital role in reinforcing the resistance to deformation by the HP relation and in understanding fracture mechanisms, melting kinetics, and transport properties in materials. The GB is a region separating two grains of the same phase. Since the two grains differ in mutual orientations, thus the GB represents a transition area, where the atoms shift from their regular positions compared to the interior of the grain [29, 36]. For a more superficial understanding, the GB is assumed to be an interface between two adjacent grains with an amorphous structure [29]. To define this interface more specifically, Gibbs [37] proposed the first thermodynamic description of interfaces. The thermodynamic state functions of the GB will be introduced later.

Generally, interfaces represent structure defects in a crystal, which have a higher Gibbs energy than a single crystal. To minimize the total Gibbs energy of the system, these interfaces will interact with other lattice defects like dislocations and foreign atoms. The interaction with dislocations leads to an impedance effect for dislocations. While the interaction with foreign atoms results in an accumulation of solute atoms in the interface area, called the GB segregation [29, 36].

1. 3. 2 Interaction between grain boundary and dislocations

The experimental method also has been carried out to investigate the properties of the GB. Tsuchiyama et al. observed the movement of dislocations in high nitrogen austenitic steels using the Transmission Electron Microscope (TEM) [38]. Fig. 1. 4 shows the image they observed of the dislocations piled up at the GB and new dislocations emitted from the GB when yield happened. Although this is a particular dislocation structure called planer dislocations, the image shows the new slip system activated from the GB to the adjacent grain by the piled-up dislocations.

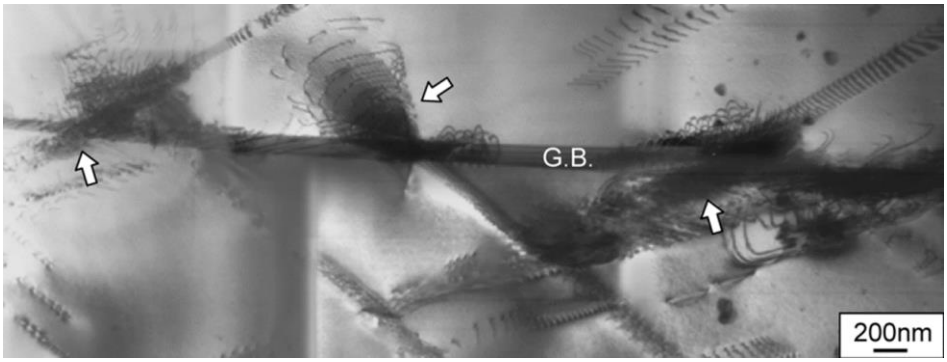

Fig. 1. 4 TEM image of dislocations at or around the GB when yield occurs.

Li et al. [39] investigated the IF steels with ultrafine grain (UFG) size and coarse grain (CG) size by TEM. They found that the dislocation density was reduced in UFG samples but increased in CG samples with tensile straining. In addition, the dislocation absorption at the GB had been observed in UFG. These results were caused by the shortage of motivated dislocations in UFG. It supposes that the GB also has a capacity for dislocations, and the GB will emit new dislocations when the capacity reaches the limit.

Ono et al. [40] analyzed the behavior of fine-grain ultra-low carbon (ULC) steels under strain aging. They found that the hardening effect of strain aging can be divided into two patterns by aging temperature. The fixed effect by the cloud of solute C atoms was adopted in low-temperature annealing. On the other hand, the dislocations at the GB may reverse when the annealing temperature increases. Then this reversion caused a hardening in tensile properties. That means the number of dislocations in the GB also influences the mechanical properties.

1. 3. 3 Types of grain boundary segregation

GB segregation is a term that describes the concentration of solution elements at GB in solids. Because GB performed as obstruct for dislocations, and the impediment effect changed when the number of solution atoms changed, it is reasonable that the level of GB segregation also influences the strength of the GB. As mentioned before, atoms segregate into the GB, which can be seen as a free surface, reducing Gibbs energy of the system. However, the mobility or diffusion behavior of each atom is different due to its various properties, such as the interstitial elements diffusing much faster than the substitute elements. This will also limit the behavior of GB segregation.

Many quantitative analyses on GB segregation have been carried out by the indirect method of measuring its effect on the GB energy and deducing the level of segregation from the Gibbs adsorption isotherm. Hondros made some reasonable approximations in a dilute binary system [41]. The level of GB segregation was induced by the mathematical formula and can be obtained with the help of GB energy, the fraction of bulk addition and the ambient temperature. With the AES technology developed [42-44], the segregation of GB can be directly measured. The fracture surface analysis areas will be imaged using the focused electron beam in the ultra-high vacuum. Then the auger electron maps of each element with a spatial resolution will be identified so that the quantitative analysis of the segregation levels can be made. The AES and grain boundary energy approaches have been studied in many alloying elements to determine the grain boundary enrichment ratio, representing their GB segregation ability. Part of the relation is shown in Fig. 1. 5.

The linear relationship between grain boundary enrichment ratio and bulk solubility of alloying elements indicates that elements with low solubility can also have a high level of GB segregation, such as C and B. Comparing with the interstitial elements, substitute elements exhibited a lower ability of GB segregation, which might be due to the difference of the rate of volume diffusion.

Based on previous AES data, three typical concentration patterns by GB segregation are collected by Stein [46], which are shown in Fig. 1. 6. Considering the mechanism of AES, the signal will remain constant until the observed impurities disappear when there is a precipitate, as shown in the Fig. 1. 6 (a). On the other hand, the GB segregation also exhibited a gradient concentration pattern, which can be distinguished to two basic types of segregation: the equilibrium and the non-equilibrium. As mentioned before, the GB segregation lowers the whole system`s Gibbs free energy. The difference will be asymptotically approached in the equilibrium segregation with each other or the bulk. The system reaches homogeneous without time dependence, and the segregation only be experimentally observed in a few atom layers [47], as shown in the Fig. 1. 6 (b). The non-equilibrium segregation consistently exhibits the inhomogeneous system and depends on the diffusion processes and kinetic events, which involves the binding of solute atoms to vacancies and the diffusion of vacancies to GB. It is a continuous time-course process that needs to be

described by the variables such as the time rates of the change of temperature and pressure, as shown in the Fig. 1. 6 (c).

1. 3. 4 Methods of quantitative evaluation of grain boundary segregation

The influence on the k_y by solute atoms can be considered due to the GB segregation. To give a quantitative relationship between the k_y and GB segregation, it is necessary to evaluate the concentration of GB segregation when adding solute atoms. The most used thermodynamic model is the McLean model [29]. This approach is based on an equal Gibbs energy of the components in equilibrium. With the assumption that the interface represents the GB, a free surface with a segregation site for atoms, the thermodynamic state functions can be summarized by Eq. (3).

$$\frac{X_{gb}}{X^*_{gb}-X_{gb}} = \frac{X_0}{1-X_0}\exp\left(\frac{G}{RT}\right) \tag{3}$$

Where the X_{gb}, X^*_{gb}, X_0, G and R are the concentrations of solute atoms at the GB, the fraction of available sites to all segregation sites in the GB layer, the bulk concentration of solute atoms, free energy of segregation, and gas constant, respectively. In this model, the fraction of available sites to all segregation sites in the GB layer is considered as 1, which means all the sites at the GB can be segregated for foreign atoms. With this assumption, Eq. (3) can thus be expressed as Eq. (4), as follows:

$$\frac{X_{gb}}{1-X_{gb}} = \frac{X_0}{1-X_0}\exp\left(\frac{G}{RT}\right). \tag{4}$$

The concentration of the atoms segregated at the GB can be evaluated using this equation when the free energy of segregation, G, is known. However, it is difficult to determine the exact values of G because of the variety of the reported values depending on the measurement conditions. Besides, the assumption that all segregation sites are available at the GB can hardly achieve. This might give the calculation results some error.

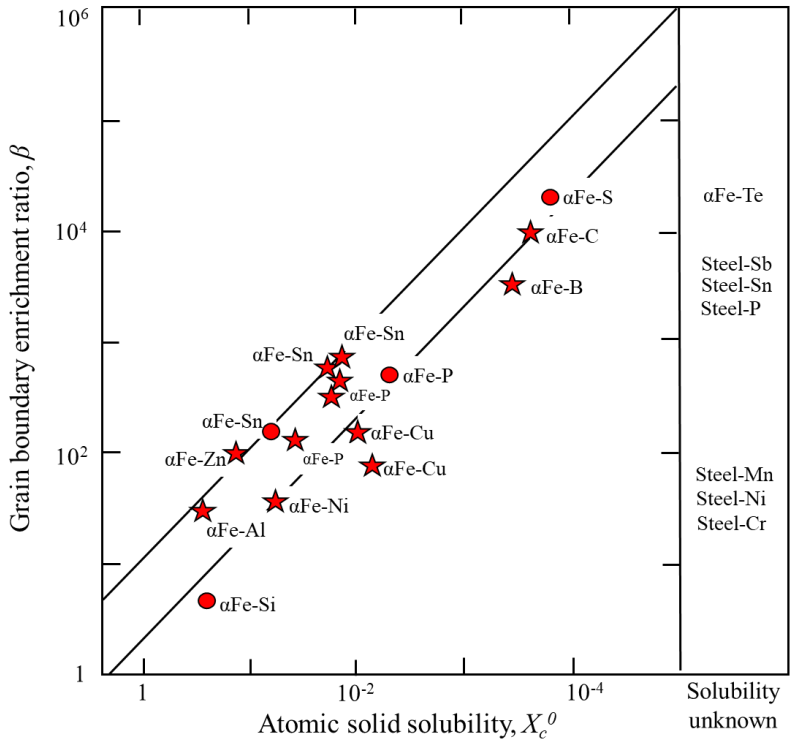

Fig. 1. 5 The relationship between grain boundary enrichment ratio and bulk solubility of alloying elements by Seah and Hondros [45].

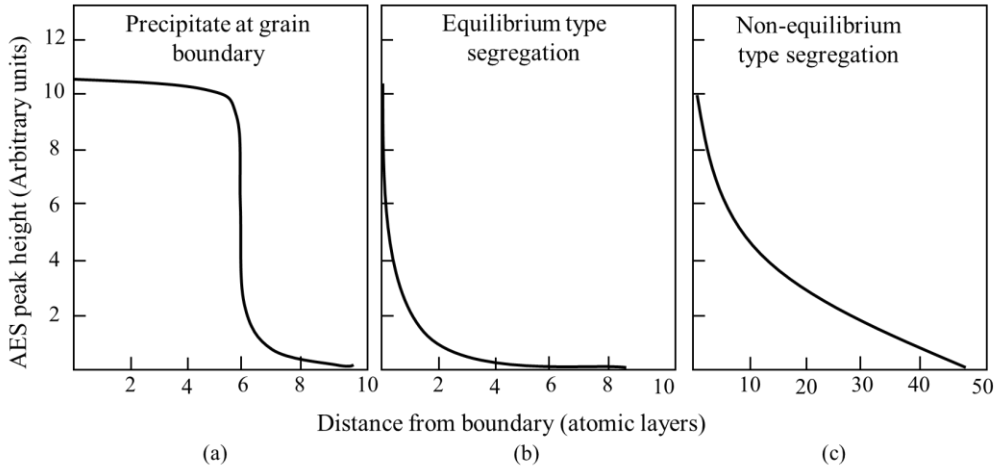

Fig. 1. 6 Typical concentration patterns by grain boundary segregation.

1. 3. 5 Relationship between Hall-Petch coefficient and grain boundary segregation in Fe-C binary alloys

Considering the relation between the τ_{cr} and the concentration of GB segregation, it can be inferred that the situation of C atoms and N atoms at the GB is different. Because the k_y seems more sensitive to the adding C content in Fe-C alloys, C atoms are supposed to have a strong tendency to segregate at the GB.

To quantify the relation between the concentration of GB segregation with the k_y, the McLean model was used to calculate the friction of GB segregation to approximate the real value [25]. As a result, the concentration of C segregated at GB exhibits a linear relation with the k_y, shown in Fig. 1. 7. Although there is an error in the calculation, this result still develops a new direction for analyzing the relationship between GB segregation and the k_y.

1. 3. 6 Hall-Petch coefficients in Fe-M (M=Si, Mn, Al, Ni, Cr) binary alloys

The interstitial elements represented by C and N have already been studied so far, and they have been proved to positively influence the k_y. Substitute elements are also commonly used in the steel manufacturing industry. Since the diameter and electronegativity of substitute elements are different from interstitial elements, several substitute elements were chosen to determine the influence on k_y.

Fig. 1. 8 shows the tensile test results of Fe-M (M=Si, Mn, Al, Ni, Cr) binary alloys [27, 28, 48]. Since the critical grain boundary shear stress is relevant to stopping dislocations, substitute atoms with more considerable volume should significantly affect the k_y. However, the k_y of these substitute elements added in IF steels show various tendencies with each other. Although Si, Mn and Ni showed a positive effect, Al and Cr nearly exhibited no effect on the k_y.

The concentration of substitute elements segregated at the GB was calculated utilizing the McLean model. Fig. 1. 9 shows the results of the influence of substitute elements segregated at the GB on critical grain boundary shear stress. Although the Y-axis differs from Fig. 1. 8, the critical grain boundary shear stress is the same as the k_y to some extent. The X-axis of Fig. 1. 9 represents the excess part of the substitute elements at the GB and in the grain, which means an

extra concentration of atoms segregated at the GB. Like the interstitial elements, the substitute elements segregated at the GB also perform a linear relationship with the k_y. It illuminates that the k_y can possibly be predicted by the concentration of GB segregation.

1. 4 Other influence factors on grain boundary segregation

1. 4. 1 Influence of annealing temperature on the Hall-Petch coefficient

The addition of C and N will enlarge the k_y due to the increase of C and N concentration segregated at GB. However, there is another way to achieve a similar rise in GB segregation. Based on the McLean model adopted in the previous study, reducing the annealing temperature will also cause an increase in the concentration of GB segregation. To figure out the influence of the annealing temperature on the k_y, Fe-C and Fe-N alloys under low temperature aging at different times was carried out [49]. The aging temperature is 373K, at which the Fe atoms can hardly diffuse, but the C atoms and N atoms can move free. The results are displayed in Fig. 1. 10.

The increase of the k_y was enhanced along with the increase of annealing time. To find out the exact reason for this enlargement of the k_y. The 3DAP was applied to observe the distribution of C and N atoms at the GB. The observation results are shown in Fig. 1. 11. The interfacial excess atoms of C and N in the base alloys without and with 6ks' aging was compared. The left side of this graphic indicates that C in Fe-C alloys slightly increased by the aging and tiny N mixed in the alloys. On the other hand, the right side of the graphic exhibit that N in Fe-N alloys sharply increased by the aging though some C mixed in the alloy and they kept almost no change. Since the concentration of C and N segregated at the GB by aging treatment also leads to the increase of the k_y, the relation between each atom and the k_y has been summarized in Fig. 1. 12. It is supposed that the interfacial excess of C and N atoms also have a linear relationship with the k_y, which is coincident to the theoretical explanation of pile-up model.

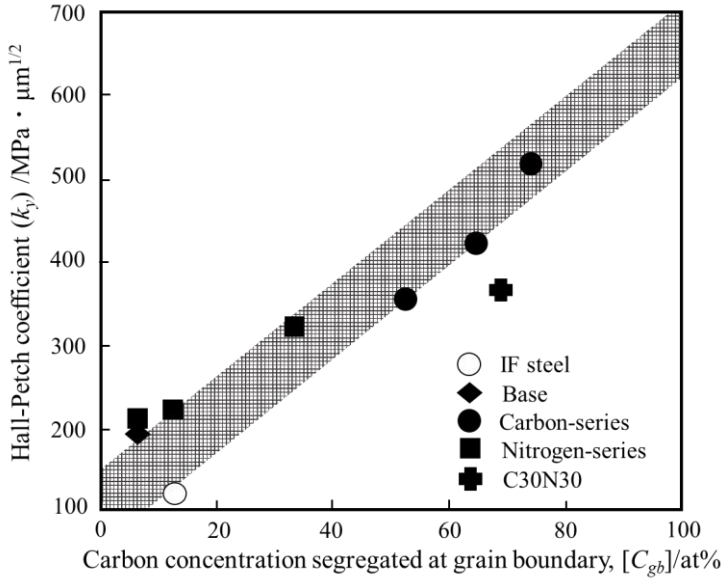

Fig. 1. 7 The relationship between the grain boundary concentration of Carbon segregated at GB and Hall-Petch coefficient (k_y).

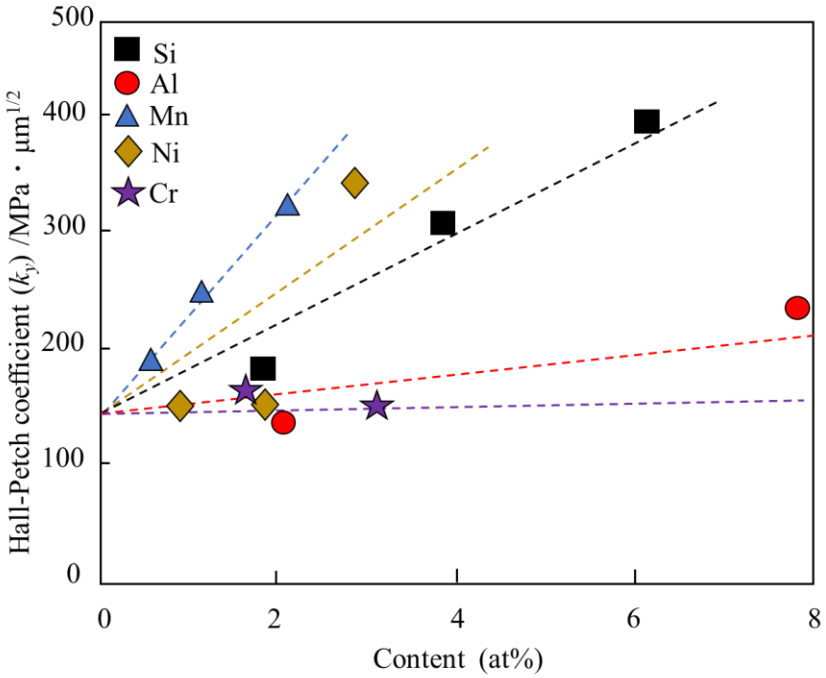

Fig. 1. 8 The relationship between the content of alloy elements addition and Hall-Petch coefficient (k_y).

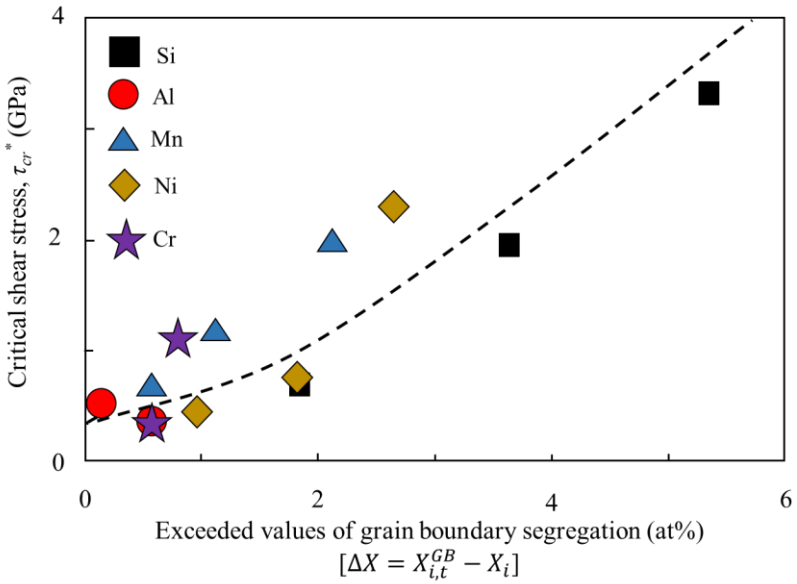

Fig. 1. 9 The relationship between the exceeded values of grain boundary segregation and Hall-Petch coefficient (k_y).

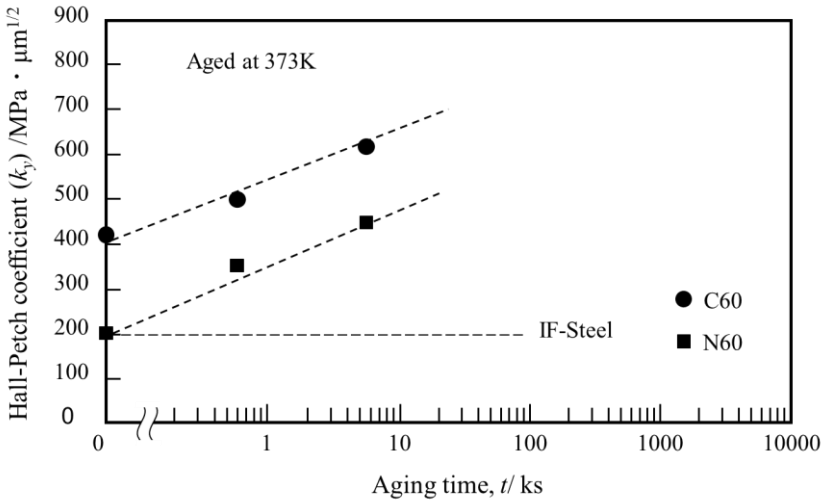

Fig. 1. 10 The relationship between aging time and Hall-Petch coefficient (k_y) in Fe-C and Fe-N binary alloys.

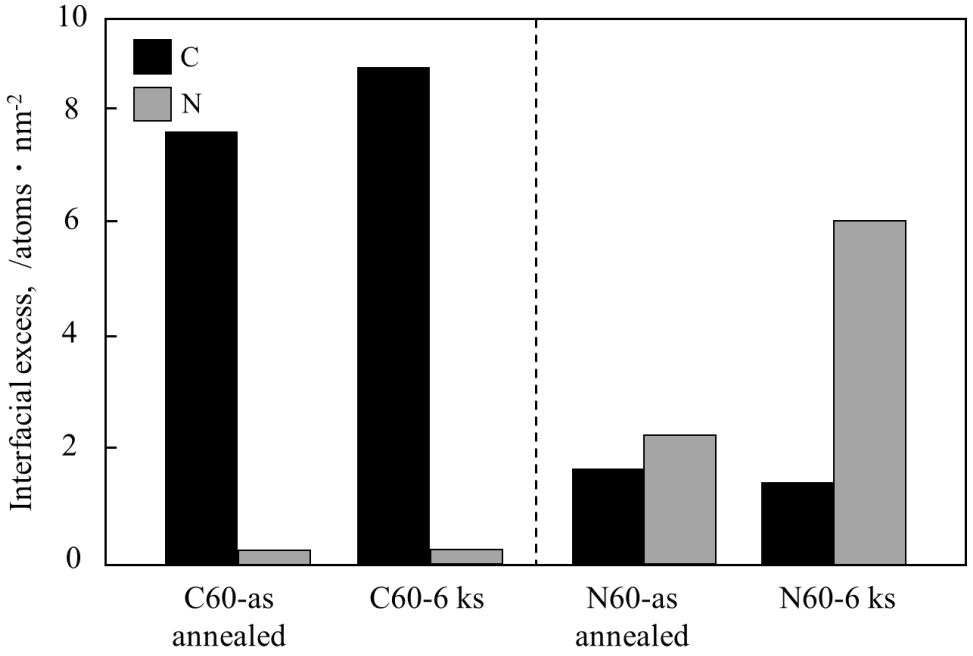

Fig. 1. 11 Interfacial excess atoms of 3DAP in Fe-C and Fe-N alloys before and after aging.

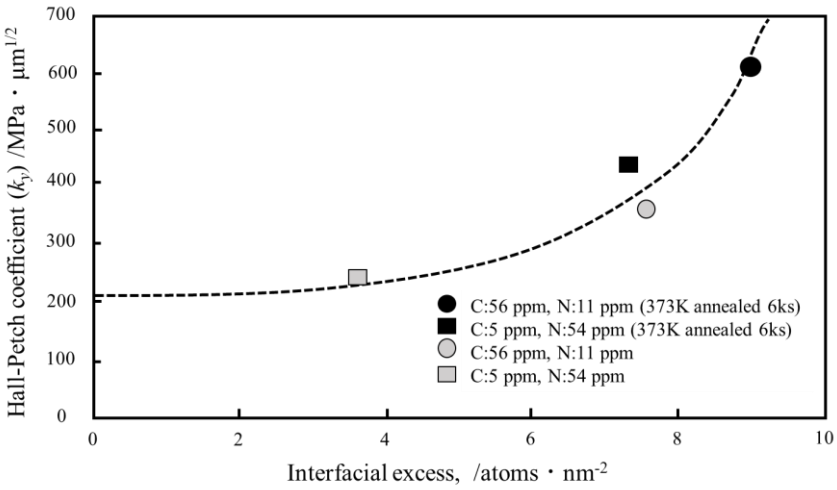

Fig. 1. 12 The relationship between interfacial excess and Hall-Petch coefficient in Fe-C and Fe-N alloys with and without aging.

1. 4. 2 Influence of the interaction between atoms on Hall-Petch coefficient in Fe-C-M ternary alloys

Since the Fe-M binary systems had been investigated, the enlargement of the k_y is due to the concentration of alloying elements segregated at GB. The GB segregation can be explained by the interaction between one kind of foreign atom with Fe atoms at GB. In the metal industry, complex alloy elements will be added to gain desirable properties, and it is not enough only considering GB segregation a binary system. Because C is a dominant element controlling the k_y, it is necessary to determine the influence of C with other elements` multi-addition on the k_y.

Since some of the alloying elements show a strong tendency with C to form the carbide, like Mn and Cr, there might be an attraction effect between C and those elements in specific circumstances. Nishizawa summarized the interaction between C and some alloying elements in austenite and ferrite steels by thermodynamic analysis [50]. Based on other researchers` literature [51, 52], a diagram was made to show the interaction parameter between each element and C, as shown in Fig. 1. 13. The positive values of the interaction parameter represent a repulsive and the negative ones represent an attractive interaction. Si has a repulsive interaction with C and Mn/Cr has an attractive interaction with C, coinciding with their ability to form carbide. On the other hand, the level of GB segregation of C might change under the effect of this interaction.

Rugy et al. [53] investigated the Fe-Si and Fe-Si-C steels by AES and low energy electron diffraction (LEED). They concluded that the segregation enthalpy of Si was lower than interstitial elements like C, N, S, P in binary systems, which made Si have a lower tendency to segregate at GB. However, there was a strong site competition between Si and C in Fe-Si-C systems, which reduced the level of Si`s GB segregation. These experimental results were verified using thermodynamic calculations by Souni [54] later.

Funakawa et al. [55] investigated the tensile properties of Fe-C-Cr ternary alloys with different content of chromium addition in extra low carbon steels. They found that the k_y decreased with Cr addition increased, which is different from the result in Fe-Cr binary steels [28]. The reason has been concluded that the concentration of C segregated at GB reduced by the chromium carbide precipitation.

These results found in Fe-C-M ternary systems indicates that although substitute elements exist, C still effectively influences the k_y by GB segregation. Furthermore, substitute elements have a much slower speed in diffusion than interstitial elements, which might result in a non-equilibrium situation.

Considering the slow diffusion rate of chromium as a substitute element, the concentration of Cr segregated at the GB might not be sufficient to interact with C. Nakada et al. [26] studied a Fe-C-P ternary system to figure out the change of the k_y in IF steel and ultralow carbon steel. They found that the k_y in Fe-P steels almost had no change with adding P. While the k_y decreased in Fe-C-P steel, resulting from the reduction of C segregation at GB by the addition of P. These results infer that the C concentration of segregation at GB is a critical factor for the change of the k_y.

1. 5 Research objectives

This research is focused on clarifying the relationship between the Hall-Petch coefficient (k_y) and the concentration of grain boundary (GB) segregation in Fe-C and Fe-N steels. Comparing the traditional evaluation method, the McLean model, a more accurate and simple method, the Hillert-Ohtani model was introduced. Previous data was adopted to fix the error by the McLean model and gain a more precise relationship between the k_y and the concentration of GB segregation. In addition, an effort to obtain steels with higher k_y was attempted with this relationship. The feasibility of low temperature annealing, and the co-segregation effect will be discussed.

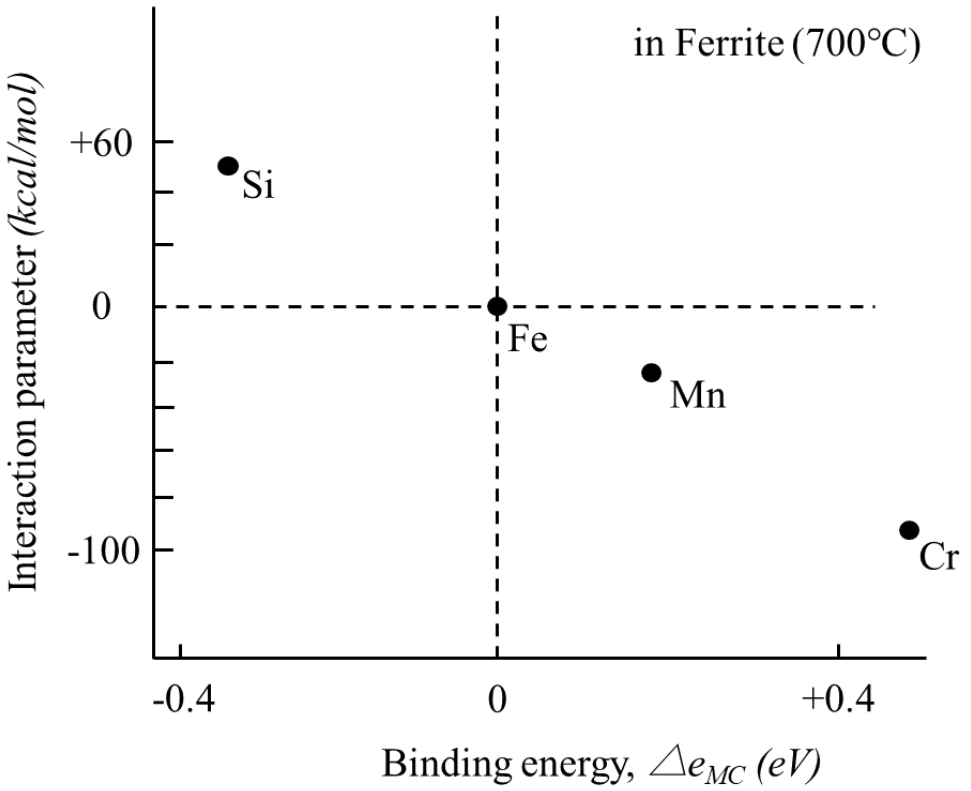

Fig. 1. 13 The interaction parameter between alloying elements and C in ferrite.

This paper is composed of five parts.

In Chapter 1, the background of this study was introduced.

In Chapter 2, the verification of thermodynamic models for predicting the GB segregation of C and N in ferritic steels will be developed. The concentrations of C and N segregated at the GBs in Fe-C, Fe-N binary alloys, and Fe-C-N ternary alloys were calculated using the McLean and the Hillert-Ohtani (HO) models. The calculated datum will be compared with experimental values obtained by three-dimensional atom probe tomography (3DAP). Then the prediction formula based on the relationship with the k_y, and the C concentration of GB segregation will be summarized.

In Chapter 3, tensile tests will be carried out in Fe-C alloys with different temperatures annealing to control the concentration of C segregated at GB through the change in the solubility of C in the ferritic matrix. The annealing temperature will affect the solubility of C in the ferritic matrix as well as the level of segregation at GB. The k_y of these annealed steels will be tested and compared with the predicted ones in Chapter 2, verifying the accuracy of the HO model in predicting the GB segregation under different temperature annealing. Besides, the relationship between the solubility and the GB segregation of C addition was figured out.

In Chapter 4, Si and Mn will be added in ultralow carbon steels to investigate the grain boundary segregation due to the interaction of C-Si and C-Mn. As a repulsive interaction with C, Si will be added to increase the concentration of C segregated at grain boundary. Besides, it will be shown that Mn has an attractive interaction with C, the addition of which is also expected to raise the grain boundary segregation of C. Furthermore, the relationship between the Si or Mn content and the k_y in co-addition ternary steels will be discussed.

In Chapter 5, the results of Chapter 2, Chapter 3 and Chapter 4 will be summarized.

Chapter 2 Prediction of Hall-Petch coefficient in ferritic steels with interstitial elements: Carbon and Nitrogen

2.1 Introduction

For the grain refinement strengthening in steel, it has been demonstrated that the yield strength of ferrite is significantly enhanced by the segregation of the carbon and nitrogen atoms at the grain boundary (GB), reflected by an increase in the slope of the Hall-Petch plot, which is called the Hall-Petch coefficient (k_y). Previous research has obtained the calculated results of the concentration of C segregated at GB in Fe-C ferritic steels by the McLean model and found a linear relationship between the concentration of C segregated at the GB and the k_y [25]. It strongly supports the prediction that the GB segregation will lead to an enlargement of the k_y.

The McLean model is simplified from the complex thermodynamic description with several assumptions [29]. Considering the actual situation of GB segregation, some assumptions may affect the accuracy of the calculated results. The McLean`s classical approach is based on a binary equilibrium system. In this system, A atoms solute in bulk, where has B solute positions; m atoms segregate at the GB with n segregation sites, as shown in Fig. 2. 1.

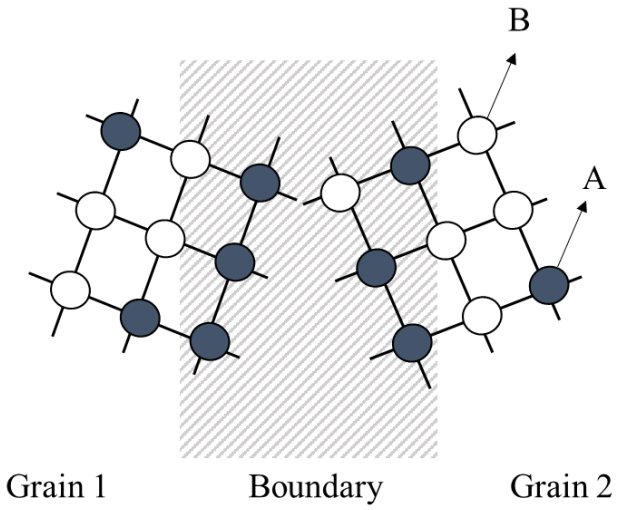

Fig. 2. 1 Sketch of the grain boundary segregation behavior by McLean approach

Then the internal energy U can be written [45],

$$U = mu_1 + AU_1 - kT[\ln n!\, B! - \ln(n-m)!\, m!\, (B-A)!\, A!] \quad (5)$$

where k, T, U_1 and u_1 are the Boltzman constant, temperature, and internal energy of atoms in bulk and at the GB, respectively. In Eq. (5), the term at the end of the right side is related to the configurational entropy of atoms in bulk and at the GB. The minimum of U can be obtained when the system reaches equilibrium. After mathematical simplification, the frequently used form of the McLean model is obtained in Eqs. (6)-(8),

$$\frac{X_{gb}}{1-X_{gb}} = \frac{X_0}{1-X_0} exp\left(-\frac{G}{RT}\right) , \tag{6}$$

$$X_0 = \frac{A}{B} , \tag{7}$$

$$X_{gb} = \frac{m}{n} . \tag{8}$$

In Eq. (6), the X_{gb}, X_0, G and R are the concentrations of solute atoms at the GB, the bulk concentration of solute atoms, the free energy of segregation, and the gas constant, respectively. Eqs. (7) and (8) explain the derivation of the X_0 and the X_{gb}, indicating that the results calculated by the McLean model represent the coverage of atoms located on a free surface. In Eq. (5), the difference between the internal energies, u_1-U_1, can be replaced by G, the Gibbs free energy of segregation. The concentration of GB segregation can be derived from Eq. (5) by Eq. (9).

$$X_{gb} = \frac{X_0 \cdot exp\left(-\frac{G}{RT}\right)}{1+X_0 \cdot exp\left(-\frac{G}{RT}\right)} . \tag{9}$$

In Eq. (9), the concentration of GB segregation can be easily obtained by the fraction of solute atoms, X_0, which approximates the concentration of addition atoms, and the Gibbs free energy of segregation, G.

Although using the G parameter can simplify the calculation largely, all entropy contributions are neglected except the configurational entropy, which determines the GB composition. In other words, the essence of GB segregation can hardly be reflected only by using the G parameter.

In addition, Eqs. (7) and (8) indicate that the GB segregation in the McLean model is represented by the coverage of atoms on a free surface, which means a ratio of the occupied segregation sites. Since the GB segregation depends on the diffusion of atoms, which occurs by the movement of atoms from one atomic site to another, it should be mentioned that the interstitial atoms have a different mechanism with the substitute atoms when diffusing in the Fe matrix. For substitute atoms, their diffusion occurs only if a vacancy is present due to the more significant volume than

interstitial atoms, which makes the diffusion process cost more energy and develop very slowly. For interstitial atoms, their diffusion is not on a lattice site but on an interstice. These diffusing atoms are free to move to any adjacent interstice unless those be already occupied. Therefore, the rate of diffusion is much faster than the substitute atoms.

On the other hand, the site location and saturation also affect the value of GB segregation. In the bcc-Fe lattice, interstitial atoms prefer to segregate into the octahedral sites than the tetrahedral sites, influencing the saturation of segregation. The saturation of site segregation is an indistinct concept with many explanations [56-59]. That affects the accuracy of the calculated value of GB segregation, which needs an explicit answer.

In the McLean model, the fraction of available sites to all segregation sites in GB is assumed to equal 1, which means that all the octahedral sites are saturated with segregated atoms in the lattice. However, considering the interaction of these adjacent atoms, such a saturated state is unlikely to be realized. In some cases, only a part of the sites can be available for GB segregation in saturation. Hondros and Seah [56] showed that the McLean model should be written as

$$\frac{X_{gb}}{X^*_{gb}-X_{gb}} = \frac{X_0}{1-X_0} exp\left(-\frac{G}{RT}\right) . \quad (10)$$

The X^*_{gb} is the fraction of available sites to all segregation sites in the GB layer. The saturation limits vary in different situations and should be considered. For example, the X^*_{gb} is found to vary between 0.38 and 0.65 in copper for antimony segregation and 0.27 for segregation of antimony in body-centered cubic iron [57, 58]. The exact X^*_{gb} in Fe-C alloys for C segregation needs to be ensured.

The previous three-dimensional atom probe tomography (3DAP) analysis showed that nitrogen atoms had a very little segregated level compared with carbon atoms when co-addition with carbon. Takahashi et al. [60] supposed that there was a site competition effect between C and N atoms when co-segregated at GB. Furthermore, the k_y in Fe-N steels showed the same enlargement as in Fe-C steels under low temperature annealing. It indicates that N has a similar ability to enlarge the k_y as C, but the short of GB segregation ability astricted the enlargement of k_y in Fe-N alloys. Araki [49] and Takahashi [60] used the McLean model in Fe-C-N ternary systems to quantify the relationship between the k_y and the concentration of GB segregation. The McLean

model was extended to the ternary equation without considering the more complex circumstance in ternary systems. That makes the calculated error bar become larger.

Disturbed by so many inaccurate factors, previous conclusions made by the McLean model need to be verified. In this chapter, A more accurate thermodynamic model was introduced. Based on previous data on Fe-C and Fe-N steels, the concentration of GB segregation was recalculated and the relationship between the k_y and GB segregation was discussed. In addition, the interaction of C and N when co-added was also investigated.

2.2 Methodology

2.2.1 The Hillert-Ohtani model

Considering the total Gibbs energy of the system, Hillert proposed a thermodynamic theory for estimating the concentration of segregated atoms at GB [30]. The theory states that the GB has a constant thickness and the atoms at the GB can be regarded as belonging to a separate phase, which makes the grain and the GB two different phases with different thermodynamic situations. The relation was illustrated by the molar Gibbs free energy diagram.

The equilibrium between the grain and GB phases can be illustrated in a molar diagram shown in Fig. 2. 2. The α-phase matrix is composed of A atoms. B atoms are added to the matrix leading to the GB segregation. All symbols quantity refers are given as a superscript to the right, such as the G^{gb}, G^{α} is the Gibbs free energy of GB and matrix. The $X^{\alpha}{}_{B}$, $X^{gb}{}_{B}$ is the concentration of B content in the matrix and at GB. The surface tension explains why the value of G^{gb} is higher than the G^{α} from the GB in the α-phase matrix. When the system reaches equilibrium, the total Gibbs free energy is expected to be minimum, which can be presented by Eq. (11).

$$d\left(G^{\alpha} + G^{gb}\right) = 0 \tag{11}$$

The Eq. (12) and Eq. (13) exhibit the change of Gibbs energy in this process of dN_A mol A atoms and dN_B mol B atoms moving from matrix to the GB. The $\mu^{gb}{}_{A}$, $\mu^{gb}{}_{B}$, $\mu^{\alpha}{}_{A}$, $\mu^{\alpha}{}_{B}$ represent the chemical potential of A, B atoms in GB and in bulk, respectively.

$$\left(\mu_A^{gb} \cdot dN_A - \mu_A^{\alpha} \cdot dN_A\right) + \left(\mu_B^{gb} \cdot dN_B - \mu_B^{\alpha} \cdot dN_B\right) = 0 \tag{12}$$

$$\left(\mu_A^{gb} - \mu_A^{\alpha}\right) \cdot dN_A + \left(\mu_B^{gb} - \mu_B^{\alpha}\right) \cdot dN_B = 0 \tag{13}$$

In general, dN_A and dN_B can be any random values when the system reaches equilibrium, then the solution for Eq. (13) is easily obtained by Eqs. (14) and (15).

$$\mu_A^{gb} - \mu_A^{\alpha} = 0 \tag{14}$$

$$\mu_B^{gb} - \mu_B^{\alpha} = 0 \tag{15}$$

However, since the GB has been seen as a separate phase with a constant thickness, Eqs. (14) and (15) are not suitable as the solution. Hillert`s theory has an assumption that the number of atoms at the GB is constant, which makes the equation can be soluted under the condition:

$$dN_A + dN_B = 0 \ . \tag{16}$$

With the help of this condition, Eq. (17) can be obtained, as follows:

$$\mu_A^{gb} - \mu_A^{\alpha} = \mu_B^{gb} - \mu_B^{\alpha} \ . \tag{17}$$

It is sufficient to require that the Gibbs free energy should not change when an A atom moves from the GB to the matrix and a B atom moves to the opposite direction at the same time. The equilibrium condition is thus,

$$\frac{dG^{gb}}{dX_B^{gb}} = \frac{dG^{\alpha}}{dX_B^{\alpha}} \tag{18}$$

The equilibrium concentration in the GB is thus found by a parallel-tangent construction based on the composition of the matrix.

The concentration of B in the GB segregation, $X^{gb}{}_B$, can be calculated by the content of the additional element, $X^{\alpha}{}_B$. Besides, the Gibbs energy under specific temperatures is also needed. However, since the thermodynamic information of the GB is insufficiently known, it is difficult to obtain the available values of G^{gb}. It is still hard to figure out $X^{gb}{}_B$ only by the Hillert model.

To deal with this problem, Ohtani et al. [61] assumed and proved that the G^{gb} would be thermodynamically equivalent to the Gibbs free energy of the liquid phase, G^{liq}. Ohtani used thermodynamic calculation to express the formula of the Gibbs energy of the GB. To gain the exact solution of these equations, the thermodynamic parameters of the liquid phase are substituted for those of the GB. Then these calculated results were compared with the experimental and showed a good agreement.

Under this approximation, Eq. (18) can be rewritten as Eq. (19) as follows:

$$\frac{dG^{liq}}{dX_B^{gb}} = \frac{dG^{\alpha}}{dX_B^{\alpha}} \ . \tag{19}$$

This formula is combined with Hillert`s theory and Ohtani`s assumption. Thus, we named this the Hiller-Ohtani (HO) model. Compared with the McLean model, the HO model is irrelevant to the number of substitute sites at the GB, which seems more accurate in the calculation. The equilibrium solute concentrations in both the matrix and GB phase can be evaluated by the HO model from the contact values by drawing the parallel tangent (or parallel contact surface) of the free energy curves (or curved surfaces) obtained by Thermo-calc.

Based on the previous research, the HO model will be verified by the experimental data from 3DAP. The calculation was performed under the following conditions: temperature = 973 K, number of moles = 1 mol, and atmospheric pressure = 101325 Pa. The TCFE12 database was used in this study.

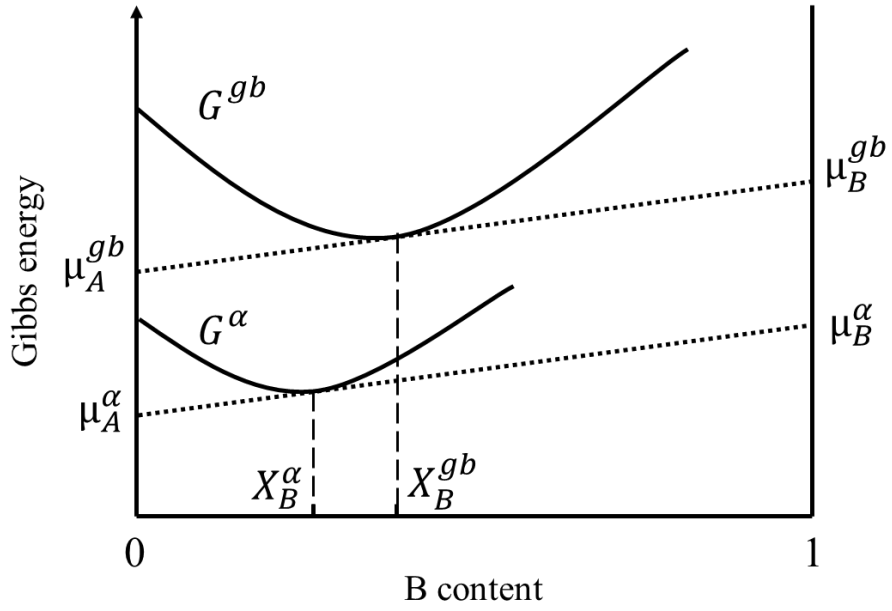

Fig. 2. 2 The evaluation of the segregation from a ferritic matrix to a grain boundary.

2.2.2 Experimental and calculated data from previous research

The calculations were applied to the steels used in Takeda's previous work [25]. The chemical compositions of the steels are listed in Table 2. 1.

Specimen	Carbon addition (mass ppm)	Nitrogen addition (mass ppm)	Hall-Petch coefficient (k_y) (MPa·μm$^{1/2}$)	GB Segregated Carbon (at%) (By the McLean model)
IF-steel	0 (4)	0 (10)	114	0
Base	5	9	188	26.19
N30	11	24	220	43.84
N60	5	54	212	26.19
C30	28	11	358	66.52
C30N60	35	26	360	71.29
C60	56	11	516	79.89

Table. 2. 1 The experimental data and the calculation results of the specimens.
(Numbers in brackets represent Carbon and Nitrogen addition without Ti fixed).

All the specimens were annealed at 973 K in a ferrite single-phase region, followed by water quenching. For the calculation of the McLean model, the Gibbs energies of segregation for carbon and nitrogen were quoted from Grabke's report as 78 kJ/mol and 58 kJ/mol, respectively [62]. The concentration of C segregated at GB will be restricted by various X^*_{gb} for comparison.

2.2.3 Assumption on the number of atoms at the GB

Since the 3DAP only shows the number of solute atoms per unit area, the interfacial excess at the GB (atoms/1 nm^2) cannot be directly compared with the calculated results expressed as the atomic fraction. Therefore, the interfacial excess must be converted to the concentration of atoms segregated at the GB expressed with atomic fraction. Then we attempted a rough estimation as follows. In the case of Fe-C and Fe-N, a 1 nm^2 area has approximately 16 (4 × 4) atoms of Fe (diameter: 0.25 nm). In this study, the GB was considered as a two-atom-thick layer (0.5 nm thick), as Fig. 2. 3 shows.

Based on this situation, the GB layer had 32 (16 × 2) Fe atoms. In addition, it is assumed that the segregated C and N atoms occupy the octahedral sites even in the GB layer, one Fe atom possesses three octahedral sites, and thus, there are 96 (32 × 3) interstitial sites per 1 nm^2 of GB area. If all the sites were available for segregation, the value of X^*_{gb} could be regarded as 1. The concentration of C or N segregated at the GB can be calculated by dividing the number of segregated atoms (interfacial excess) by the number of interstitial sites in the GB layer.

2.2.4 Simulation of the interaction between carbon and nitrogen at the grain boundary

Considering the different tendencies of the k_y shown in Fig. 1. 3 [25], the k_y might not be influenced simply by the addition of alloying elements. Due to the impurities mixed in those specimens, the behavior is possibly changed by the interaction between C and N. Based on the conclusion by Ohnuma et al. [63], the HO model can be maximum expanded to a five-element system, which can be written as:

$$\mu_A^{gb} - \mu_A^{\alpha} = \mu_B^{gb} - \mu_B^{\alpha} = \mu_C^{gb} - \mu_C^{\alpha} = \cdots \ . \tag{20}$$

To identify the interaction between C and N when they are co-segregated at the GB, the calculation in Fe-C-N ternary steels was carried out by the HO model. With the point of GB segregation, the small increment of the k_y in Fe-N steels need to be discussed. Two series of steels are considered. Fe-N steels with different amounts of C added and Fe-C steels with N added were investigated. The change of the calculated GB segregation before and after the addition of impurity was summarized to explain the C-N interaction.

2.3 Results and analysis

2.3.1 Verification of two thermodynamic models

Fig. 2. 4 (a) and Fig. 2. 4 (b) display the estimated concentrations of C and N segregated at the GB, obtained by the McLean model with different values of X^*_{gb}. When X^*_{gb} is 1, the calculated result shows that approximately 90% of the GB was filled with C, which is a very unlikely situation. The amount of segregated C varies from approximately 90% to 10% when X^*_{gb} is changed from 1 to 0.1. The calculated data for N also decreased with a reduction in X^*_{gb}, although

the amount of segregated N is much smaller than that of C. This observation indicates that a suitable X^*_{gb} is essential for obtaining an accurate prediction using the McLean model.

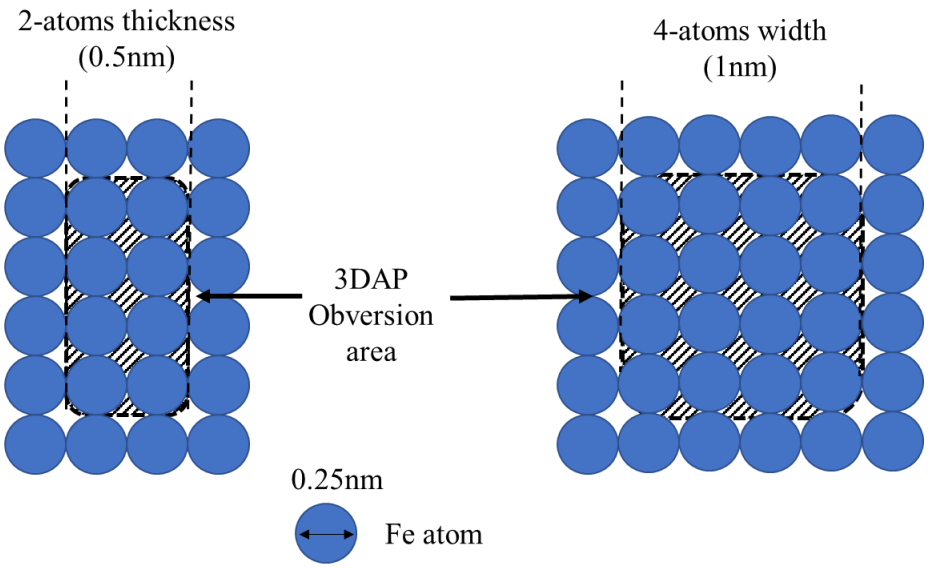

Fig. 2. 3 Sketch map of the grain boundary structure.

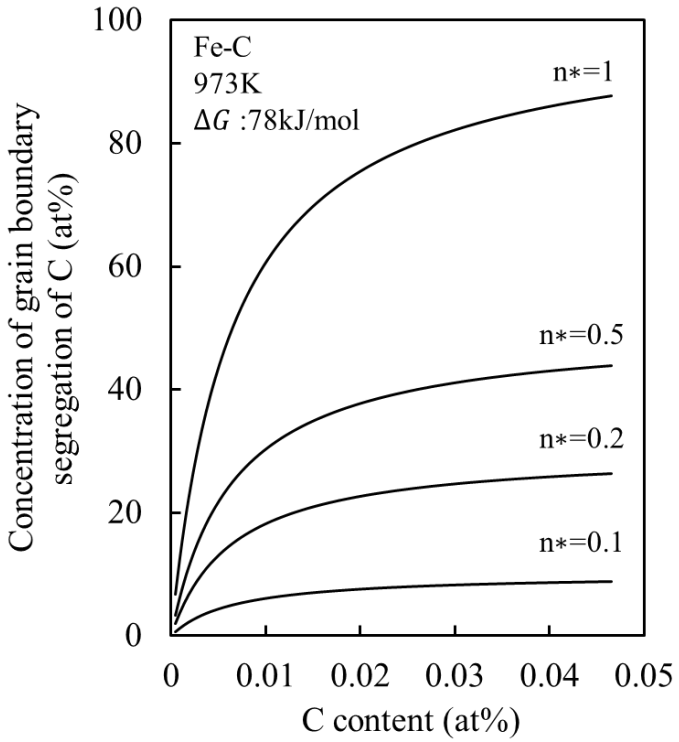

(a) C in Fe-C

Fig. 2. 4 Concentrations of C (a) and N (b) segregated at GB calculated with the McLean model using the different n*.

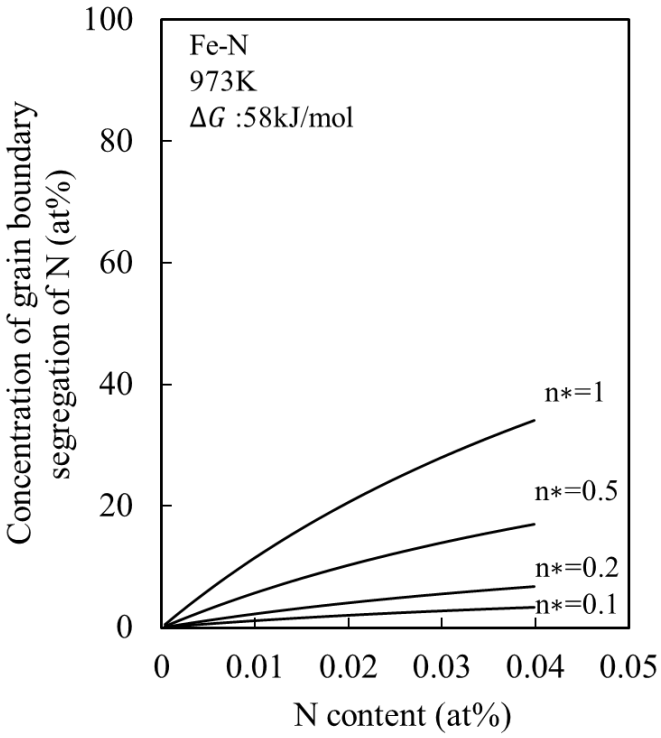

(b) N in Fe-N

Fig. 2. 4 Concentrations of C (a) and N (b) segregated at GB calculated with the McLean model using the different n^*.

In Figs. 2. 5 (a) and 2. 5 (b), the bold red lines show the concentrations of C and N segregated at GB that were calculated using the HO model. The values estimated by the McLean model, as shown in Figs. 2. 4 (a) and 2. 4 (b), are also presented with the broken lines for comparison.

In addition, the experimental results of 3DAP for C60 and N60 are plotted with quadrilateral marks. It was found that the results of the HO model were close to the experimental results for both the Fe-C and Fe-N alloys. Thus, it was inferred that the HO model was nearly reliable in predicting the concentration of atoms segregated at the GB. The McLean model was also consistent with the experimental results when X_{gb}^{*} was approximately 0.1, which means that the segregated C and N would be saturated when approximately one-tenth of all the interstitial sites were filled in the GB.

2.3.2 Concentrations of C and N segregated at GB in Fe-C-N ternary alloys under C-N interaction

The HO model has been proved to show higher accuracy than the McLean model in predicting the concentration of the GB segregation in Fe-C and Fe-N binary systems. In the case of Fe-C-N ternary alloys, the interaction between the C and N atoms is also anticipated by the HO model, which might change the segregation behavior of both elements.

Fig. 2. 6 (a) shows the changes in the concentration of C segregated at GB as a function of the C content with the addition of N at 0 at%, 0.005 at% and 0.01 at%. Fig. 2. 6 (b) shows the concentration of N segregated at GB as a function of the N content with the addition of C at 0 at%, 0.005 at% and 0.01 at%. These calculations were performed using the HO model. Fig. 2. 6 (a) indicates that there is little change in the value of segregated C, even when N was coexistent in steel. On the other hand, Fig. 2. 6 (b) shows that the amount of segregated N declined drastically with an increase in the coexisting C. Only 0.005 at% C caused a 70% decrease in the value of segregated N.

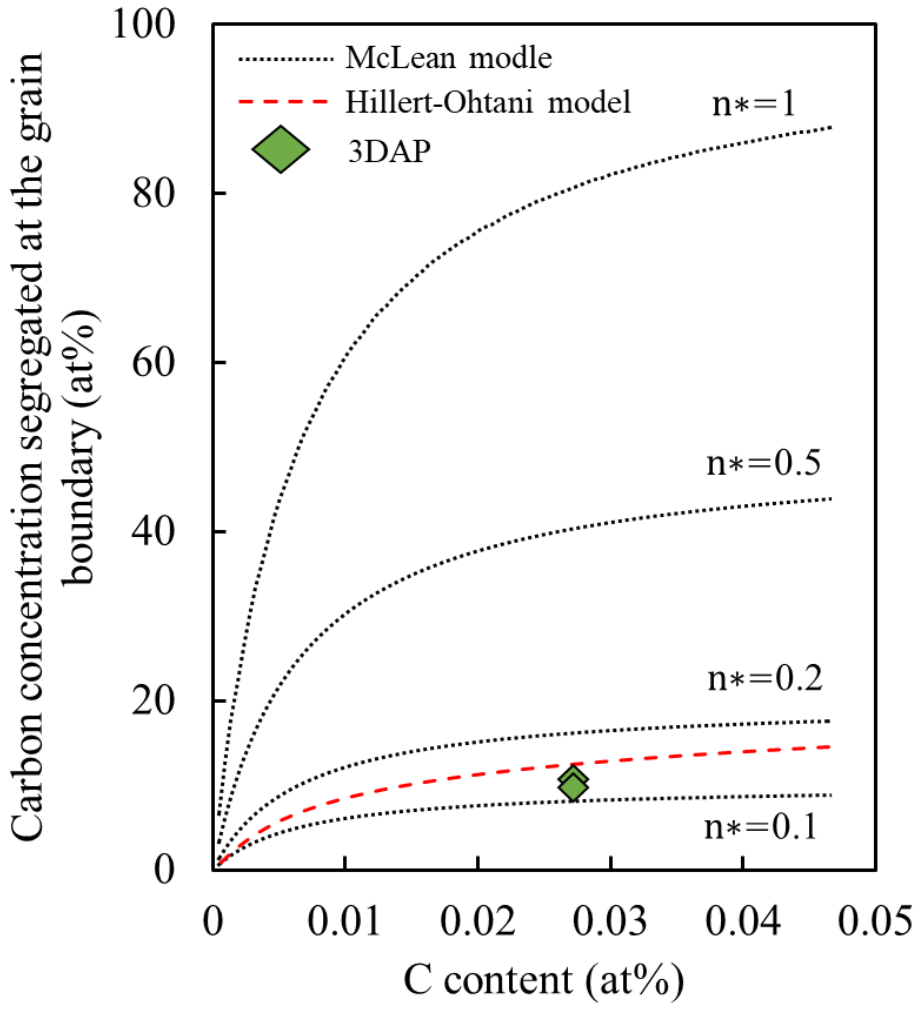

(a) C in Fe-C

Fig. 2. 5 Concentrations of (a) C and (b) N segregated at the grain boundary calculated with the Hillert-Ohtani model and experimental values obtained by 3DAP.

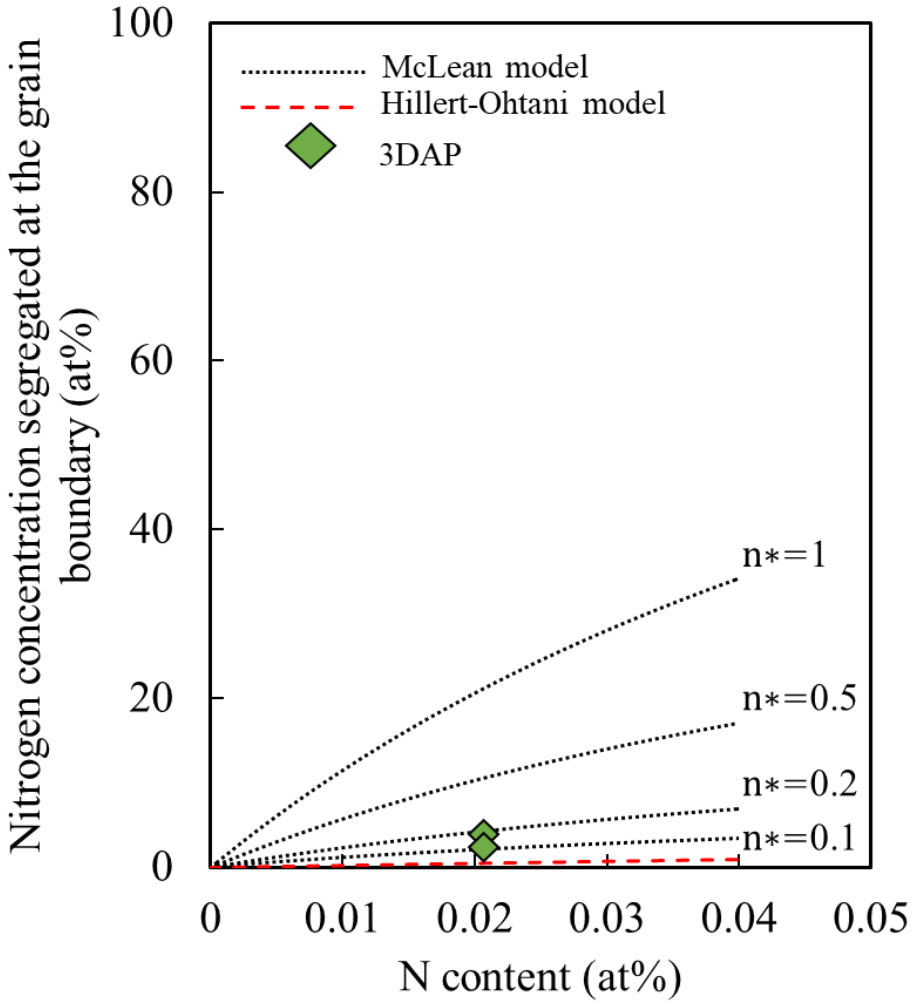

(b) N in Fe-N

Fig. 2. 5 Concentrations of (a) C and (b) N segregated at the grain boundary calculated with the Hillert-Ohtani model and experimental values obtained by 3DAP.

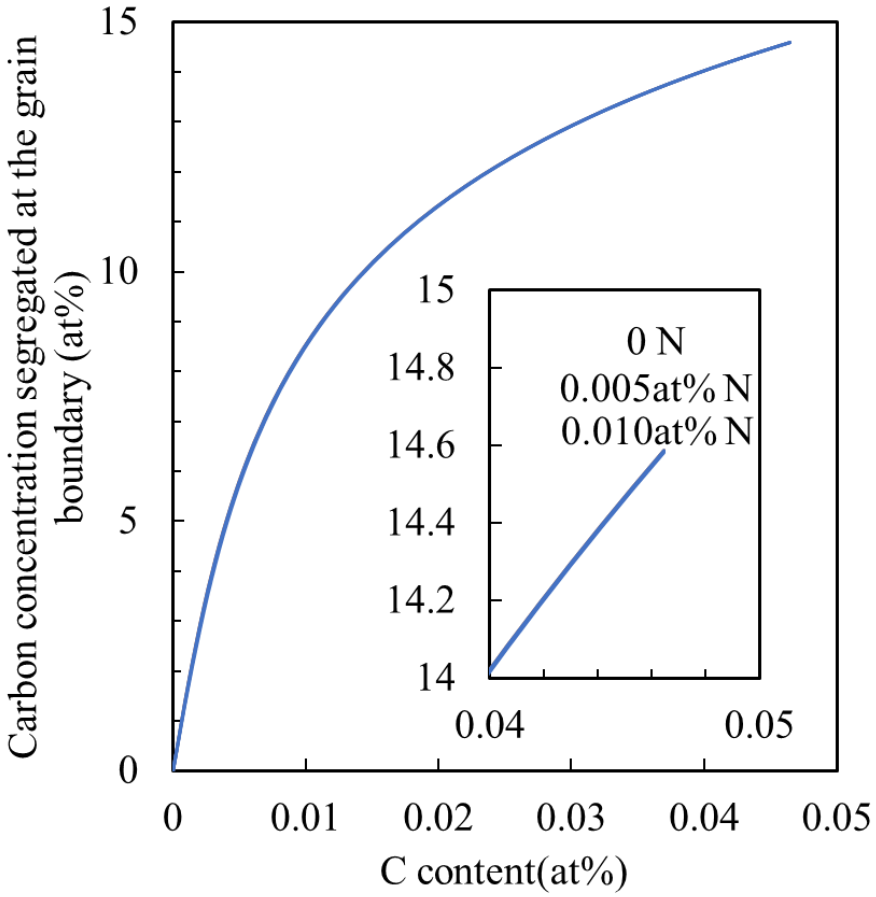

(a) C in Fe-C-N

Fig. 2. 6 Concentrations of (a) C and (b) N segregated at the grain boundary in Fe-C-N ternary alloys, calculated by the Hillert-Ohtani model.

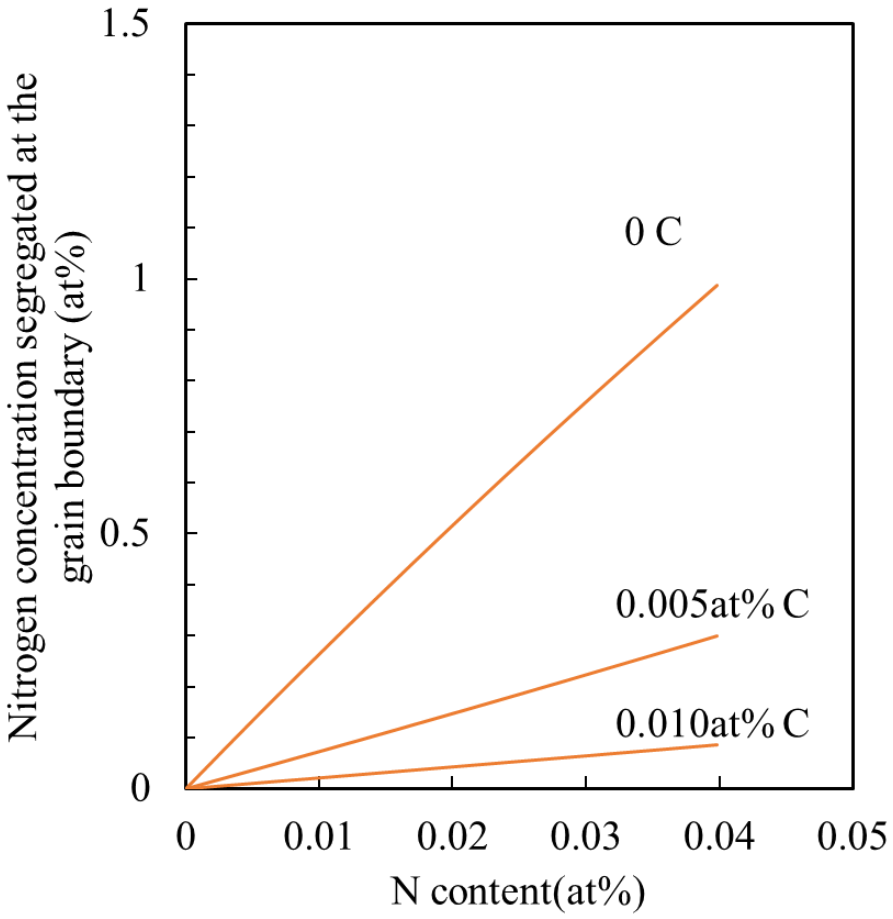

(b) N in Fe-C-N

Fig. 2. 6 Concentrations of (a) C and (b) N segregated at the grain boundary in Fe-C-N ternary alloys, calculated by the Hillert-Ohtani model.

The results suggest that the tendency of C atoms to segregate at the GB is much stronger than that of N, and thus, the segregation behavior of C was less affected by N atoms. In contrast, N segregation was significantly hindered by C. There might have been a similar site competition between C and N like C and P [26], which makes N atoms repulsed by C atoms under co-addition. That interaction can explain the abnormal change of the k_y in Fe-N steels, shown in Fig. 1. 3. Fe-N steels were mixed with C impurity, which formed a Fe-C-N ternary system. The k_y of Fe-N steels became dominant by the C impurity not the segregated N because of the reduction of the concentration of N segregated at the GB.

2.3.3 Relationship between grain boundary segregation and Hall-Petch coefficient

Since the HO model can provide a more reasonable prediction of the equilibrium C and N concentrations segregated at the GB than the McLean model, the relationship between grain boundary segregation and the k_y was reconsidered. The concentration of C and N segregated at GB in Fe-C-N alloys was calculated by the HO model, and the reported Hall-Petch coefficients (k_y) were plotted as a function of the calculated C and N concentrations in Fig. 2. 7 (a).

It can be seen that the value of segregated (C+N) at GB exhibits a linear relationship with the k_y. The C60 (56 ppm C, 11 ppm N) steel exhibited the maximum amount of segregation of 12.6 at% C, which resulted in an enlargement of k_y to approximately $500 MPa \cdot \mu m^{1/2}$. In comparison, IF steel with no segregation had a very low k_y of approximately 100 $MPa \cdot \mu m^{1/2}$. That means the GB segregation indeed leads to the enlargement of the k_y.

Considering the much stronger segregation tendency of C, the effect of N on the Fe-C-N ternary alloys should be very small. To prove this hypothesis, the k_y values were again plotted as a function of C, ignoring N, as shown in Fig. 2. 7 (b). Comparison of Figs. 2. 7 (a) and (b) reveals that the effect of N on k_y is negligibly small. Therefore, it can be inferred that the enlarged k_y mainly resulted from the segregated C in the Fe-C-N alloy because of the much stronger tendency of C to segregate at the GB compared to N. However, this does not mean that the segregated N atoms had no effect on k_y. As previously demonstrated, the enhanced N segregation by low-temperature aging at 373 K indicates that the k_y of ferritic steel increases with increasing

concentration of N segregated at the GB [49].

In conclusion, the k_y in Fe-C-N ternary alloys is mainly dominated by the concentration of C segregated at GB. To quantify the relationship between the concentration of C segregated at the GB, C_{seg}, and the k_y, previous results have been summarized and presented by Eq. (21), as shown in Fig. 2. 8.

$$k_y(C) = 28.8 \cdot X_{C-seg} + 95.03 \quad (21)$$

Data from other researchers were added [64, 65], which coincident well with Eq. (21). This result strongly supports the suspicion that the k_y will be enlarged along with the increase of GB segregation in ferritic steels.

As a result, it can be concluded that by using thermodynamic calculations with the HO model, the k_y of ferritic steels can be roughly predicted from their chemical composition and the heat treatment temperature. In addition to the above discussion, the effect of substitutional elements, such as Mn or Si, on the amounts of segregated C and N should also be considered because these elements interact with the interstitials and alter the equilibrium concentrations at GB. Therefore, the macroscopic mechanical properties of steels might be influenced by Mn and Si through not only simple solid solution strengthening but also the changing of the Hall-Petch coefficient. This is the next step towards deeply understanding the mechanism of grain refinement strengthening.

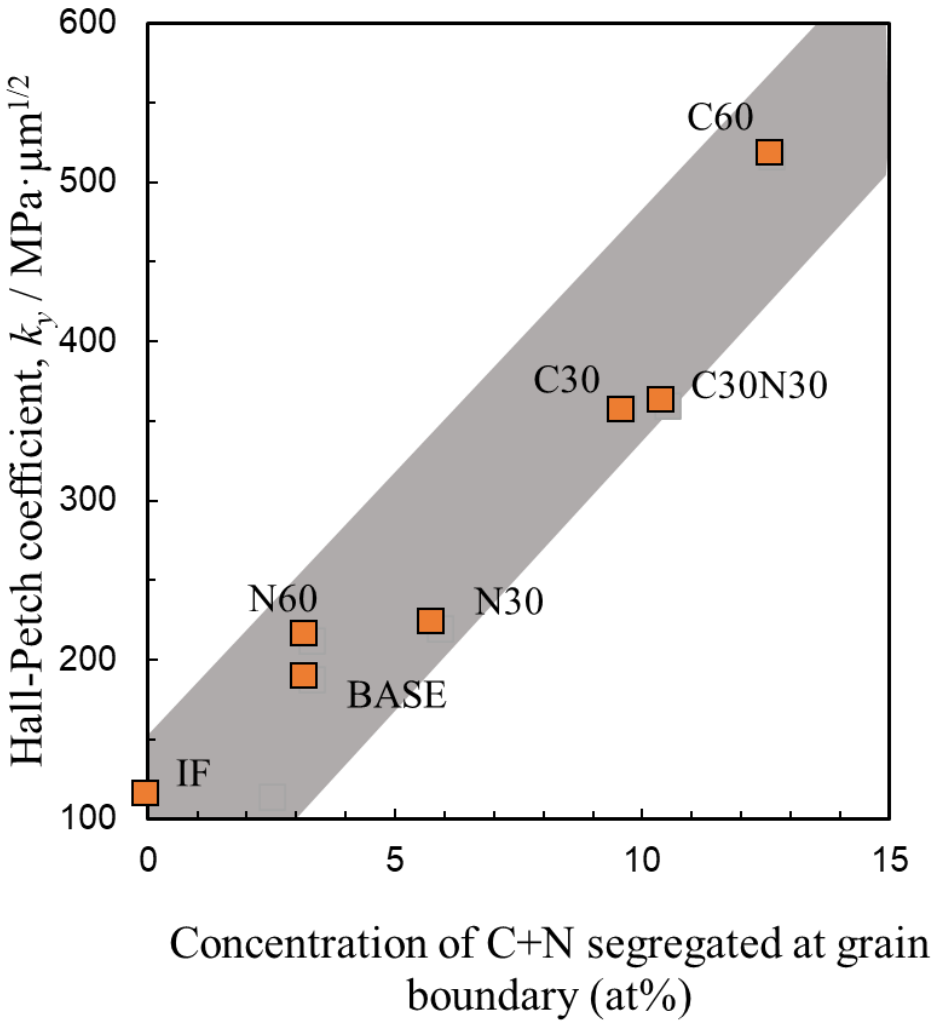

(a)

Fig. 2. 7 Relationship between Hall-Petch coefficient (k_y) and concentration of (a) C+N or (b) C segregated at the grain boundary calculated with Hillert-Ohtani model.

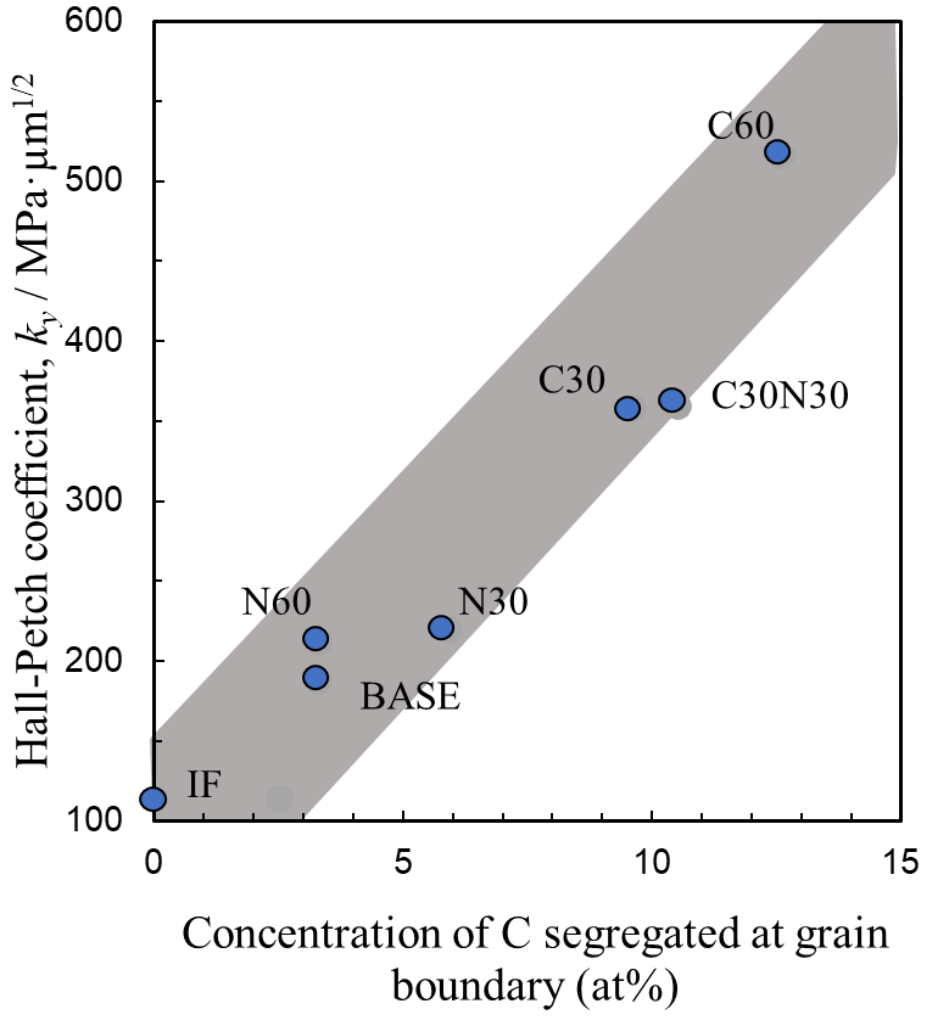

(b)

Fig. 2. 7 Relationship between Hall-Petch coefficient (k_y) and concentration of (a) C+N or (b) C segregated at the grain boundary calculated with Hillert-Ohtani model.

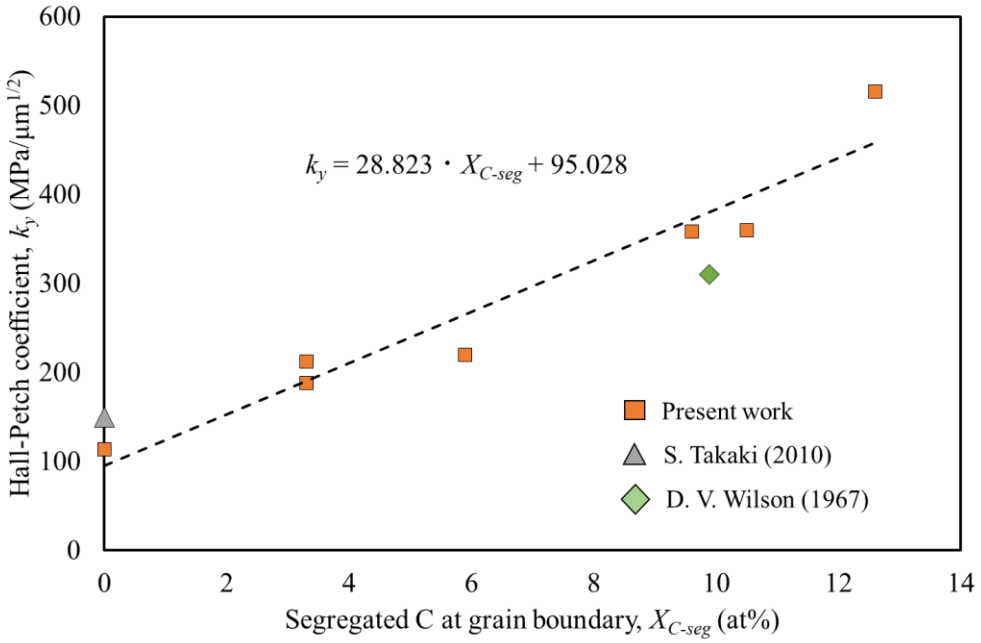

Fig. 2. 8 The relationship between the concentration of Carbon segregated at the grain boundary and the Hall-Petch coefficient, k_y.

2.4 Conclusions

(1) Thermodynamic calculations using the Hillert-Ohtani model can provide a reasonable prediction of the equilibrium concentrations of C and N segregated at the GB. The McLean model can yield similar results when the fraction of available sites in the GB layer is assumed to be saturated at 0.1.

(2) The Hall-Petch coefficient (k_y) of ferritic steels increased linearly with increasing concentrations of C and N segregated at GB. Therefore, using the above thermodynamic calculations, we can predict the k_y of the Fe-C-N alloys by the chemical composition and heat treatment temperature.

(3) Carbon has a much stronger segregation tendency than nitrogen, which caused a site competition between C and N atoms when co-addition. The segregated N atoms at GB will be replaced by C atoms resulting in the enlargement of the Hall-Petch coefficient（k_y) only by the effect of C.

Chapter 3 Influence of annealing temperature on the Hall-Petch coefficient in ferritic steels with interstitial elements: carbon

3.1 Introduction

In Chapter 2, the Hillert-Ohtani (HO) model was proved to obtain a high accuracy in predicting the concentration of grain boundary (GB) segregation. With the help of this model, the concentration of C segregated at GB was estimated in Fe-C binary alloys. Besides, the linear relationship between segregated C and the Hall-Petch coefficient (k_y) was quantitatively summarized by a mathematical formula that coordinates with the pile-up theory. It becomes available to develop the method to gain the high k_y steels by controlling the concentration of GB segregation.

It has been known that the level of GB segregation can be changed by controlling the amount of additional content. The calculation in Chapter 2 denotes that the concentration of C segregated at GB will increase when the C content is increased. Additionally, the McLean model explains that the GB segregation level will also increase when the surrounding temperature becomes lower [29], which proposes another way to enlarge the GB segregation to obtain the high k_y steels. Araki investigated the change in tensile properties of Fe-50 mass ppm carbon alloys under various times of low-temperature aging (170℃) [49]. The results indicated that the increase in aging time promoted the GB segregation of C and increased the k_y. It announced the feasibility of enhancement of the k_y by lowing temperature.

Based on the iron-carbon phase map, the solubility will change with the solution temperature. The solubility limits the number of solution atoms in bulk, which can also affect GB segregation because the excessive atoms have to move into GB when the bulk is saturated. That might be the mechanism of the rising k_y under low-temperature aging in Fe-C alloys. However, it must be noticed that excess aging can lead to the formation of precipitates, which will reduce solution C, resulting in decreasing the GB segregation. Since the aging treatment has been investigated among certain temperatures, such as 100℃ and 170℃ utilized only in the bake hardening process, general heat treatment temperature needs to be investigated.

Considering the α-iron area in the iron-carbon phase diagram, the solubility of C relies on the solution temperature. The GB segregation of C might simply be promoted by decreasing the solution temperature if there are no precipitate nucleates. Nevertheless, reducing the solution temperature might not constantly increase the GB segregation of C because the solubility of C has a different tendency above and below the A1 line. In addition, the C content in the matrix is also related to the formation of precipitates, which probably happen during the heat treatment process. Therefore, an accurate calculation method is required to help to control the solution temperature enlarging the k_y.

Based on Hillert's theory, the difference between the G_{gb} and the G_{α} increase when a new boundary is created in a system. Using the mathematical derivation, Hillert concluded that no matter how thick a grain boundary may be, a much larger addition or a much lower temperature is required to increase segregation [30]. That coincides with the McLean`s conclusion, thus, the HO model can be used in this study.

In this Chapter, the k_y of Fe-50C ferrite steels was studied by annealing treatment under different annealing temperatures. The concentration of C segregated at GB was evaluated by the HO model to determine the relationship between the changing GB segregation and the k_y. The predicting formula obtained in Chapter 2 was extended, studied, and verified by these experimental data to confirm the influence on the k_y by the annealing temperature.

3. 2 Methodology

3. 2. 1 Calculation of the Hall-Petch coefficient in Fe-C binary alloys under different annealing temperatures

To figure out the solubility of C under different annealing temperatures, the Fe-C phase diagram was calculated by Thermo-Calc 2022 (Thermo-Calc software). The database TCFE12 was utilized. The concentration of C segregated at GB under different solution temperatures was calculated by the HO model. The content of C was set from 0 to 100 mass ppm in interstitial free (IF) steels. The calculation was performed under the following conditions: temperature = 873, 923, 973, 1023, 1073, 1123, and 1173 K, number of moles = 1 mol, and atmospheric pressure = 101325 Pa. The

TCFE12 database was used in this study.

The quantitate description of the relationship between the k_y and the GB segregation obtained in Chapter 2 was adopted to predict the k_y of specimens under different temperatures annealing. Then, the predicted k_y was compared with the experimental k_y obtained in the tensile tests to verify the quantitate description and the HO model.

3. 2. 2 Preparation of specimens and heat treatment

25 kg ingots with a 110 mm square cross-section were manufactured by vacuum melting. The ingots were homogenized at 1523 K for 3.6 ks and then hot-rolled to a thickness of 10mm. A 90% cold rolling was followed by hot rolling. After wire-electrode cutting to the standardized shape, the cold rolled specimens were annealed at 1023 K, 973 K, 923 K, and 873 K in the salt bath furnace from 0.06 ks to 3.6 ks to control the grain size and the level of GB segregation, then quenched into water. The schematic diagram of the manufactory is illustrated in Fig. 3. 1. The specimens with various GB segregation levels were conducted. To prevent aging at room temperature, samples were put in the freezer with 223 K after quenching and quickly carried out during the experiments. The chemical compositions of the steel used in the study are listed in Table 3. 1.

3. 2. 3 Tensile tests and observation of the microstructures

The Instron tensile tester, SHIMADZU AG100kNX, was used. The tensile test was carried out at an initial strain rate of 1.38 mm/min for plate test pieces standardized by JIS13B at 293 K to measure the yield strength. The dimension of the tensile specimen is shown in Fig. 3. 2. In this study, the yield strength of specimens was defined as the lower yield stress or the 0.2% offset yield strength when specimens exhibit continuous yielding. The yield strength obtained in tensile tests was plotted against the inverse of the square root of the grain size based on the Hall-Petch relationship, and the k_y was estimated by the least-square method.

The microstructure was observed with an optical microscope (OM) and transmission electron microscopy (TEM, JEOL JEM-2010). To prepare the specimens for the OM observation, small

pieces were cut from the tensile test samples in the transverse direction. After the wet grinding by abrasive papers to #2400, the specimens were proceeded with alumina powders and buff polishing. Finally, the chemical corrosion was followed by a 3% nital (Nitric acid: Alcohol=3:97). The specimens for TEM observation were mechanically punched to disks of 3 mm diameter and polished to about 100 μm thickness by wet grinding. Then twin-jet electropolishing was carried out to fabricate thin foil specimens.

Table 3. 1 The chemical compositions of the steel used in the study (mass ppm).

	C	N	Si	Mn	P	S	O	Al	Fe
Fe-50C	48	6	<30	<30	<20	3	16	80	Bal.

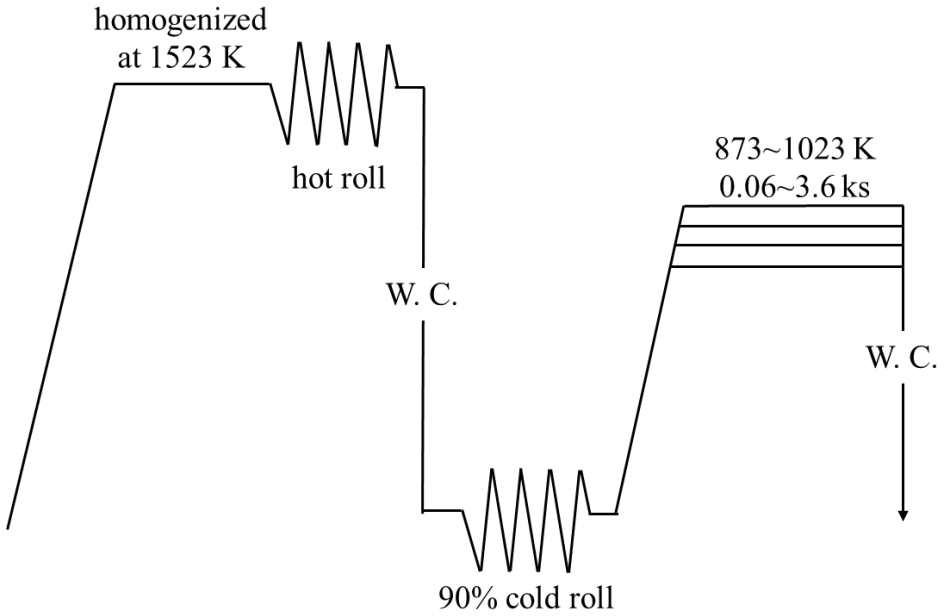

Fig. 3. 1 Manufactory process diagram of specimens.

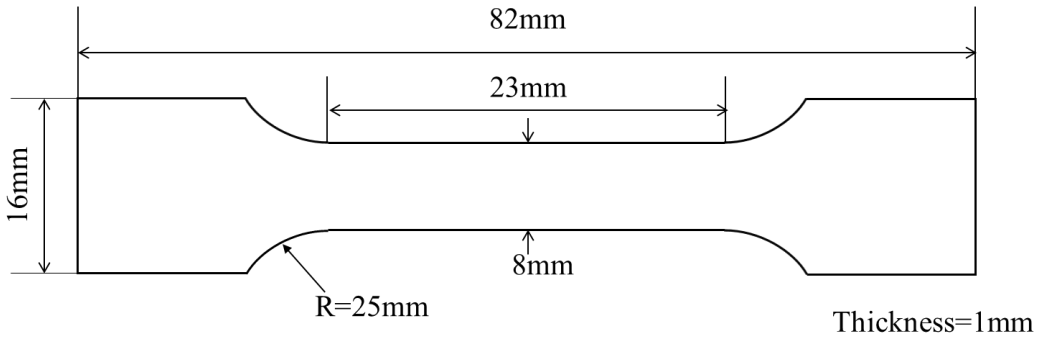

Fig. 3. 2 Dimension of the tensile specimen

The grain size was measured by the quadrature method [66]. The sketch diagram is shown in Fig.3. 3. The rectangle observation area (S) contains three kinds of grains. Grains intersected with the sides of the rectangle (a). Grains intersected with one side of the rectangle (b) and grains in the rectangle without any intersection (c). These grains contribute 1/4, 1/2, and 1 in the total number of grains (N), respectively. The grain size can be obtained by taking the square root of a, under the shape of a grain is seen as a square approximately. Then the total number of grains (N) in the square area, the average area per grain (s) and the nominal grain size (d) can be obtained by Eqs. (22), (23) and (24).

$$N = \frac{1}{4}a + \frac{1}{2}b + c \tag{22}$$

$$s = \frac{S}{N}, \tag{23}$$

$$d = \sqrt{s}. \tag{24}$$

3. 2. 4 Electric resistivity measurement

An electric resistivity measurement was carried out to estimate the solution and precipitation behavior during the annealing treatment. The constant current device (made by Takasago International Corporation) and digital voltmeter (made by Yokogawa Test & Measurement Corporation) were used to measure the electric resistance by a four-terminal measurement method [67]. The schematic diagram of the electrical circuit applicated in this study is shown in Fig. 3. 4. The wire specimens with a scale of 50 mm*1 mm*1 mm were prepared by wire-electrode cutting, followed by wet grinding subsequently. After holding in liquid nitrogen for 60 s, the electrical resistivity was measured twice by changing the current direction, and the average values were calculated. Based on Matthiessen's rule for electrical resistivity ($\rho = \rho_L + \rho_i$), ρ_L stems from the lattice vibration and is temperature dependent. In contrast, ρ_i represents the effects of solute atoms, defects, etc., and is independent of temperature. Therefore, by measuring in liquid nitrogen, the impact of ρ_L becomes approximately zero.

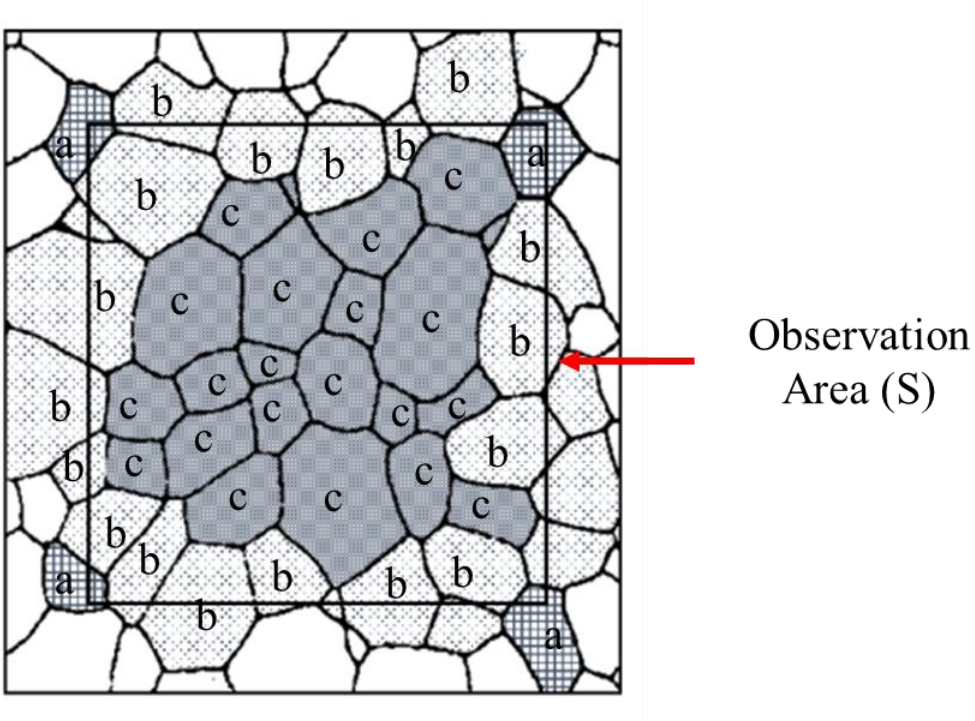

Fig. 3. 3. The evaluation of the grain size by the quadrature method

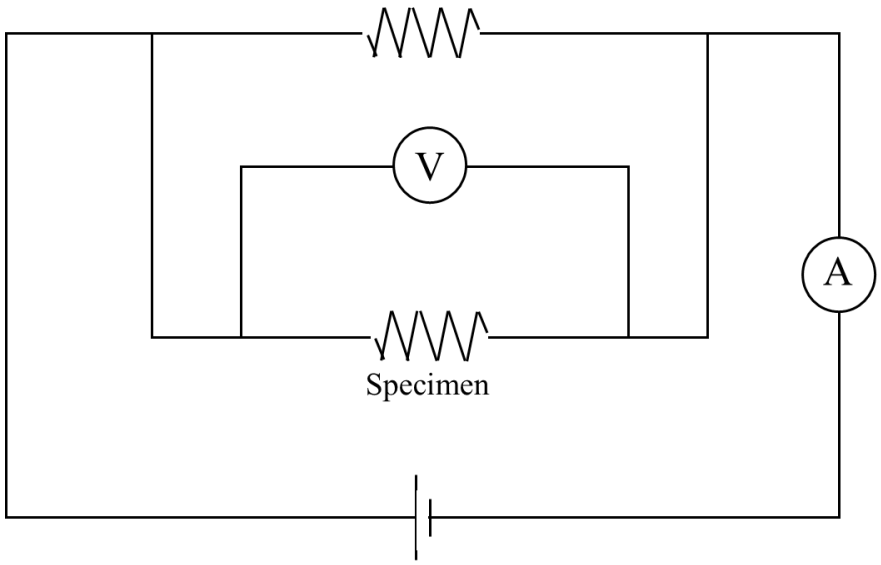

Fig. 3. 4 Schematic diagram of an electrical circuit.

3. 3 Results and analysis

3. 3. 1 Prediction of the Hall-Petch coefficient in Fe-C binary alloys with various annealing temperatures

Based on Eq. (21) between the k_y and GB segregation, the concentration of C segregated at GB with various annealing temperatures were calculated at first. Fig. 3. 5 shows the calculated values of C segregated at GB under different annealing temperatures in Fe-C binary alloys by the HO model. The calculated results of Fe-C alloys under various annealing temperatures are similar to those in Chapter 2. The concentration of C segregated at GB, $X_{c\text{-}seg}$, increases along with the addition of C content. On the other hand, the values of $X_{c\text{-}seg}$ decreased with the rise of annealing temperature, which corresponds to conclusions by other researchers [29, 49]. The calculated value of C at 1173K almost reduces to one-fourth of it at 873K, which indicates that the annealing temperature would remarkably influence the concentration of C segregated at GB in Fe-C ferritic steels.

Based on the quantitative formula of the k_y obtained in Chapter 2, the k_y values were calculated at a: 1023 K, b: 973 K, c: 923 K and d: 873 K, as shown in Fig. 3. 6. The k_y exhibited the highest level at 873K.

As mentioned previously, the concentration of C segregated at GB relies on the solubility of C in the α-Fe matrix. The predicted tendency of the k_y is reasonable only when C addition all solutes in the α-Fe matrix. When the annealing temperature is reduced, the solubility of C might disturb the actual segregation behavior of C. To find the influence of the solubility on the value of segregated C, the phase diagram of Fe-C steels was calculated by Thermo-calc and shown in Fig. 3. 7. There are four areas in the chart, in which the shadow part, representing the bcc area, is the target area in this study. The red broken line shows 50 mass ppm C (Fe-50C alloy). The four annealing temperatures are also plotted in the diagram. When the solubility of C in the α-Fe matrix is higher than 50 mass ppm, all of C content can be soluted in bulk or segregated to the GB. On the contrary, if the solubility of C is lower than 50 mass ppm, a part of solute C will precipitate as cementite, causing a loss of solute content. The loss might influence the value of GB segregation.

As seen in Fig. 3. 7, the a (1023K), b (973K), and c (923K) were located in the BCC single-phase region. Then the concentration of C segregated at GB, and the corresponding k_y could be predicted. On the hand, d (873K) was located near the border. That supposes the precipitation might happen during annealing, resulting in a deviation from the predicted value.

3. 3. 2 Tensile strength of Fe-50ppmC alloys under different annealing temperatures

The nominal stress-strain curves of Fe-50ppmC alloys annealed at (a) 1023 K, (b) 973 K, (c) 923 K, and (d) 873 K are shown in Fig. 3. 8. The specimens b, c and d were annealed for 0.2, 0.6, 1.8 and 3.6 ks at each temperature to control the grain sizes, respectively. Because the growth speed of grain size is too fast at 1023 K, the annealing time were 0.03, 0.06, 0.2, and 0.6 ks to obtain a similar grain size with the specimens annealed at other temperatures. The obtained yield stress was marked with black fork marks. The 0.2% offset yield strength was adopted as the yield stress because lower yield points were not clear in most stress-strain curves.

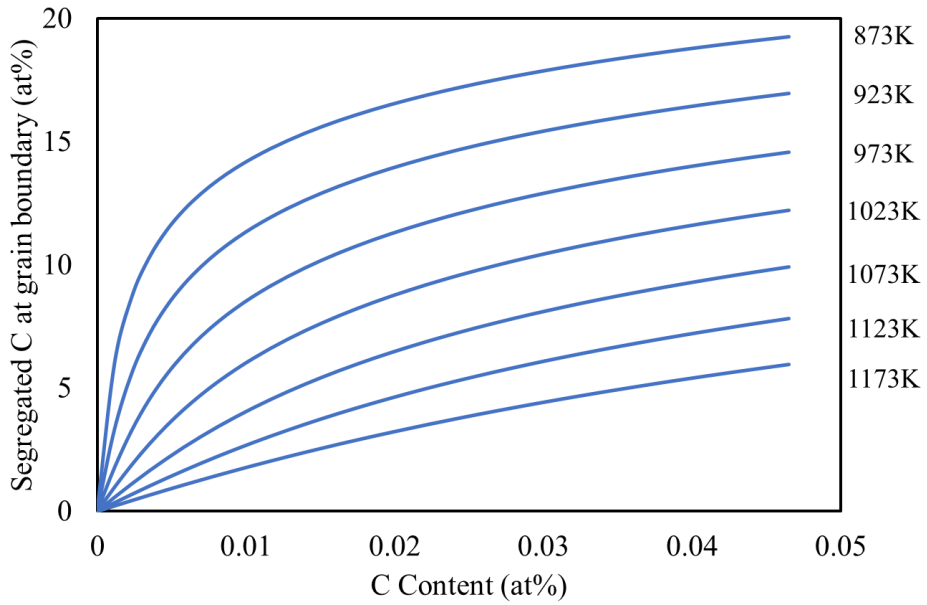

Fig. 3. 5 The calculated results of the carbon concentration of grain boundary segregation under different solution temperatures.

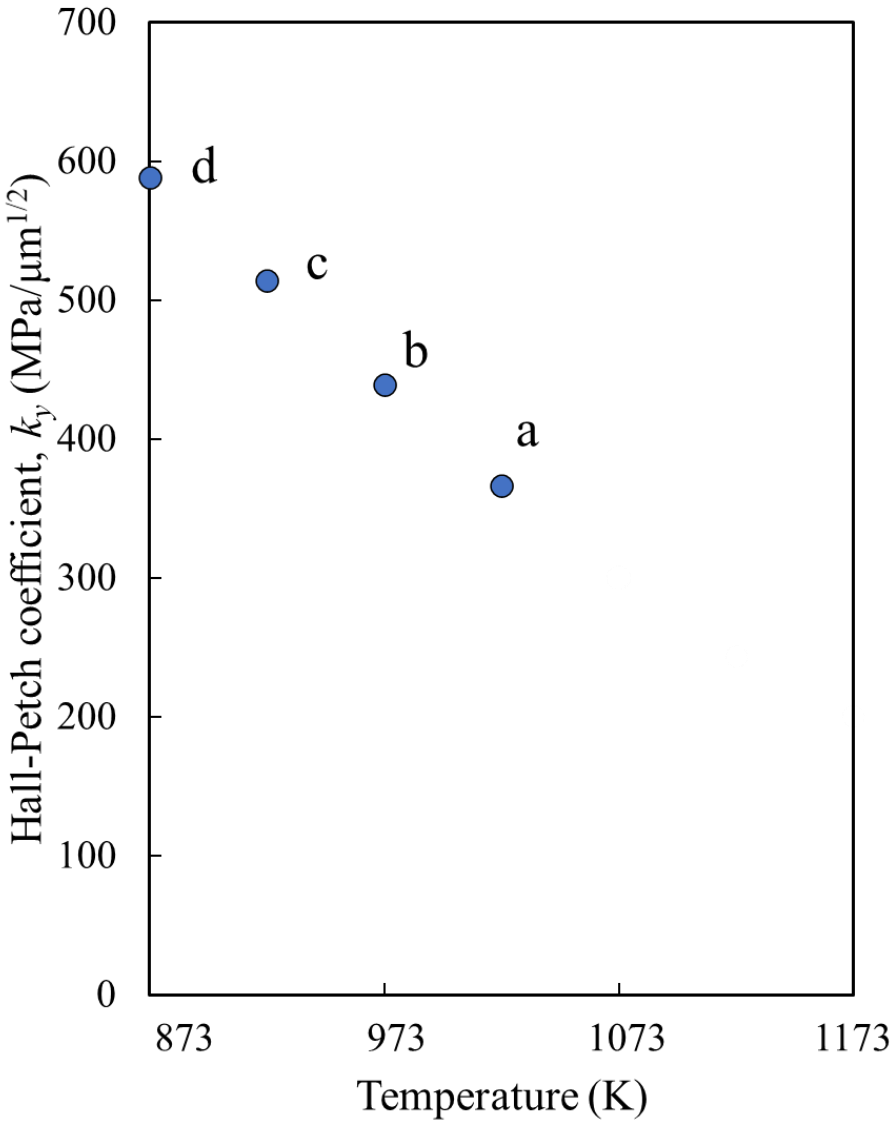

Fig. 3. 6 The calculated results of predicted Hall-Petch coefficients under various annealing temperature.

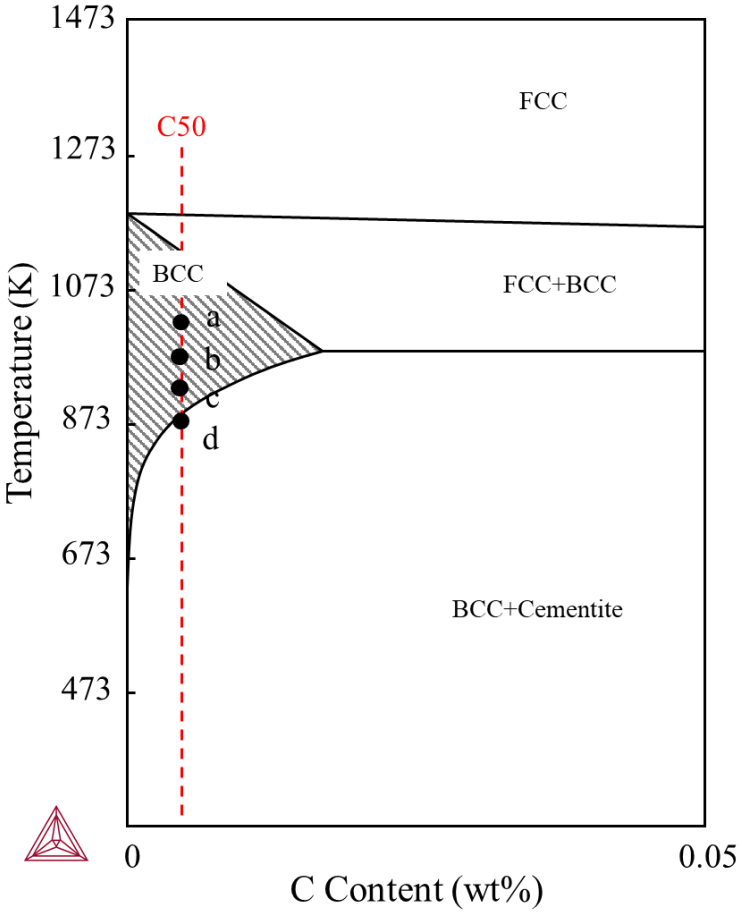

Fig. 3. 7 The phase diagram of Fe-50C binary alloys.

Yield stress of the specimens increased with the reduction of annealing time and annealing temperature. The Hall-Petch plots of Fe-50 ppmC steels annealed in (a) 1023 K, (b) 973 K, (c) 923 K, and (d) 873 K were shown in Fig 3. 9, respectively. The friction stress has been proved only weakly influenced by the solute C in Fe-C alloys [49]. In this study, the friction stress, σ_0, was calculated using the Cracknell`s formula [21] by the content of C, X_c, written in Eq. (25).

$$\sigma_0 = 40 + 4500 \times X_C \tag{25}$$

Since X_c are in the ferritic area at all four annealing temperatures, all C atoms will be solute in the α-matrix, making the friction stress constant. It can be seen that the k_y of specimens annealed under (a) 1023 K, (b) 973 K, and (c) 923 K were near the predicted results. However, the specimen (d) under 873 K annealing exhibited an abnormally low k_y, which should be larger than that of (c) 923K by predicting. Based on the calculated phase diagram of Fe-C alloys, the solubility of C in α-Fe only has a contrary trend near 1000 K. It is supposed that the precipitation might happen at 873 K during the annealing process resulting in a decrease in GB segregation.

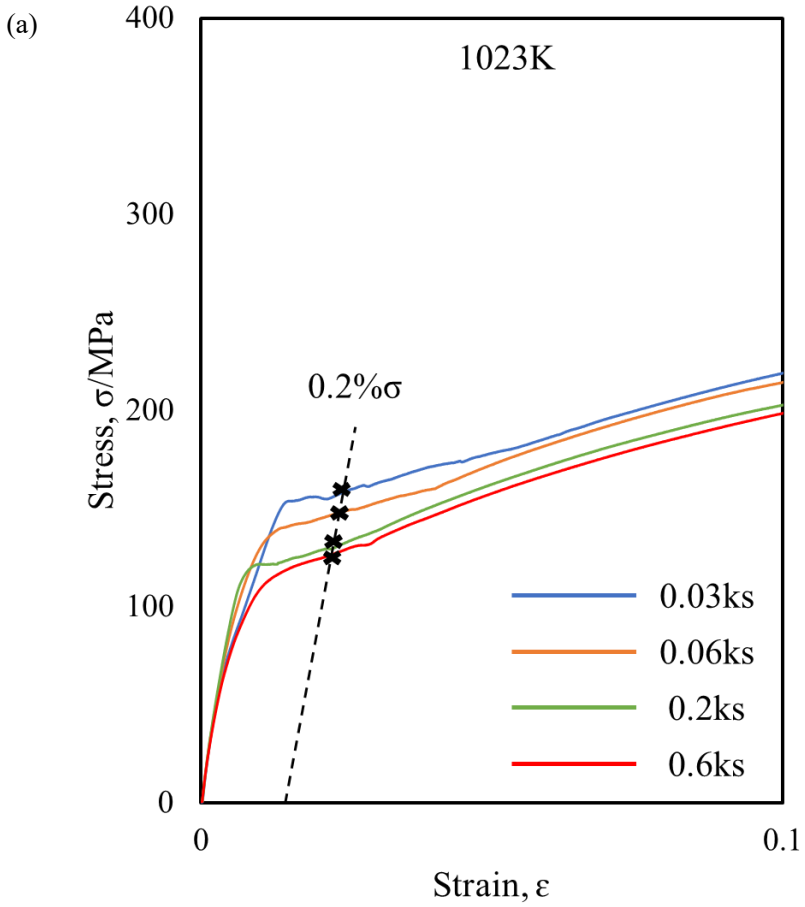

(a)

Fig. 3. 8 The nominal stress-strain curves in Fe-50C steels annealed in (a) 1023 K, (b) 973 K, (c) 923 K, and (d) 873 K.

(b)

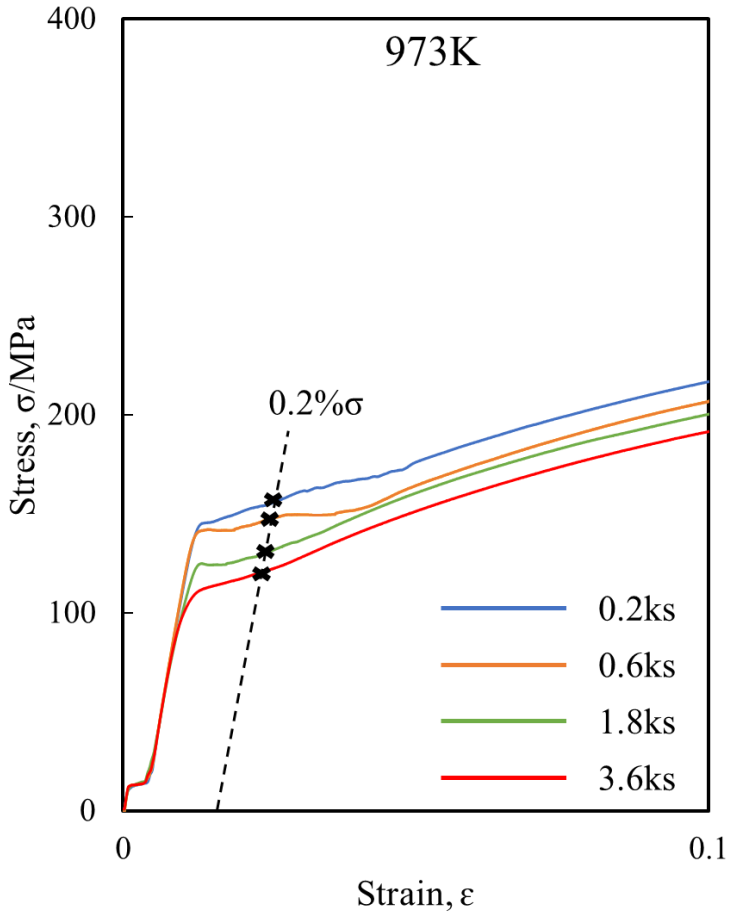

(b)

Fig. 3. 8 The nominal stress-strain curves in Fe-50C steels annealed in (a) 1023 K, (b) 973 K, (c) 923 K, and (d) 873 K.

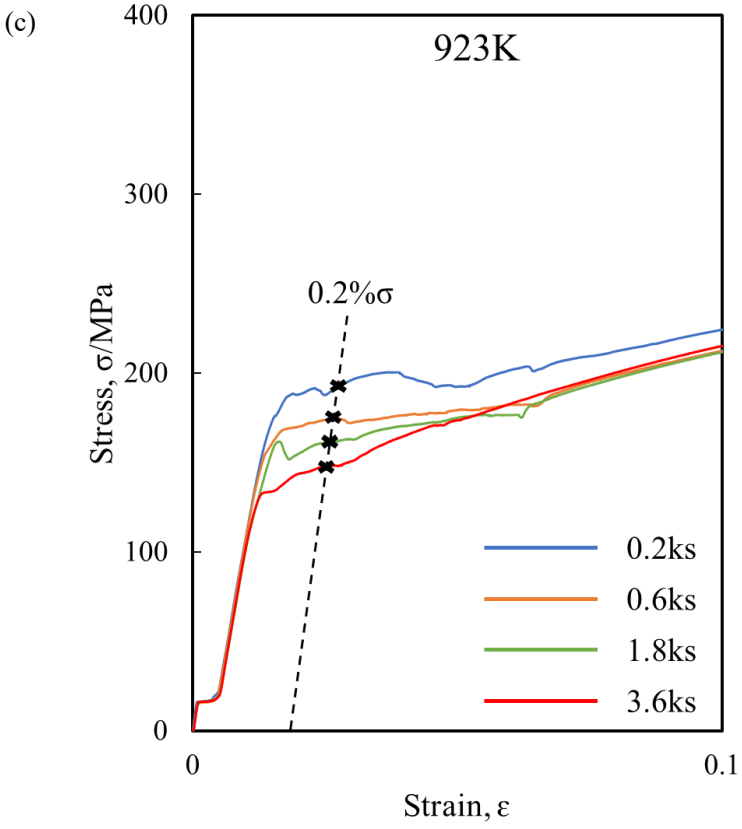

(c)

Fig. 3. 8 The nominal stress-strain curves in Fe-50C steels annealed in (a) 1023 K, (b) 973 K, (c) 923 K, and (d) 873 K.

(d)

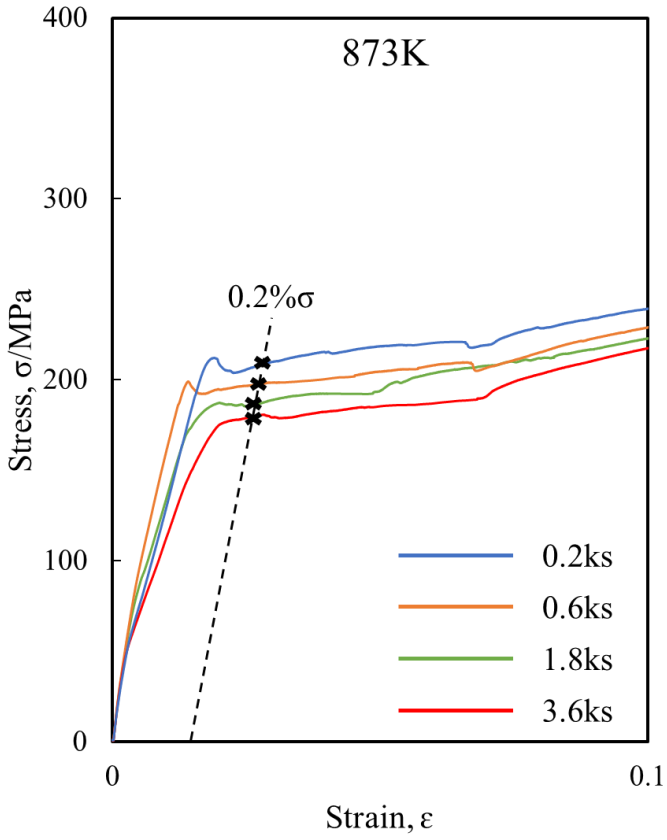

(d)

Fig. 3. 8 The nominal stress-strain curves in Fe-50C steels annealed in (a) 1023 K, (b) 973 K, (c) 923 K, and (d) 873 K.

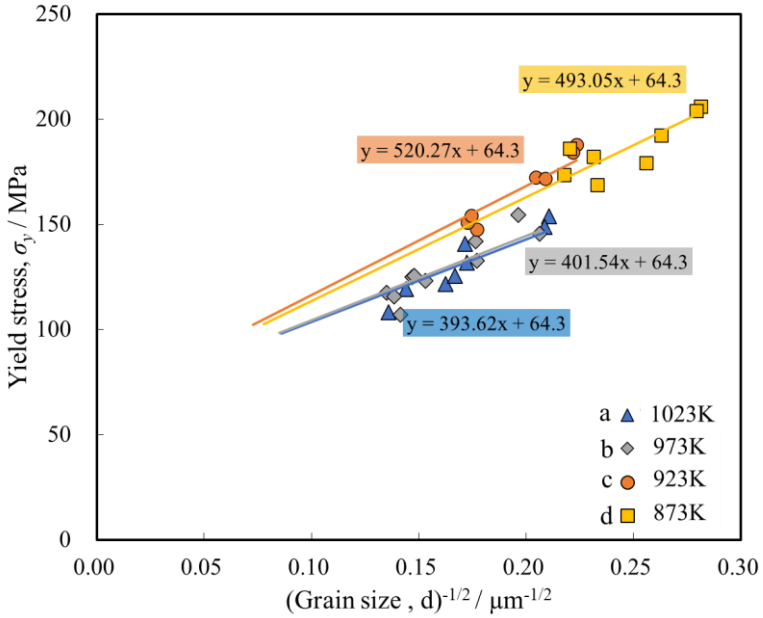

Fig. 3. 9 The Hall-Petch profile of Fe-50C steels annealed in (a) 1023 K, (b) 973 K, (c) 923 K, and (d) 873 K.

3. 3. 3 Verification of the calculated and experimental Hall-Petch coefficients of Fe-50C steels under different annealing temperatures

Fig. 3. 10 shows the predicted and experimental Hall-Petch coefficients (k_y) under different annealing temperature. The orange and blue circles represent the experimental and predicted results, respectively. The experimental k_y of the specimens annealed at 1023 K (a), 973 K (b), and 923K (c) are close to the calculated ones, while the k_y of specimen annealed at 873K (d) exhibits a large deviation from the predicted value. With the suspension of forming precipitates, further investigation was carried out to identify whether there were any precipitates in the specimen annealed at 873 K.

The OM images of Fe-50C steels annealed at 1023 K (a), 973 K (b) 923K (c) and 873K (d) with different annealing times are represented in Fig. 3. 11. The annealing temperature and time were tagged on the top of each image, under which the calculated average grain size was shown. The grain size of each series specimen exhibited an increasing tendency with the annealing temperature or time raised. However, the microstructures of all specimens showed clear grains with no precipitate, which could hardly explain the unusual change of the k_y in (d) 873 K.

TEM observation was also carried out on the specimens with annealing at 873 K for 3.6 ks. Based on the phase map, if the precipitate forms, they prefer to nucleate at the GB first. The TEM observation on the GB is shown in Fig. 3. 12. The precipitates were barely observed at GB or in bulk. The diffraction pattern analysis was carried out on the line perpendicular to the GB. Position 1: upper grain boundary, Position 2: grain boundary, and Position 3: lower grain boundary were observed. As a result, no clear evidence shows there are any precipitates.

When C forms precipitate, the electrical resistivity (ρ) will reduce due to the loss of solute C. The measured results are shown in Fig. 3. 13, in which the previous data were plotted for comparison. The specimens with annealing at 873 K and 973 K for 3.6 ks were investigated. Compared with the apparent reduction of ρ in Fe-60C aged at 373 K, which is due to the formation of precipitates, the electric resistivity results in this study could be seen as unchanged.

These results show no clear evidence that the precipitate appears when annealed at 873 K. Considering the rough prediction by the relationship between the GB segregation and the k_y, the

usual k_y at 873 K might be due to the uncertainty of the calculated solubility or the non-equilibrium GB segregation of C caused by low temperature annealing.

3. 3. 4 Prediction of the Hall-Petch coefficient in ferritic steels of arbitrary composition

Assuming that the calculated phase diagram is accurate and the equilibrium segregation state of C at GB is obtained, based on our theory the following predictions can be introduced. In Fig. 3. 14, the relationship among the k_y predicted by the HO model, the concentration of C at GB and the annealing temperature is summarized with the surface abcd. The solubility limit is indicated by surface ABCD. In addition, the blue line represents the calculated results of Fe-50ppm C alloy adopted in this study, on which the black plots exhibit the relationship between the experimental k_y and the annealing temperature. Curve PP` is the intersecting line of these two surfaces. At the right side of the PP` line, which means the annealing temperature goes below or the C content raises over this line, the is k_y expected not increased due to precipitation of cementite. Therefore, in the range of this figure, it is expected that the maximum k_y will be obtained when 100 ppm C is dissolved at 1000 K.

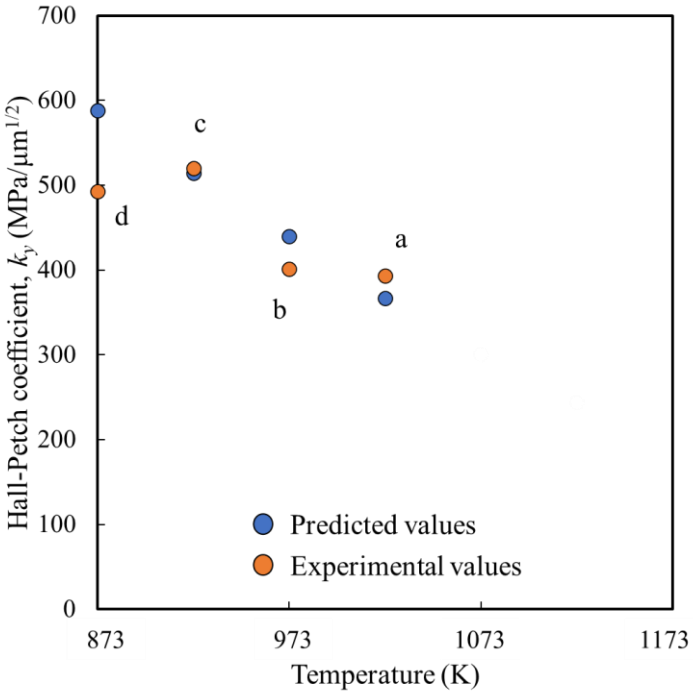

Fig. 3. 10 The predicted and experimental Hall-Petch coefficient (k_y) under annealing at (a) 1023 K, (b) 973 K, (c) 923 K and (d) 873 K, respectively.

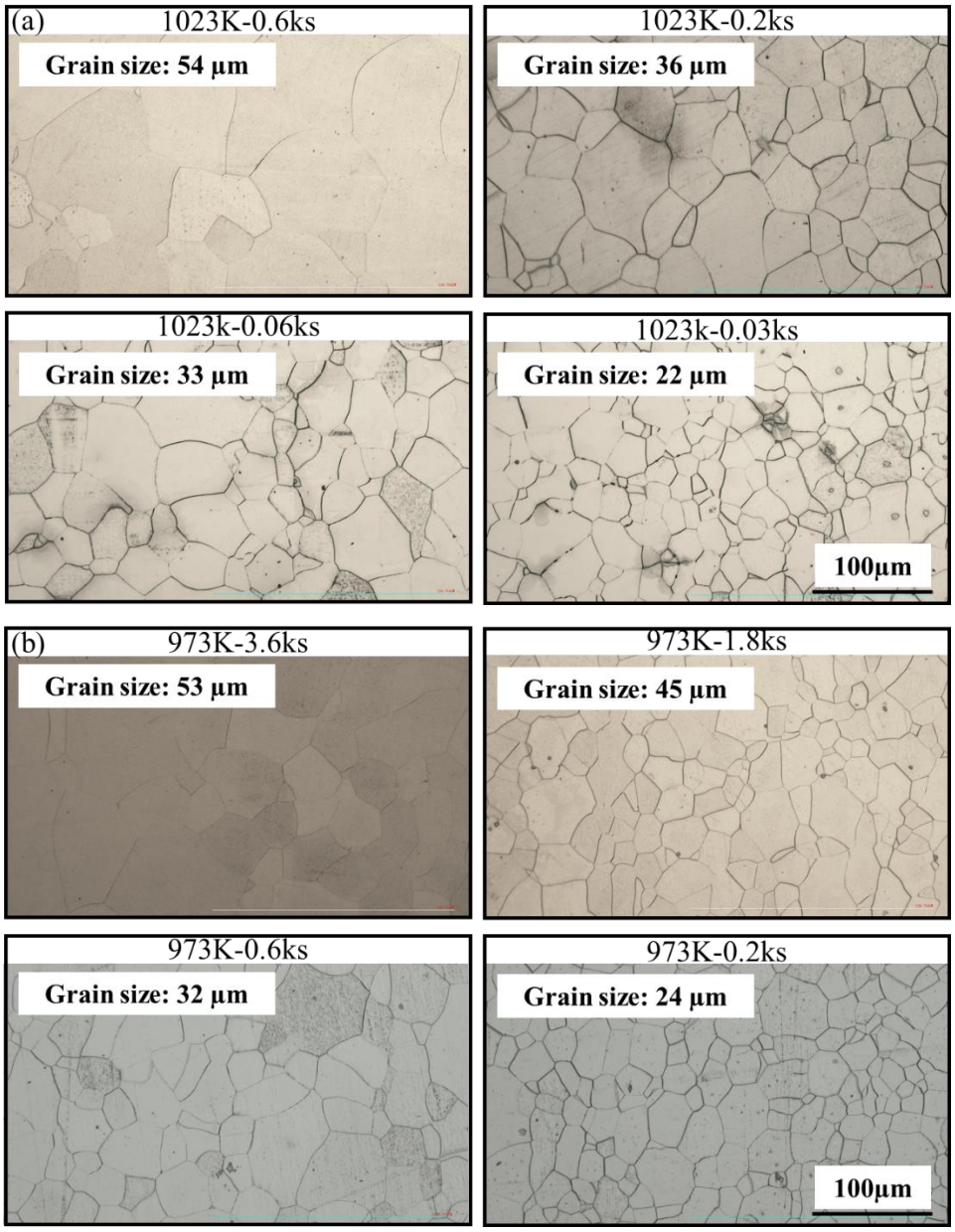

Fig. 3. 11 OM images of Fe-50C steels annealed at (a) 1023 K, (b) 973 K, (c) 923 K and (d) 873 K for different annealing time.

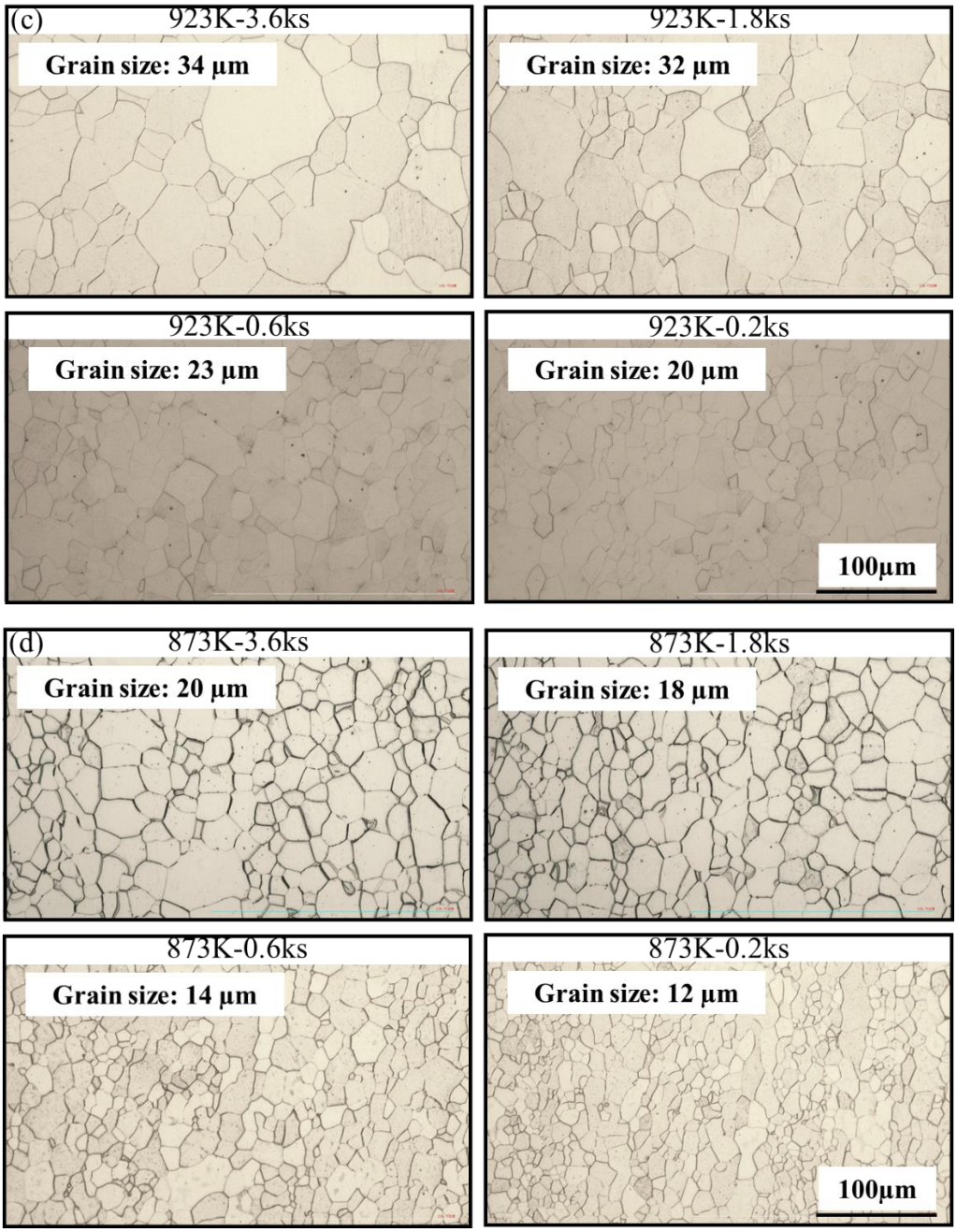

Fig. 3. 11 OM images of Fe-50C steels annealed at (a) 1023 K, (b) 973 K, (c) 923 K and (d) 873 K for different annealing time.

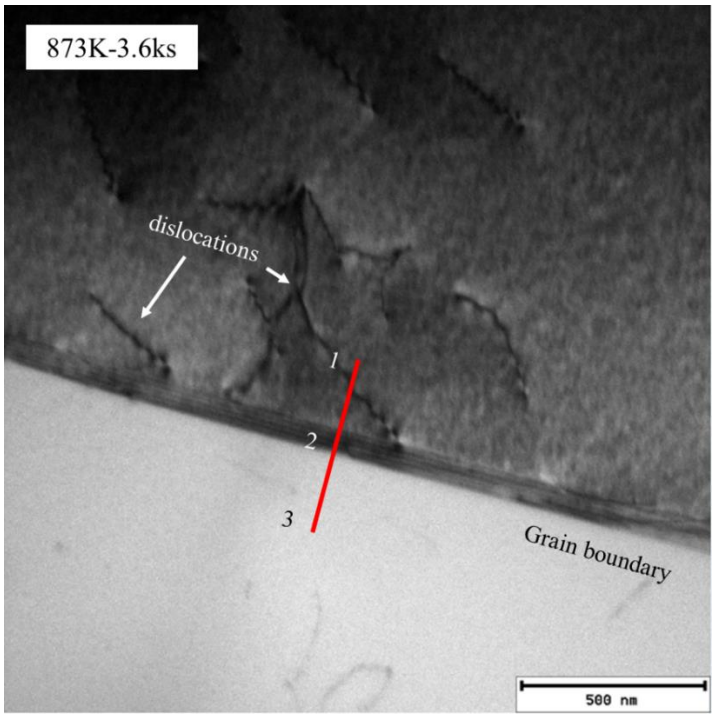

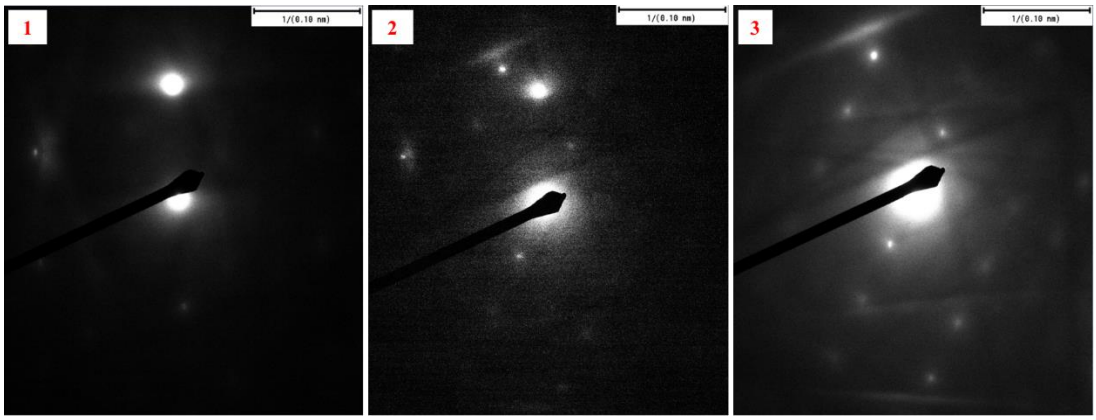

Fig. 3. 12 TEM images on the grain boundary of Fe-50C specimen annealed at 873 K for 3.6ks.

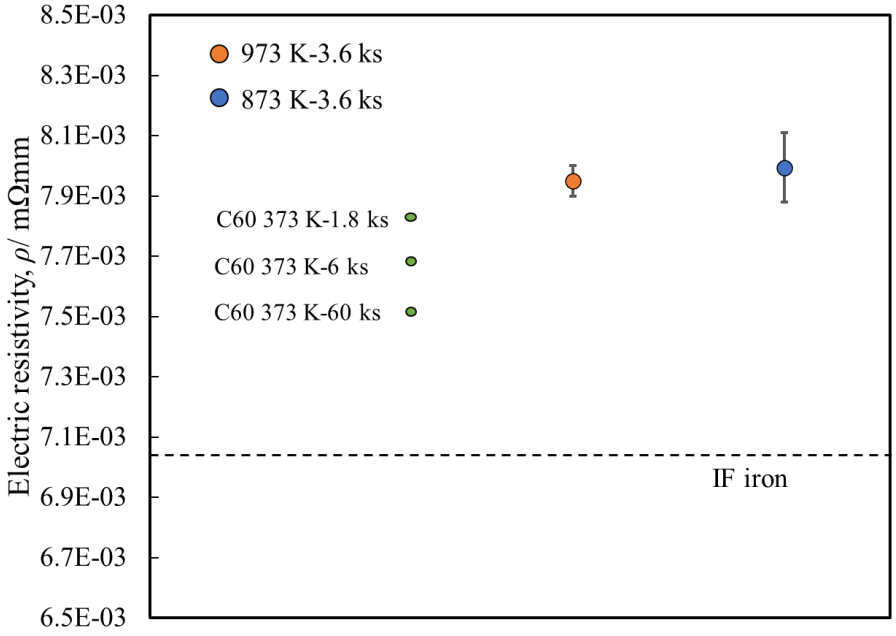

Fig. 3. 13 Changes in electric resistivity of C50 with annealing at 973 K and 873 K.

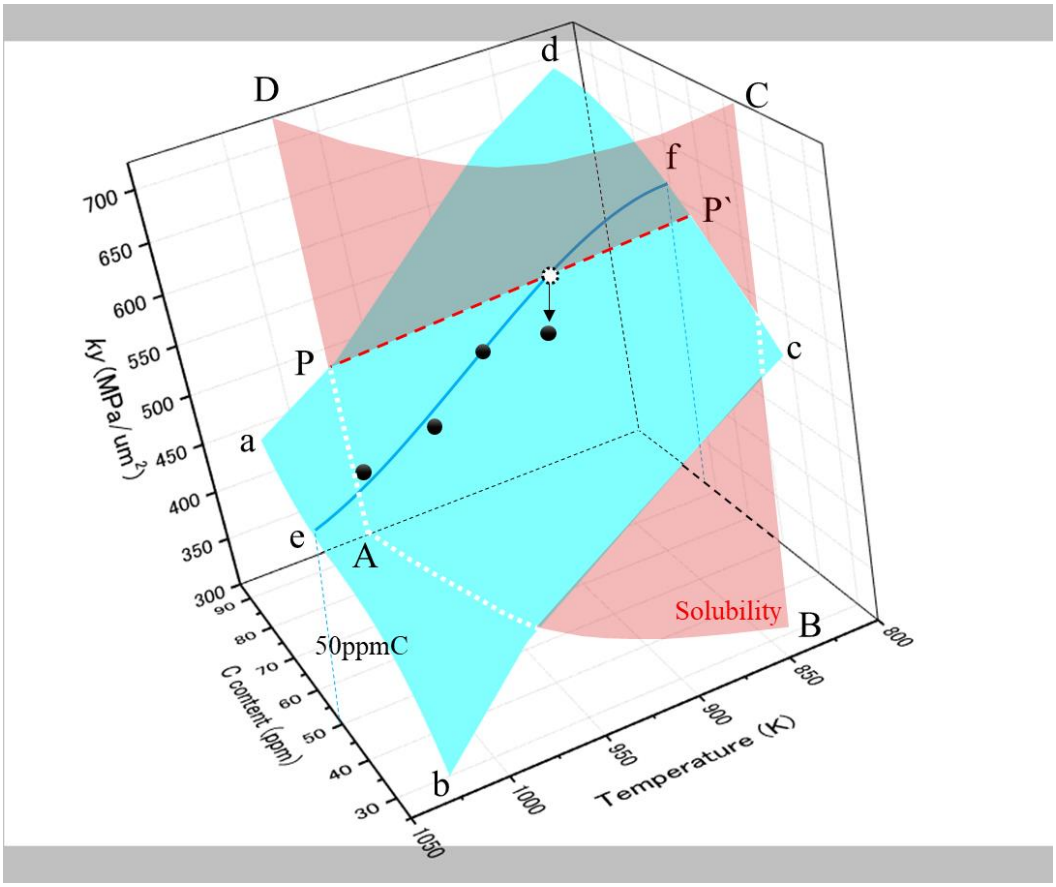

Fig. 3. 14 The relationship among the C content, the annealing temperature, and the Hall-Petch coefficient (k_y).

3. 4 Conclusions

1. Reducing the annealing temperature can increase the carbon concentration segregated at grain boundary and enlarge the Hall-Petch coefficient (k_y).
2. The Hall-Petch coefficient (k_y) obtained in the tensile test coincident well with the predicted values by the mathematical formula, which describes the relationship between the concentration of carbon segregated at the grain boundary and the Hall-Petch coefficient (k_y) summarized in Chapter 2.
3. Fe-C alloys with high Hall-Petch coefficient (k_y) can be gained by raising the C content or reducing the annealing temperature. However, precipitate becomes easy to form when the annealing temperature reduces, which may cause a negative influence on the Hall-Petch coefficient (k_y).

Chapter 4 Co-addition effect of interstitial and substitutional elements on Hall-Petch relationship: Manganese-Carbon and Silicon-Carbon

4.1 Introduction

The relationship between the Hall-Petch coefficient (k_y) and the concentration of segregated carbon at the grain boundary (GB) in Fe-C ferritic steels has been studied in Chapter 2. The value of k_y increased linearly with the raising concentration of C segregated at GB. Based on this relationship, the control of the k_y by changing the solubility of C via annealing temperature in C-added α-Fe was achieved in Chapter 3. Moreover, these various k_y roughly followed the linear relationship predicted by the mathematical formula obtained in Chapter 2. This not only provides experimental evidence to the pile-up theory but also develops a new way to strengthen steels by grain refinement strengthening in steels.

So far, we have mainly discussed the strengthening effect of segregated C at the GB. The site-competition interaction between the co-added C and N atoms in ferritic steels was discussed in Chapter 2. It was found that C atoms show a repulsive interaction with N atoms. The concentration of N at GB reduced by co-segregation of C, leads to C atoms being the dominant factor in increasing the k_y even in the N-based steels. These results indicated that the strong interaction between atoms at the GB may play a more important role than the change in solubility.

In the steel manufacturing industry, not only interstitial elements like C and N are used to improve the properties of alloys, but also substitutional elements, such as silicon and manganese, are added to obtain the specific properties of some alloys. The influence of the substitutional elements on the k_y of ferritic steels has been extensively studied in the past. Jiang et al. [48] investigated the k_y of ferritic steels c, Al, Mn, Ni, Cu, and Cr individually in Fe-M (M=Si, Al, Mn, Ni, Cu, Cr) binary alloys [27, 28, 41]. With the exception of Cr, which showed no effect, the remaining substitutional elements increased the k_y value, with Si and Mn being the most effective candidates. Compared with the relatively small interstitial atoms, the substitutional atoms are larger than the Fe atoms, resulting in different crystal lattice strains. Due to the interaction with dislocations and atoms, the added substitutional atoms might form a different circumstance at the GB, which leads

to the additional enhancement of the k_y. On the other hand, since the driving force of C segregation into the GB can be changed by adding substitutional elements, this could increase the amount of segregated C in the GB. Therefore, it is worth investigating the strengthening effect of the co-addition of C and substitutional elements.

In general, interactions between solute atoms may be involved in controlling the segregation level of alloying elements at GB in multicomponent systems [68, 69]. When two atoms form an attractive or repulsive interaction, their GB segregation tends to be enhanced or hindered by the interaction. From the literature [50, 51, 52], C atoms also have a repulsive interaction with Si atoms, which would lead to the reduction of Si at GB. In the ternary Fe-Si-C system, the k_y can be enhanced due to the additional segregated C and Si atoms compared to the binary Fe-C system. On the other hand, Mn atoms are known to have attractive interactions with C atoms. The segregated Mn atoms at the GB could also cause additional carbon segregation due to the attractive interaction. However, these two assumptions are all unidirectional. The interaction between Si or Mn and C at the GB will be more complicated in the actual situation.

In a Fe-M-C (M=Mn or Si) ternary system, although the equilibrium concentration of Mn or Si can be easily determined by the HO model, the substitutional elements such as Mn and Si rarely have sufficient time to reach equilibrium in the practical annealing situation due to their slow diffusion rate [29, 58]. In this non-equilibrium situation, the Mn or Si atoms could maintain their initial position even after annealing. In contrast, C is in equilibrium in bulk and at the GB, which is suitable for the application of the para-equilibrium theory.

In this chapter, two types of ternary alloys, Fe-yMn-C (y=0.5, 1, 2 wt%) and Fe-xSi-C (x=1, 2, 3 wt%), were investigated. The concentration of C was calculated using a thermodynamic calculation software called CaTCalc, which is suitable for para-equilibrium calculation. The influence of each element on the k_y value was considered independently to clarify the co-addition interaction.

4. 2 Methodology

4. 2. 1 Preparation of specimens and heat treatment

1.5 kg ingots with a cross-section of 30 mm×53 mm were manufactured by vacuum melting. The ingots were homogenized at 1473 K for 3.6 ks and then hot rolled to a thickness of 10 mm. A 90% cold rolling was followed by hot rolling. After cutting the wire-electrode into the standardized shape, the cold-rolled specimens were annealed at 973 K in the salt bath furnace from 0.06 ks to 3.6 ks to control the grain size and quenched into water. The schematic diagram of the manufactory process is illustrated in Fig. 4. 1. The chemical compositions of the steel used in this study are listed in Table 4. 1.

For tensile tests and observation of the microstructures, the same methodologies were adopted in Chapter 3.

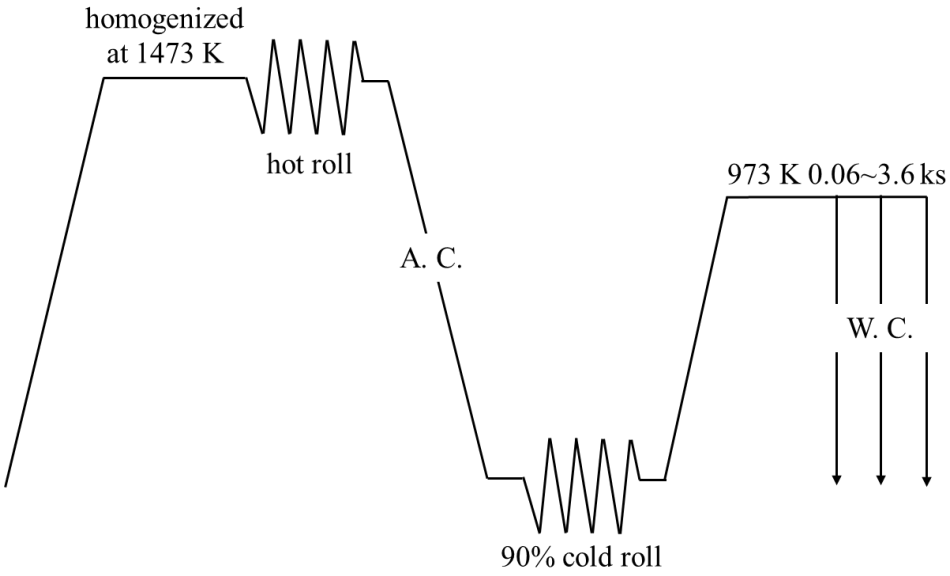

Fig. 4. 1 The manufactory process diagram of specimens

Table 4. 1 The chemical compositions of the steel used in the study (wt%).

	C	Si	Mn	P	S	Ti	Fe
Fe-1Si-C	0.006	0.92	<0.01	<0.002	<0.001	-	Bal.
Fe-2Si-C	0.006	1.93	<0.01	<0.002	<0.001	-	Bal.
Fe-3Si-C	0.006	2.92	<0.01	<0.002	<0.001	-	Bal.
Fe-0.5Mn-C	0.0054	<0.01	0.45	<0.002	<0.001	<0.001	Bal.
Fe-1Mn-C	0.0051	<0.01	0.93	<0.002	<0.001	<0.001	Bal.
Fe-2Mn-C	0.0057	<0.01	1.98	<0.002	<0.001	<0.001	Bal.

4. 2. 2 The para-equilibrium theory

Numerous studies have investigated the effect of alloying elements on phase transformation in Fe-C-X alloys. It was found that when the interphase reaches an equilibrium state, transformation can occur with or without the partition of alloying elements [58]. Kirkaldy et al. [59] concluded that an alloying element may be unsegregated but remain in substantial local equilibrium during the transformation. This particular equilibrium mode, which strongly deviates from the usual one, must be described by unique kinetics. This transformation mode, named by Hillert [72-74], is called the para-equilibrium mode, in which the substitutional alloying element plays no role in the transformation and proceeds under pure C diffusion control.

Gilmour *et al.* [75] used this conclusion to quantitatively investigate the constitution of the Fe-C-Mn system concerning the α/γ interphase. In the situation of ortho-equilibrium, when the system reaches equilibrium,

$$\mu_{Fe}^{\alpha} = \mu_{Fe}^{\gamma} \ , \tag{26}$$

$$\mu_{Mn}^{\alpha} = \mu_{Mn}^{\gamma} \ , \tag{27}$$

$$\mu_{C}^{\alpha} = \mu_{C}^{\gamma} \ . \tag{28}$$

Eq (26), (27), and (28) are established. On the other hand, the condition of para-equilibrium is different because Mn is unsegregated, which can be described by Eq (29).

$$x_{Fe}/x_{Mn} = constant \tag{29}$$

Then the description of the para-equilibrium is expressed as Eq (30) and Eq (31). The parameter *Y* represents the mole fraction of Fe or Mn.

$$\mu_{C}^{\alpha} = \mu_{C}^{\gamma} \tag{30}$$

$$Y_{Fe}\mu_{Fe}^{\alpha} + Y_{Mn}\mu_{Mn}^{\alpha} = Y_{Fe}\mu_{Fe}^{\gamma} + Y_{Mn}\mu_{Mn}^{\gamma} \tag{31}$$

Combining these equations with Hillert theory in which GB is considered as a separate phase, these formulas can be extended at the α/GB interface by the parallel-tangent construction given in Eq (32).

$$\mu_{C}^{GB} - \mu_{C}^{\alpha} = (Y_{Fe}\mu_{Fe}^{GB} + Y_{Mn}\mu_{Mn}^{GB}) - (Y_{Fe}\mu_{Fe}^{\alpha} + Y_{Mn}\mu_{Mn}^{\alpha}) \tag{32}$$

Eq (32) can be rewritten as Eq (33) when the Ohtani`s assumption is applied, which provides a way to calculate the concentration of C in bulk and at the GB under the co-addition with Mn.

$$\mu_C^L - \mu_C^\alpha = (Y_{Fe}\mu_{Fe}^L + Y_{Mn}\mu_{Mn}^L) - (Y_{Fe}\mu_{Fe}^\alpha + Y_{Mn}\mu_{Mn}^\alpha) \quad (33)$$

Therefore, the concentration of C segregated at the GB will be calculated under the condition that Mn or Si is unsegregated in the Fe-(Mn/Si)-C ternary system. The thermodynamic software: Chemical and Thermodynamic Equilibrium Calculator (CaT-Calc) was used to perform these complex calculations. CaT-Calc is a software that performs thermodynamic equilibrium calculations using the Gibbs Energy minimization method.

4. 3 Results and analysis

4. 3. 1 Hall-Petch relationship in Fe-(Mn/Si)-C ternary alloys

The Hall-Petch (HP) plots of Fe-Mn-C (a) and Fe-Si-C (b) ternary alloys obtained by tensile tests are shown in Fig. 4. 2. In addition, the previous experimental data of Fe-C binary alloys (Fe-60 mass ppm C without Mn or Si) are also represented by dashed lines to illustrate the effects of Mn and Si content. From Fig. 4. 2, it can be seen that the yield stress of Fe-Mn-C and Fe-Si-C ternary alloys in the tensile tests exhibits a linear relationship with the square root of grain size, which is consistent with the typical HP relationship. However, the HP plots of Fe-Mn-C and Fe-Si-C ternary alloys show different tendencies under the influence of Mn or Si substitutional addition. The k_y increases in the Fe-Mn-C ternary alloys compared to the Fe-C alloys, indicating that the co-addition of Mn and C increased the critical GB shear stress. The k_y value also increases along with additional Mn content, while the friction stress of Fe-Mn-C alloys hardly changes, which might be due to the weak effect of Mn on solid solution strengthening. On the other hand, the Fe-Si-C alloys show a more significant increment in k_y than the Fe-Mn-C alloys. Moreover, the k_y remains almost constant, while the friction stress improves with additional Si content, suggesting that Si has a strong solid solution strengthening ability.

In order to investigate the influence of substitutional elements on the k_y in the C-bearing steels, the change in k_y as a function of substitutional element content was plotted separately in Fig. 4. 3. Experimental data of Fe-(Mn/Si)-C ternary alloys are indicated by blue circles, and the data of binary Fe-(Mn/Si) alloys and IF steels are shown by dashed lines for comparison. The addition of C leads to a remarkable increase in k_y in Fe-Mn and Fe-Si steels. However, the increase in k_y

shows two different trends. The k_y of the Fe-Mn-C alloys increases gradually with Mn content. This increment is similar to that of Fe-Mn alloys, indicating that the effect of Mn and C on k_y is simply added up. On the other hand, in the Fe-Si-C alloys, k_y initially increases with the addition of Si and later remains unchanged, while in the Fe-Si alloys, the k_y increases linearly with the Si content shown in Fig. 4. 3 (b). This indicates that a co-effect might occur in Fe-Si-C alloys at the GB compared to Fe-Si alloys.

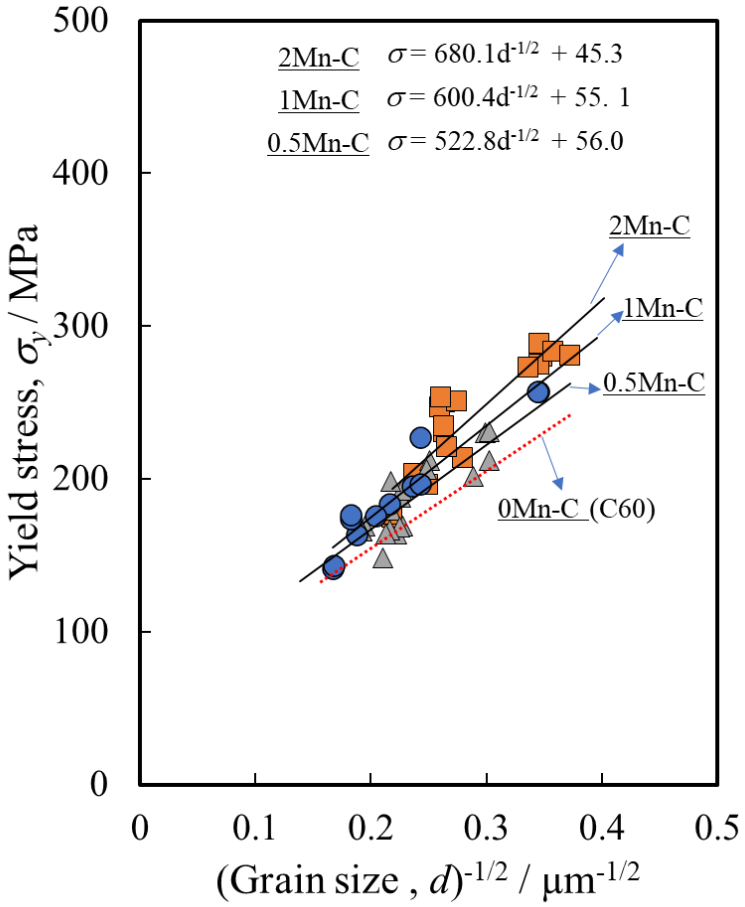

(a) Fe-Mn-C

Fig. 4. 2 The Hall-Petch profile of (a) Fe-Mn-C and (b) Fe-Si-C ternary alloys compared with the previous experimental data of binary alloys.

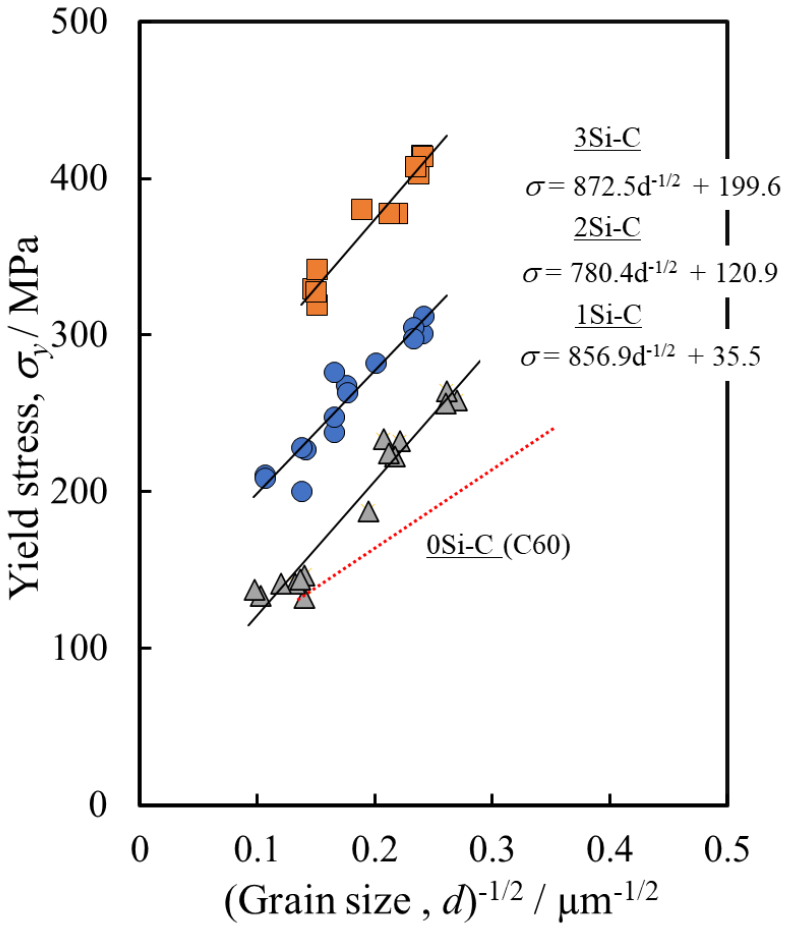

(b) Fe-Si-C

Fig. 4. 2 The Hall-Petch profile of (a) Fe-Mn-C and (b) Fe-Si-C ternary alloys compared with the previous experimental data of binary alloys.

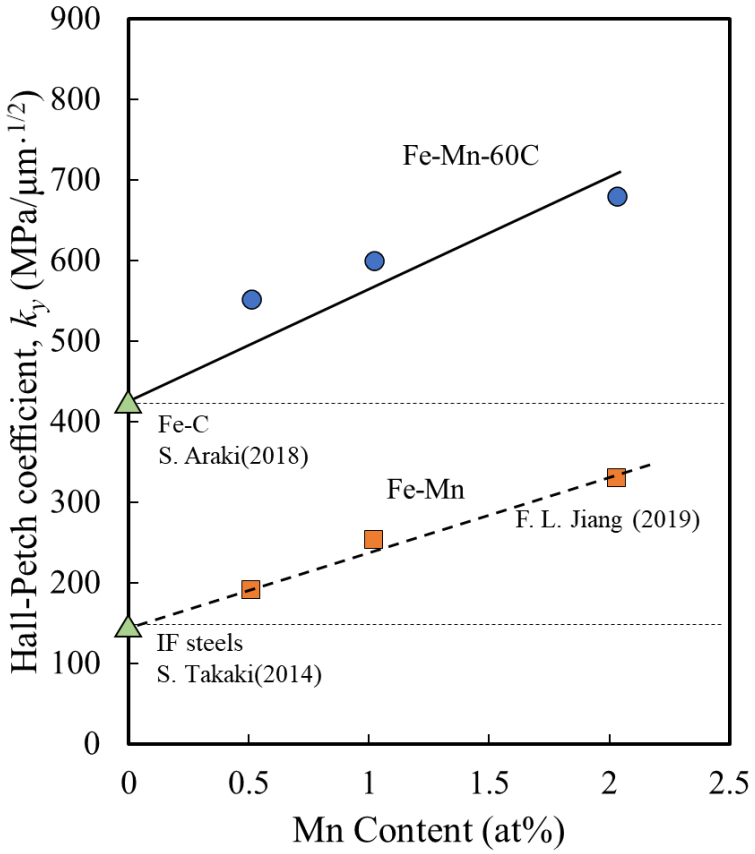

(a) Fe-Mn-C alloys

Fig. 4. 3 The Hall-Petch coefficient in (a) Fe-Mn-C and (b) Fe-Si-C alloys compared with the previous experimental data.

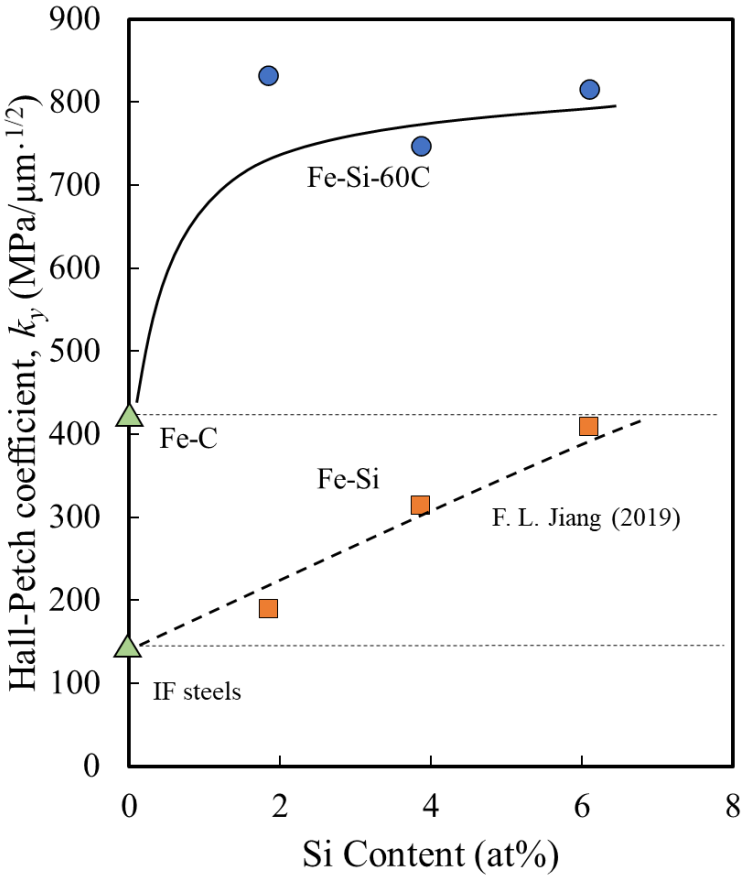

(b) Fe-Si-C alloys

Fig. 4. 3 The Hall-Petch coefficient in (a) Fe-Mn-C and (b) Fe-Si-C alloys compared with the previous experimental data.

4. 3. 2 Grain boundary segregation in Fe-(Mn/Si)-C ternary alloys

To explain the difference in the k_y between Fe-Mn-C and Fe-Si-C alloys, the behavior of each element on GB segregation needs to be investigated. Based on the HO model and that with para-equilibrium theory, the concentrations of Mn, Si, and C segregated at the GB were calculated. Three GB segregation situations were considered here to figure out the actual segregation behavior of each alloying element, namely, the para-equilibrium situation in Fe-(Mn/Si)-C ternary systems (blue), the equilibrium situation in Fe-(Mn/Si) binary systems (orange), and the equilibrium situation in Fe-(Mn/Si)-C ternary systems (green). The results are shown in Fig. 4. 4. The bars with light colors represent the corresponding concentration of C segregated at the GB. The dashed line represents the value of segregated C in Fe-C alloys shown in Chapter 2 for comparison. In the para-equilibrium situation, Mn or Si is unsegregated and remains its original composition at GB, thus the calculated values are equal to the average content of the alloys. In such a situation, the Gibbs free energy of the total system is not minimized, though it is only a temporary situation, as assumed. In the two equilibrium situations for the binary and ternary alloys, the substitutional elements, Mn or Si, are assumed to diffuse completely and cause segregation at GB with sufficient time, making the system stable with the minimum Gibbs free energy.

In Fig. 4. 4 (a), the concentration of Mn segregated at the GB shows an obvious difference between the para-equilibrium and the equilibrium situations, while the two equilibrium ones seem to be close to each other. Comparing the para-equilibrium and equilibrium situation, it can be indicated that Mn itself has a significant tendency to segregate at the GB, which is nearly five times higher than the concentration in bulk. On the other hand, Fig. 4. 4 (b) reveals that, the concentration of Si at GB is greatly affected by C addition. The concentration of Si in the para-equilibrium situation and in the equilibrium of binary systems is only slightly different, which means the tendency of segregation of Si at the GB is much lower than that of Mn.

The interstitial element C was discussed individually. The concentrations of C segregated at the GB in Fe-Mn-C and Fe-Si-C alloys, were calculated and divided into two situations: para-equilibrium and equilibrium. As shown in Fig. 4. 5, Orange lines represent the equilibrium situations, and blue lines represent the para-equilibrium ones. The dashed black line corresponds

to the segregated C concentration in Fe-C alloys. The C concentration in para-equilibrium and the equilibrium system exhibit an opposite trend. In the para-equilibrium situations, the segregated C decreases with the addition of Mn or Si. On the contrary, in equilibrium systems, the values of C increases with the addition of Mn or Si. The addition of C has little effect on the Mn concentration at the GB. Also, the value of C segregated at the GB changes little in these three situations. This indicates that Mn also hardly affects the concentration of C segregated at the GB. However, in the equilibrium situation, the concentration of Si segregated at the GB reduces to a shallow level under C addition. This could be due to the strong repulsive interaction between C and Si at the GB, which is so effective that almost all Si atoms were expelled from the GB even though the C content in bulk is only 1/100 times that of Si. Focus on the concentration of C segregated at the GB, it tends to be reduced with the addition of Si in the para-equilibrium but increased with the decrement in Si segregation in the equilibrium. These opposite tendencies also suggest that C and Si must have a repulsive interaction at GB and within the grain.

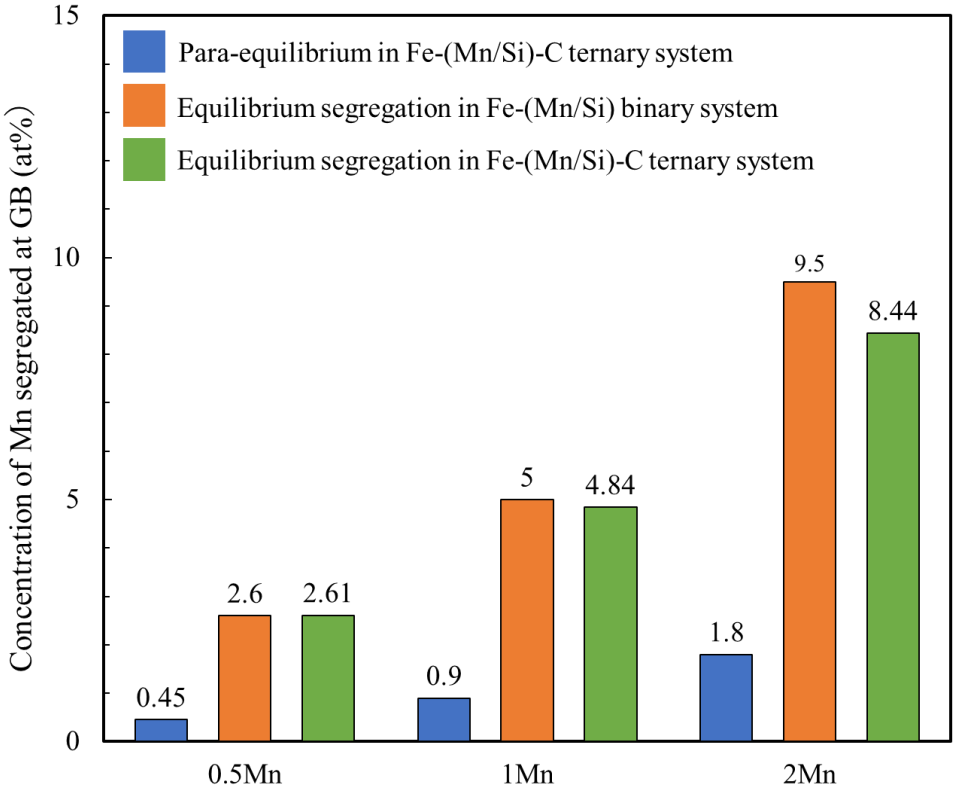

(a) The concentration of Mn segregated at the grain boundary in different situations

Fig. 4. 4 The calculated concentration of (a)Mn and (b)Si segregated at the grain boundary.

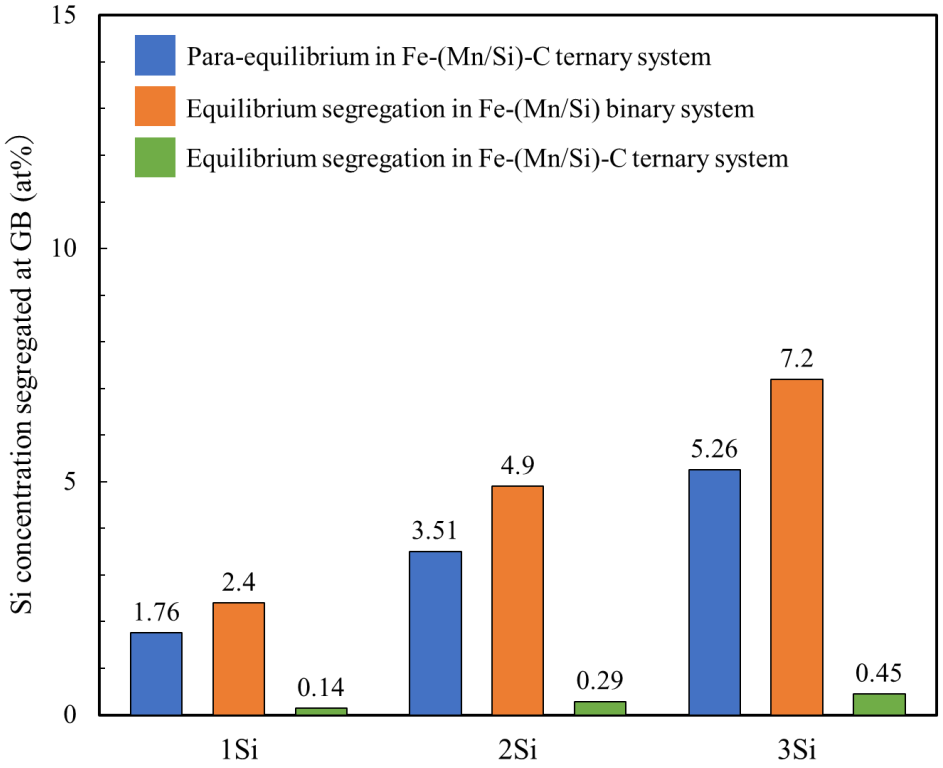

(b) The concentration of Si segregated at the grain boundary in different situations

Fig. 4. 4 The calculated concentration of (a)Mn and (b)Si segregated at the grain boundary.

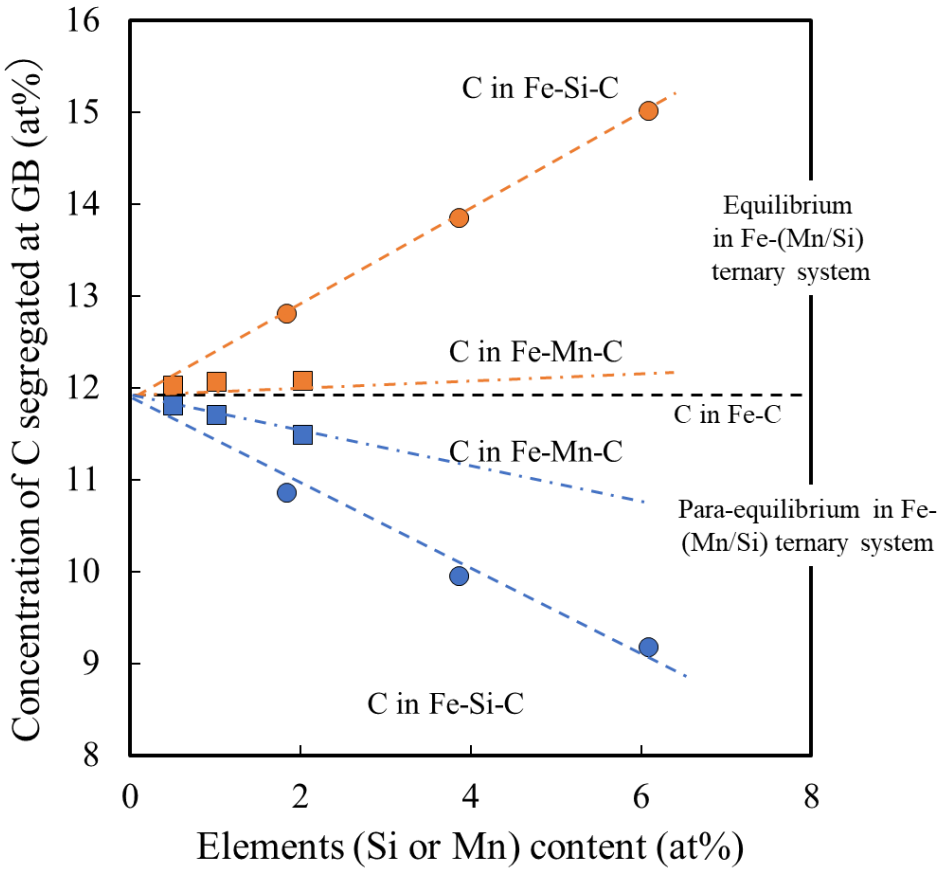

Fig. 4. 5 The concentration of C segregated at the grain boundary.

4. 3. 3 Hall-Petch coefficients in Fe-(Mn/Si) binary alloys

Before discussing the relationship between k_y and GB segregation in ternary Fe-(Mn/Si)-C systems, the relationship in binary Fe-(Mn/Si) systems was investigated to reveal the individual effects of the segregated Mn/Si on the k_y. The binary systems are also divided into two cases: para-equilibrium and equilibrium. The conclusion obtained in Chapter 2 supposes that the effect of additional elements on the k_y can be roughly predicted by the linear relationship between the GB segregation and the k_y. Since the effect of C has already been discussed by the experimental k_y and the calculated segregated C, the effect of Mn/Si could be investigated similarly. The experimental k_y and calculated GB segregation of Mn/Si were clarified previously, then the relationship between the concentration of Mn/Si segregated at the GB and the change of k_y was summarized in Fig. 4. 6.

As illustrated in Fig. 4. 6, orange squares indicate the para-equilibrium situation, and the blue circus indicate the equilibrium situation. No matter which situation, the addition of Mn/Si enlarges the k_y. The two lines show a much larger deviation in Fe-Mn alloys than in Fe-Si alloys. This is probably due to the stronger segregation tendency of Mn than Si, which has an effective influence on the calculated concentration of Mn segregated at the GB. For a rough prediction of the change of k_y of binary Fe-(Mn/Si) alloys, the same method as in Chapters 2 and Chapter 3 was adopted. The mathematical formulas for the relationship between the concentration of (Mn/Si) and the change of k_y can be obtained from Eq. (34), Eq. (36) (para-equilibrium) and Eq. (35), Eq. (37) (equilibrium), respectively.

$$\Delta k_y^{Para}(Mn) = 90.3 \cdot Mn_{seg} \tag{34}$$

$$\Delta k_y^{Equi}(Mn) = 19.4 \cdot Mn_{seg} \tag{35}$$

$$\Delta k_y^{Para}(Si) = 44.6 \cdot Si_{seg} \tag{36}$$

$$\Delta k_y^{Equi}(Si) = 37.4 \cdot Si_{seg} \tag{37}$$

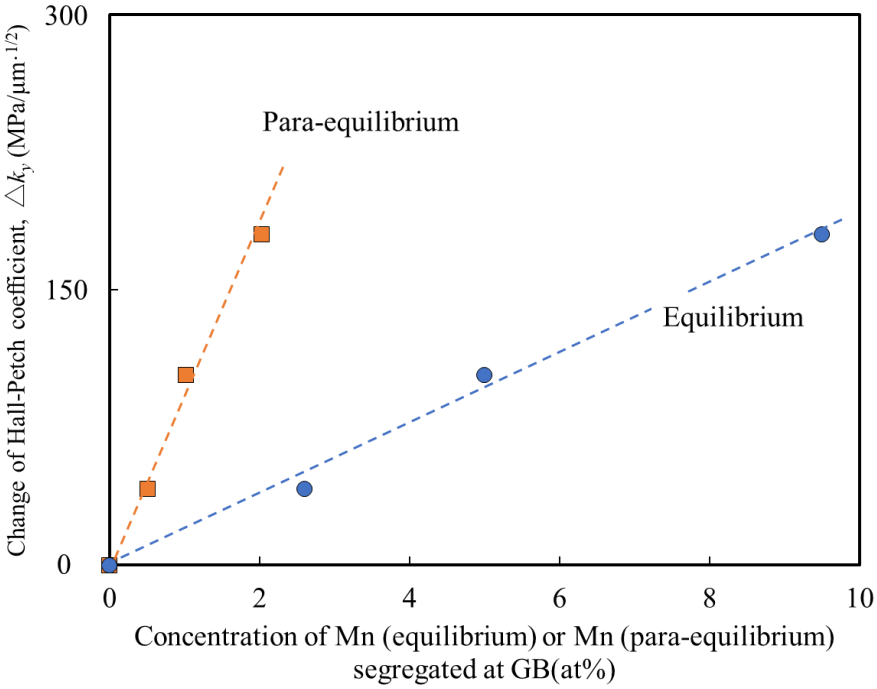

(a) The relationship in Fe-Mn alloys

Fig. 4. 6 The relationship between the concentration of (a) Mn and (b) Si segregated at the grain boundary and the change of the Hall-Petch coefficient.

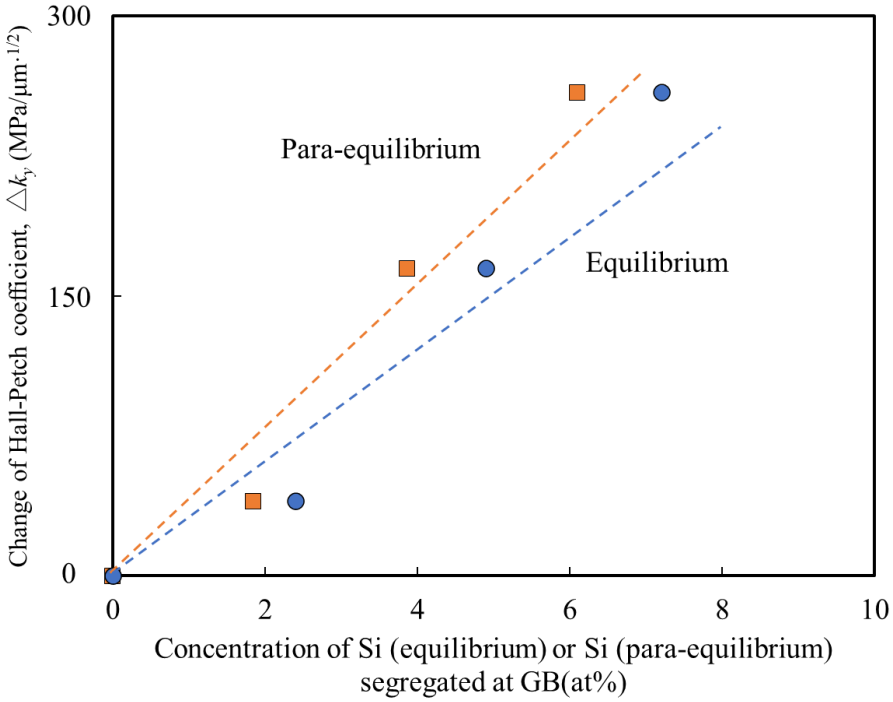

(b) The relationship in Fe-Si alloys

Fig. 4. 6 The relationship between the concentration of (a) Mn and (b) Si segregated at the grain boundary and the change of the Hall-Petch coefficient.

4. 3. 4 Hall-Petch coefficients in Fe-(Mn/Si)-C ternary alloys

So far, the linear relationship between the concentration of Mn/Si segregated at the GB and the k_y in binary systems has been determined based on the same method used in Chapter 2 for C in Fe-C alloys. In addition, the concentration of C/Mn/Si segregated at the GB in ternary Fe-(Mn/Si)-C systems was also discussed in various situations. Although the calculated values of GB segregation depend on the actual segregation situation, a certain assumption can be made that the total k_y in ternary alloys might be composed of the effects of each element on the k_y in binary alloys. In that case, the k_y of Fe-(Mn/Si)-C ternary referred to as k_y (Total), can be estimated by the following addition laws.

$$k_y \text{ (Total)} = \triangle k_y \text{ (Mn or Si)} + \triangle k_y \text{ (C)} + k_y \text{ (Fe)} \quad (38)$$

The k_y (Fe) is equal to the k_y of the IF steel. The $\triangle k_y$ (Mn or Si) and $\triangle k_y$ (C) are the increments of the k_y due to Mn/Si/C addition, which are expressed with Eq. (21) and Eqs. (34)-(37), respectively.

The results of the two situations are shown in Fig. 4. 7. In the Fe-Mn-C alloys, shown in Fig. 4. 7 (a), the calculated results in ternary equilibrium and para-equilibrium situations are close to the experimental results. The para-equilibrium and equilibrium results both exhibite an increasing tendency along with the addition of Mn content, which is roughly coordinated with experimental ones. The small deviation between the experimental and calculated values is probably due to the weak effect of the Mn-C interaction. In the Fe-Si-C alloys, the calculated results in equilibrium and para-equilibrium situations also show lower values than the experimental results. However, the deviation between the calculated and experimental results is much larger than Fe-Mn-C alloys.

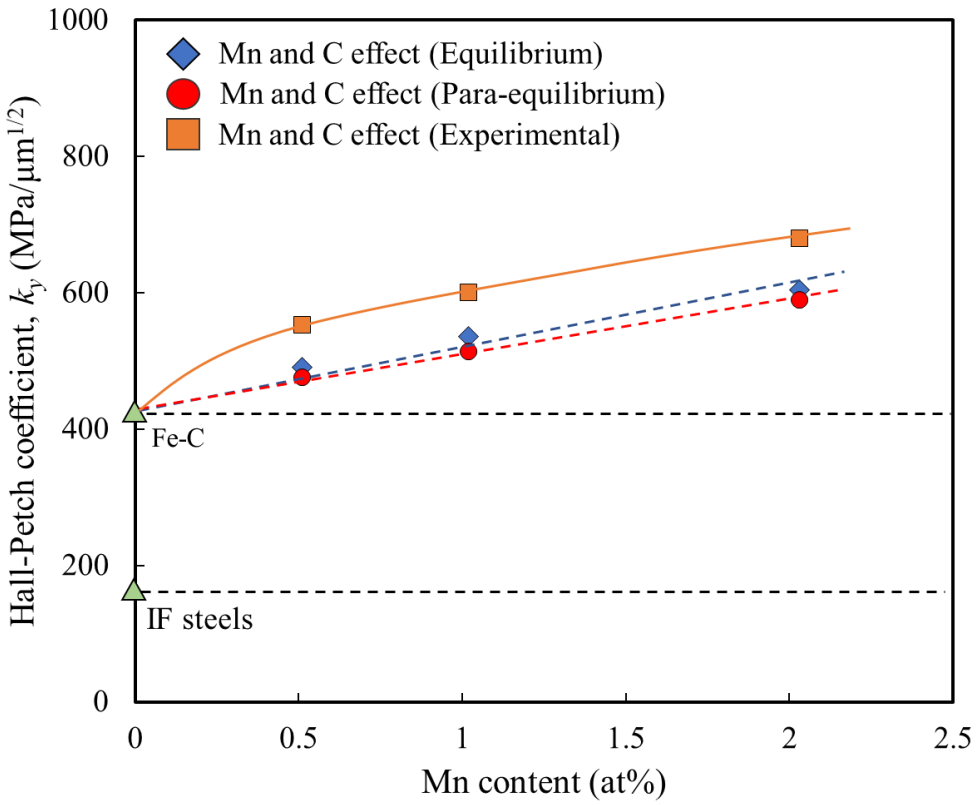

(a) Para-equilibrium and Ternary equilibrium of Mn

Fig. 4. 7 Relationship between the Hall-Petch coefficient and (a) Mn content or (b) Si content based on calculation and experiment results.

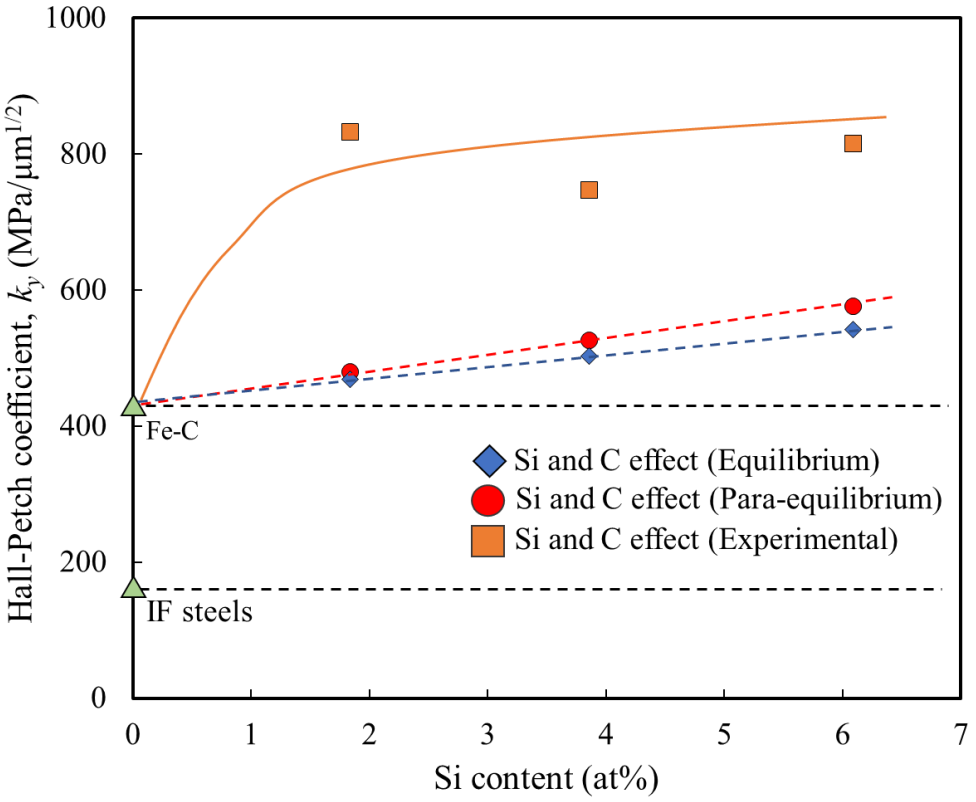

(b) Para-equilibrium and Ternary equilibrium of Si

Fig. 4. 7 Relationship between the Hall-Petch coefficient and (a) Mn content or (b) Si content based on calculation and experiment results.

4. 3. 5 Contribution of Si, Mn, C segregated at grain boundary on the Hall-Petch coefficient

The contributions of GB segregation of C, Si, and Mn to the k_y have been discussed in different situations as mentioned before. To make a more realistic prediction, it is necessary to consider the required time to reach equilibrium to find a more valid situation. According to the fast diffusion rate of C atoms in ferritic steels, the segregation of C is considered to be in the equilibrium in the experiment [76-78]. On the other hand, Si, and Mn diffuse so slowly that it would take a very long time to reach the equilibrium even at the annealing temperature of around 800 K.

Jiang *et al.* [48] considered the GB segregation kinetics based on the McLean model utilizing the volume diffusion coefficient to describe the transportation of solute elements and discussed the equilibrium GB segregation level of Mn and Si in binary Fe-(Mn/Si) alloys at 873 K. He then concluded that it would take about 3 months to reach equilibrium for Mn and Si due to their slow diffusion rate. When the annealing temperature is 973 K, as in the case of this study, 3.6 ks of annealing is not sufficient for Mn and Si to reach equilibrium. With such short annealing time, Mn or Si atoms would hardly move from the initial position, and no significant GB segregation will occur. For example, the average diffusion length (L) can be defined as follows:

$$L = \sqrt{2Dt} \ , \tag{39}$$

in which D is the diffusion coefficient and t is the diffusion time, respectively. It can be obtained that the diffusion length of Mn under a 3.6ks annealing at 973K is only about 0.003μm. Compared with the average grain size, Mn can hardly reach equilibrium.

Having determined the actual situation, it is now necessary to clarify why the k_y increased upon co-addition. The effect of the concentration of C, Mn, and Si segregated at GB on the k_y was investigated in Chapter 2 (interstitial element: C) and Chapter 4 (substitutional element: Mn and Si). The contribution of each component to the total k_y can be calculated using the addition law mentioned above. Figure 4. 8 shows the k_y as a function of Mn or Si content in Fe-(Mn/Si)-C alloys in the para-equilibrium situation. To distinguish the effects of each alloy element on the k_y, the predicted values are marked by different colors.

Figure 4. 8 (a) shows the calculated results for Fe-Mn-C alloys. The dashed line shows the effect of Fe, which describes the influence of the α-Fe matrix on the k_y. The orange and gray areas

represent the effect of Mn and C, respectively. The blue area shows the deviation between the experimental and predicted values. Since all factors affecting the k_y have been considered, the deviation should result from some interaction between segregated atoms at the GB. For Fe-Mn-C alloys, the Mn-C interaction is supposed to reinforce the GB and increase the k_y. However, the deviation is so small compared to the Mn and C area that Mn and C could be regard as the main factors for increasing the k_y in Fe-Mn-C. Figure 4. 8 (b) shows the calculated results for Fe-Si-C alloys. Similar to Fe-Mn-C, the black dashed line, orange and gray areas represent the effect of Fe, Si, and C, respectively. The deviation area in Fe-Si-C alloys is much larger than that in Fe-Mn-C alloys, implying a stronger interaction between Si and C atoms at the GB, which might be the reason why Fe-Si-C alloys own a larger k_y. It is supposed that the Si-C combined effect reinforces the GB and increases the critical GB shear stress, leading to an additional increase in k_y. This could be a new way to achieve high k_y in Si and C co-addition alloys. Although Mn and C also show additional magnification, the smaller area indicates the interaction between Mn and C is weak.

It is very unfortunate that we have not figured out the reason why the k_y enlarged abnormally in Fe-Si-C alloys. Instead, we suggest a hypothesis based on previous research. Due to the co-segregation of Si and C, the structure of GB significantly changes compared with that under individual Si or C segregation, which might have an effective influence on the GB critical shear stress (τ_{cr}) in Eq. (2). In particular, considering that Si is an element that can covalently bond with C and form compounds [79-83], which is the strongest bond in nature, it is not surprisingly that similar atomic structures are generated when the concentration of Si and C are high at the GB. In fact, the molecular dynamics simulation on Ni has proved that hydrogen segregates into GB forming a hydride likely structure, which will induce the intergranular fracture due to the suppression of the emission of dislocations at GB [84]. Further research is expected to reveal how the GB structure changes due to the segregation of solute atoms and how much it changes the k_y in ferritic steels. For that purpose, the development of techniques such as atomic simulation and observation at atomic resolution will be essential.

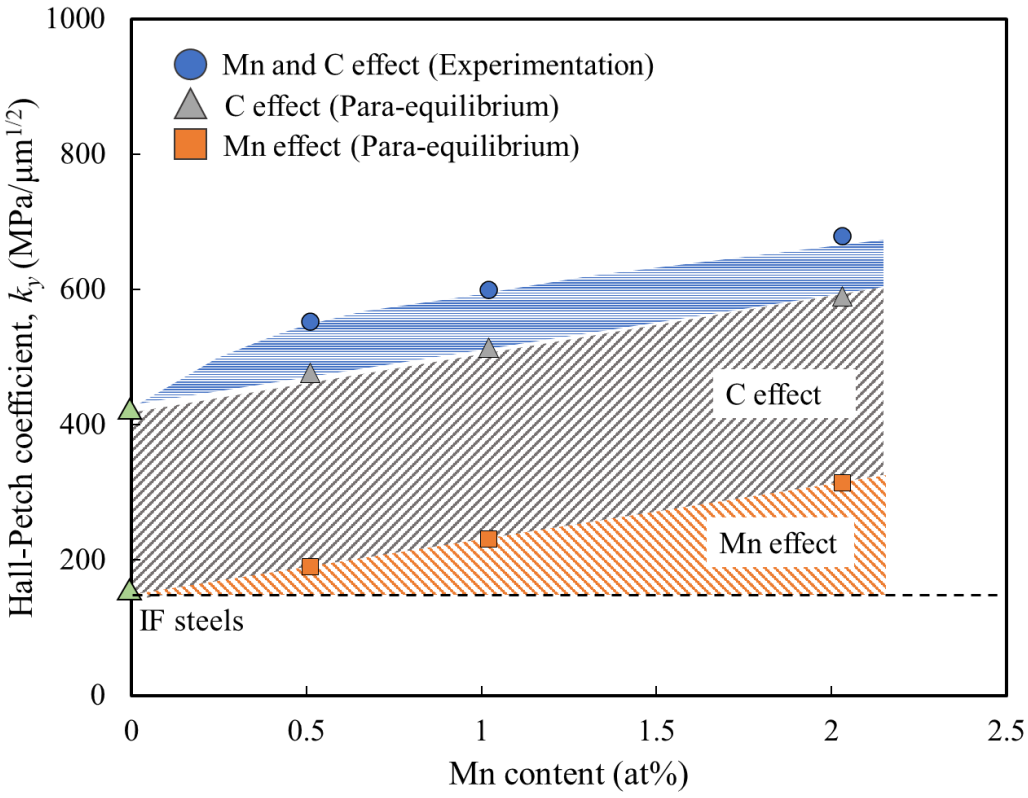

(a) Fe-Mn-C alloys in a para-equilibrium situation

Fig. 4. 8 The relationship between the concentration of (a) C and Mn and (b) C and Si segregated at the grain boundary and the Hall-Petch coefficient, k_y.

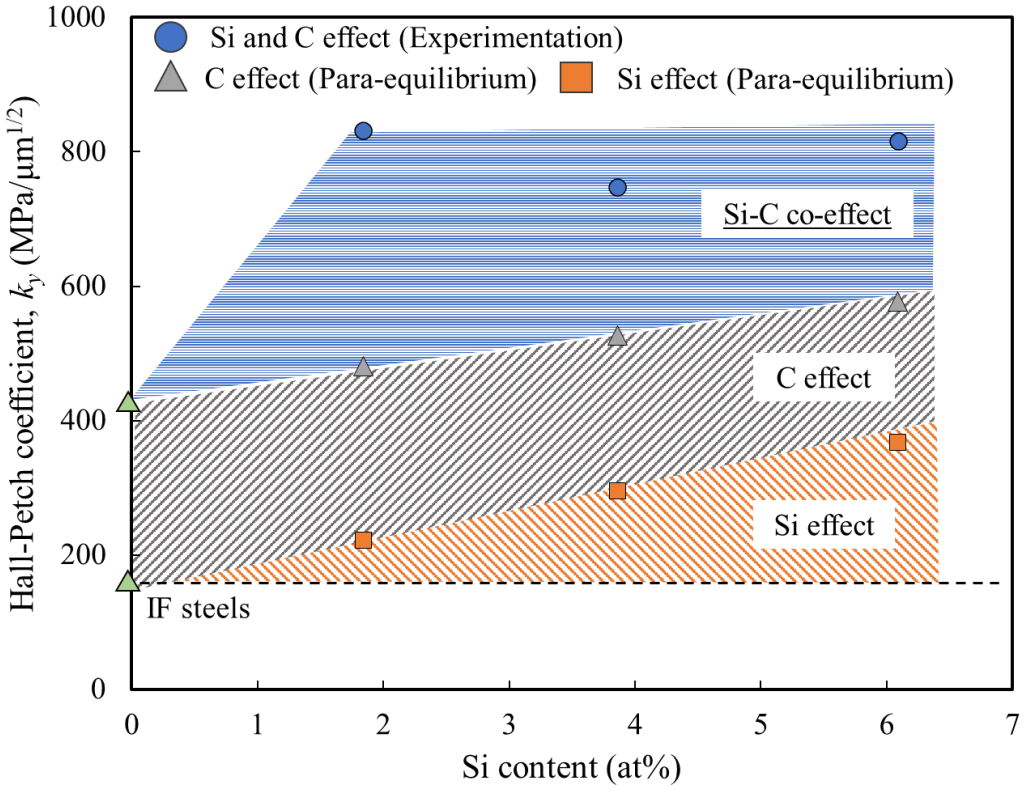

(b) Fe-Si-C alloys in a para-equilibrium situation

Fig. 4. 8 The relationship between the concentration of (a) C and Mn and (b) C and Si segregated at the grain boundary and the Hall-Petch coefficient, k_y.

4. 4 Conclusions

(1) The Hall-Petch coefficient (k_y) is enhanced by the co-addition of interstitial (C) and substitutional elements (Mn/Si), which is much greater than that in binary Fe-(C/Mn/Si) alloys.

(2) Two possible situations: Equilibrium and para-equilibrium were considered to determine the change in the concentration of Mn, Si and C segregated at the grain boundary. Mn exhibited a strong tendency of grain boundary segregation and a weak interaction with C. In contrast, Si exhibited a weak trend of grain boundary segregation and a strong repulsive interaction with C.

(3) Due to the different diffusion rates of interstitial (C) and substitutional (Mn/Si) elements, the para-equilibrium grain boundary segregation was more reasonable in this study, because which Mn and Si are unsegregated and keep the original composition at the grain boundary.

(4) In Fe-Mn-C alloys, the Hall-Petch coefficient (k_y) calculated by the concentration of Mn and C segregated at grain boundary was roughly coordinated with the experimental results. The interaction between Mn and C has a slight influence on the Hall-Petch coefficient (k_y). As a result, the Hall-Petch coefficient (k_y) can be simply predicted by the additional law considering the effects of grain boundary segregation of C and Mn.

(5) In Fe-Si-C alloys, the experimental Hall-Petch coefficients (k_y) were much greater value than the calculated ones, due to some additional interactions between Si and C atoms at the grain boundary.

Chapter 5 Summary

This study investigated the relationship between the Hall-Petch coefficient (k_y) and the concentration of grain boundary (GB) segregation in Fe-C binary and Fe-C-(Mn/Si) ternary alloys. The Hillert-Ohtani (HO) model's GB segregation evaluation method was verified experimentally compared with the traditional McLean model. The influence of annealing temperature and interaction between interstitial element: C with substitutional elements: Mn and Si on the k_y was discussed. The conclusions are summarized as follows:

Chapter 1 introduced the background and research objectives of this study.

In Chapter 2, it was purposed to find an accurate method to calculate the concentration of GB segregation and figure out the exact relationship between the k_y and segregated C/N concnentration at the GB. The concentrations of C and N segregated at the GB in Fe-(C/N) binary alloys were estimated using the McLean and the HO models. The comparison between the two models' calculated results and experimental values obtained by the three-dimensional atom probe tomography (3DAP) revealed that the HO model could gain more precise results than the McLean model. In addition, C exhibited a stronger tendency of GB segregation than N, which will decrease the N concentration at GB when co-added. In this Chapter, it was indicated that the k_y was linearly related to the calculated concentrations of segregated C at GB, the k_y can be predicted from the chemical composition and heat treatment temperature via thermodynamic calculations.

In Chapter 3, it was proposed that the k_y can be correlated with the solubility of C in Fe-C alloys by extending the study of the predicting formula obtained in Chapter 2. Based on the calculated results of the HO model, the reduction of annealing temperature will improve the GB segregation level. The k_y of Fe-50C ferrite steels was studied by annealing treatment under different temperatures to verify this. The results of experimental k_y were almost coordinated with the predicted values by the HO model, which makes the quantitative description reasonable for various C content and annealing temperature in Fe-C alloys. At the end of Chapter 3, a three-

dimensional diagram was drawn to summarize the relationship among the C content, the solution temperature, and the k_y in Fe-C alloys. With the help of this diagram, the k_y can be predicted and controlled in further studies.

In Chapter 4, the procedure was to confirm the influence on the k_y by co-addition of interstitial and substitutional elements and gain high k_y alloys. Based on Chapters 2 and 3, C has a strong tendency to segregate at the GB, significantly affecting the k_y. In addition, previous studies also indicated the apparent enlargement of the k_y by Mn and Si addition in Fe-Mn/Si binary alloys. To find out whether the co-addition of C with Mn or Si can gain higher k_y or not, Fe-Mn-C and Fe-Si-C ternary alloys were investigated. Both ternary alloys exhibited larger k_y than Fe-C binary alloys. In these two multi-systems, the equilibrium and para-equilibrium situations were considered to estimate the concentration of GB segregation. Due to the different diffusion rates of C and Mn/Si, the para-equilibrium was considered more reasonable. With this equilibrium theory, the k_y of Fe-Mn-C alloys can be predicted by the additional effects of segregated C and Mn. On the contrary, the k_y of Fe-Si-C was much greater than the predicted ones. This effect might come from the interaction between Si and C at the GB.

Chapter 5 finally summarized the results of Chapters 2, 3, and 4.

Reference

[1] E. O. Hall: Proc. Phys. *Soc. Lond. B*, 64 (1951), p. 747.

[2] N. J. Petch: *J. Iron Steel Inst*., 174 (1953), p. 25.

[3] J.F. Wallace: *J. Metals* 15 (1963), pp. 372–376.

[4] R.A. Grange: *Metall. Trans*. 2 (1971), pp. 65–78.

[5] R. Ueji, N. Tsuji, Y. Minamino, Y. Koizumi: *Acta Mater*. 50 (2002), pp. 4177–4189.

[6] M. Najaf, H. Mirzadeh, M. Alibeyki: *Mater. Sci. Eng. A* 670 (2016), pp. 252–255.

[7] E.I. Poliak, J.J. Jonas: *ISIJ Int*. 43 (2003), pp. 684–691.

[8] K. Huang, R.E. Logé: *Mater. Des*. 111 (2016), pp. 548–574.

[9] S. Saadatkia, H. Mirzadeh, J.M. Cabrera: *Mater. Sci. Eng. A* 636 (2015), pp. 196–202.

[10] T. Sakai, A. Belyakov, R. Kaibyshev, H. Miura, J.J. Jonas: *Prog. Mater Sci*. 60 (2014), pp. 130–207.

[11] H. Mirzadeh, J.M. Cabrera, A. Najafzadeh, P.R. Calvillo: *Mater. Sci. Eng. A* 538 (2012), pp. 236–245.

[12] H. Rastegari, M. Rakhshkhorshid, M.C. Somani, D.A. Porter: *J. Mater. Eng. Perform*. 26 (2017), pp. 2170–2178.

[13] E. Shafei, N. Goodarzi, K. Dehghani, A. Soltani Tehrani: *Metall. Q*. 56 (2017), pp. 104–112.

[14] R.D. Doherty, D.A. Hughes, F.J. Humphreys, J.J. Jonas, D. JuulJensen, M.E. Kassner, W.E. King, T.R. McNelley, H.J. McQueen, A.D. Rollett: *Mater. Sci. Eng. A* 238 (1997), pp. 219–274.

[15] H. Dong, X. Sun: *Curr. Opin. Solid State Mater. Sci*. 9 (2005), pp. 269–276.

[16] Kosashi. Controlled Rolling and Controlled Cooling, Tokyo, Chijin Shokan (1997), p. 211.

[17] Schiøtz, J. & Jacobsen, K. W: *Science* 301 (2003), pp. 1357–1359.

[18] Schuh, C., Nieh, T. & Yamasaki, T.: *Scr. Mater*. 46 (2002), pp. 735–740.

[19] A. H. Cottrell, B. A. Bilby: *Proc. Phys. Soc. A* 62 (1949), p. 49.

[20] J. D. Eshelby, F. C. Frank, F.R.N. XLI. Nabarro: Lond. Edinb. Dublin Philos. Mag. J. Sci. (1951) 42, pp. 351-364.

[21] A. Cracknell and N. J. Petch: *Acta Metall*. 3 (1955), pp. 186-189.

[22] J. Heslop and N. J. Petch: *Philos. Mag*. 1 (1956), pp. 866-873.

[23] R. Matoba, N. Nakada, Y. Futamura, T. Tsuchiyama and S. Takaki: *Tetsu-to-Hagane*, 93 (2007), p. 513.

[24] S. Takaki, K. Kawasaki and Y. Kimura: *J. Mater. Process. Technol*., 117 (2001), p. 359.

[25] K. Takeda, N. Nakada, T. Tsuchiyama and S. Takaki: *ISIJ Int*., 48 (2008), p. 1122.

[26] N. Nakada, M. Fujihara, T. Tsuchiyama and S. Takaki: *ISIJ Int*., 51 (2011), p. 1169.

[27] A. Hironaka, N. Nakada, T. Tsuchiyama and S. Takaki: *Mater. Sci. Forum*, 706 (2012), p. 2130.

[28] D. Akama, N. Nakada, T. Tsuchiyama, S. Takaki and A. Hironaka: *Scr. Mater*., 82 (2014), p. 13.

[29] D. McLean: Grain Boundaries in Metals, Clarendon Press, Oxford (1957), p. 116.

[30] M. Hillert: Lectures on the Theory of Phase Transformations, ed. by H.I. Aaronson (AIME, New York, 1975), p. 36.

[31] M. Guttmann, D. McLean: Grain boundary segregation in multicomponent systems, in Interfacial Segregation, ed. by W. C. Johnson, J. M. Blakely (ASM, Metals Park, 1979), pp. 261-348.

[32] W. B. Morrison: *ASM Trans. Q*., 59 (1966), p. 824.
[33] M. Matsukura and S. Nanba: *CAMP-ISIJ*, 12 (1999), p. 373 (in Japanese).
[34] M. Etou, S. Fukushima, T. Sasaki, Y. Haraguchi, K. Miyata, M. Wakita, T. Tomida, N. Imai, M. Yoshida and Y. Okada: *ISIJ Int.*, 48 (2008), p. 1142.
[35] S. Takaki, D. Akama, N. Nakada and T. Tsuchiyama: *Mater. Trans*., 55 (2014), p. 28.
[36] P. Lejcek, S. Hofmann, Crit. Rev. Sol. State. Meter. Sci. 20, 1 (1995).
[37] J. W. Gibbs, Transaction of the Connecticut Academy III, 108, 343 (1875-1878), The Scientific Papers of J. Willard Gibbs. Vol. I: Thermodynamics (Longmans, Green & Co., London, 1906)
[38] T. Tsuchiyama, Y. Fuji, Y. Terazawa, K. Nakashima, T. Ando and S. Takaki: *ISIJ Int*., 48 (2008), p. 861.
[39] H. X. Li, S. Gao, Y. Tomota, S. Li, N. Tsuji and T. Ohmura: *Acta Mater*. 206 (2021), 116621.
[40] Y. Ono, Y. Funakawa, K. Okuda, K. Seto, N. Ebisawa, K. Inoue and Y. Nagai: *Tetsu-to-Hagane*, 105 (2019), p. 452.
[41] H. D. Hondros and M. McLean: *Nature*, 224 (1969), p. 1296.
[42] Chang C.C: *Surf. Sci*., 25 (1) (1971), pp. 53-79.
[43] C.A. Shell, J.C. Rivière: *Surface Sci*., 40 (1973), p. 149.
[44] A. Joshi, P.W. Palmberg, D.F. Stein: *Metall. Trans*., 6A (1975), p. 2160
[45] M. P. Seah: *J. Phys. F; Metal Phys*., 10 (1980), p. 1043.
[46] D. F. Stein, W. C. Johnson, C. L. White: Grain Boundary Structure and Properties, Academic Press (1976).
[47] A. Joshi, D. F. Stein: *Met. Trans*., 1 (1970), pp. 2543-2546.
[48] F. Jiang, T. Masumura, T. Tsuchiyama and S. Takaki: *ISIJ Int*., 59 (2019), p. 1929.
[49] S. Araki, K. Fuji, D. Akama, T. Tsuchiyama, S. Takaki, T. Ohmura and J. Takahashi: *ISIJ Int*., 58 (2018), p. 1920.
[50] T. Nishizawa: Bulletin of the Japan Institute of Metals., 12(1973), p. 401.
[51] T. Fuwa and J. Chipman: *Trans. Met. Soc. AIME*, 215(1959), p. 708.
[52] F. Neumann and H. Schenck: *Arch. Eisenhiitt*., 30(1959), p. 477.
[53] H. de. Rugy, H. Viefhaus: *Surf Sci*., 173 (1986), p. 418.
[54] M. Es-Souni, A. Moser: *Surf Sci*, 199 (1988), pp. 439-446.
[55] Y. Funakawa, T. Ujiro: *ISIJ Int*., 50 (2010), p. 1488.
[56] E. D. Hondros, M. P. Seah: *Metall. Trans*. A 8 (1977), p. 1363.
[57] B. S. Bokstein, A. N. Smirnov: *Mater. Lett*. 57 (2003), p. 4501.
[58] P. Lejcek, J. Alloys: *Compd*. 378 (2004), p. 85.
[59] B. W. Krakauer, D. N. Seudman: *Rev. Sci. Lnstrum*. 63 (1992), p. 4971.
[60] J. Takahashi, K. Kawakami, K. Ushioda, S. Takaki, N. Nakada and T. Tsuchiyama: *Mater, Sci*., 66(2012), p. 207.
[61] H. Ohtani, M. Enoki: *Proceedings of the 5th ISSS*, (2017), p. 50.
[62] H. J. Grabke: *Steel Res*., 57 (1986), p. 178.
[63] I. Ohnuma, T. Hara and T. Ohmura: *CAMP-ISIJ*, 31 (2018), p. 753.
[64] S. Takaki, N. Nakada, T. Tsuchiyama: *CAMP-ISIJ*, 23(2010), p. 1199.
[65] D. V. Wilson: *Met. Sci. J*. 1 (1967), pp. 40-47.
[66] K. Osamura and F. Nakamura: *J. Jpn. Inst. Light Met*., 33(1983), No. 1, p. 55.

[67] JIS Handbook Iron and Steel I, Japan Standard Association, Tokyo, (2006), p. 638.
[68] M. Guttmann, D. McLean, Grain boundary segregation in multicomponent systems, in Interfacial Segregation, ed. by W. C. Johnson, J. M. Blakely (ASM, Metals Park, 1979).
[69] M. Guttmann, Interfacial segregation in multicomponent systems, in Atomistics of Fracture, ed. by R. M. Latanision, J. R. Pickens (Plenum Press, New York, 1983).
[70] G. R. Purdy, D. H Weichert, and J. S. Kirkaldy: *Trans. TMS-AIME*, 1964, vol. 230, p. 1025.
[71] J. S. Kirkaldy: Can. Z Phys., 1958, vol. 36, p. 907.
[72] M. Hillert: Internal Rep., Swedish Inst. for Metals Research, 1953.
[73] M. Hillert: The Mechanism of Phase Transformations in Crystalline Solids, 1969, Inst. of Metals, Monograph No. 33, p. 231.
[74] M. Hillert: *Jernkont. Ann*., 1952, vol. 136, p. 25.
[75] Gilmour, J.B., Purdy, G.R. & Kirkaldy, J.S: *Metall Mater Trans B* 3 (1972), pp. 1455–1464.
[76] J. K. Stanley: *Phys. Rev*., 75 (1949), p. 1627.
[77] Y. F. Babikova and P. L. Gruzin: Fiz. Metal. iMetalloved. Akad. Nauk, S. S. S. R., 5 (1957), p. 57.
[78] R. P. Smith: *Trans. Met. Soc. AIME*, 224 (1962), p. 105.
[79] K. Tagashira, N. Sumita and H. Hayakawa: *Mater. Trans. JIM*, 30 (1989), p. 10.
[80] S. Kalogeropoulou, L. Baud, N. Eustathopoulos: *Acta Metal. Mater*. 43 (1995), pp. 907–912.
[81] T. D. Shen, C.C. Koch, K.Y. Wang, M.X. Quan, J.T. Wang: *J. Mat. Sci*. 32 (1997) 3835.
[82] J. Pelleg, Mater. Sci. Eng. A 269 (1999), pp. 225–241.
[83] B. Song, S. Dong, P. Coddet, G. Zhou, S. Ouyang, H. Liao, C. Coddet: *J. Alloy. Compd*., 579 (2013), pp. 415-421.
[84] J. Chen, Y. Zhu, M. Huang, L. Zhao, S. Liang, and Z. Li: *Computational Material Science*, 196 (2021), pp.

Acknowledgments

First of all, I would like to give my heartfelt thanks to all the people who have ever helped me with this paper.

My sincere and hearty thanks and appreciations go firstly to my supervisor, Prof. Tsuchiyama, whose suggestions and encouragement have given me much insight into these translation studies. From his insightful and lively lecture, I have obtained a better understanding of translating theories and thus developed an interest in it. Working on a very busy schedule, he still gives my paper a careful reading and detailed comments. Without his keen insights and constant encouragement, it would not have been finished. Furthermore, it is my honor to benefit from his personality and diligence, which I will treasure my whole life. My gratitude to him knows no bounds.

I am also extremely grateful to the associate professor on our team, Prof. Masumura for his helpful comments on my work. My acknowledgments also go to the technology assistant in our team, Mrs. Ono, and my team member Ma for their help in my experiments.

I also want to thank all my friends and classmates who have kindly provided me with assistance and companionship in the course of preparing this paper.

In addition, many thanks go to my family for their unfailing love and unwavering support.

Finally, I am really grateful to all those who devote much time to reading this thesis and give me much advice, which will benefit me in my later study.